ASSESSING THE IMPACT OF SAHARAN DUST ON ATLANTIC REGIONAL CLIMATE AND TROPICAL CYCLOGENESIS

A Thesis

by

BOWEN PAN

Submitted to the Office of Graduate and Professional Studies of
Texas A&M University
in partial fulfillment of the requirements for the degree of

MASTER OF SCIENCE

Chair of Committee,	Renyi Zhang
Committee Members,	Kenneth P. Bowman
	Robert L. Korty
	Yuxuan Wang
	Qi Ying
Head of Department,	Ping Yang

December 2015

Major Subject: Atmospheric Sciences

ABSTRACT

Recent studies show that Saharan dust can exert substantial radiative and microphysical effects on the weather and regional climate. Moreover, the potential impacts of Saharan dust on the genesis and intensification of tropical cyclones (TCs) remain unclear. In this project, the influences of Saharan dust on the Atlantic regional climate and the genesis of TCs are investigated in the hurricane seasons of 2005 and 2006, which represent hurricane active years and inactive years, respectively. The atmospheric stand-alone version of the Community Earth System Model version 1.0.4 (CESM1.0.4), CAM5.1, is used to simulate the climate condition in full (dust) and none dust (non-dust) emission from the continents. Two regions of interest, the Atlantic TC genesis region (GNR, 50W-20W, 5N-15N) and the TC intensification region (ITR, 70W-40W, 15N-30N), are analyzed. Model output proves the important roles of Saharan Dust on the radiative budget, hydrological cycle, and TC genesis. Dust perturbs the large-scale circulation that moves the Inter Tropical Convective Zone (ITCZ) northward, enhances the West African monsoon, changes the cloud fraction, and perturbs the regional longwave and shortwave radiations. Dust favors the genesis of TCs thermodynamically by increasing the mid-level moisture in the GNR. On the other hand, the TC formation is suppressed by dust through increasing wind shear and decreasing low-level vorticity in the GNR. It is likely that the TC genesis region shifts northward with the ITCZ.

DEDICATION

To my grandfather who passed away on February 2014

ACKNOWLEDGEMENTS

I would like to thank my advisor and the committee chair, Dr. Renyi Zhang, who guides me through the course of research and the thesis writing process. I also want to express my appreciation to all my committee members, Dr. Kenneth Bowman, Dr. Robert Korty, Dr. Yuxuan Wang, and Dr. Qi Ying, for their valuable comments and support throughout the course of this research.

Thanks also go to my friends and colleagues in Dr. Renyi Zhang's group for their valuable inputs and support of my research. I appreciate my friends as well as the department faculty and staff for making my time at Texas A&M University a great experience. Special thanks go to Paige Waskow from the University Writing Center for her help and guidance on great improvement of my thesis writing. And, thanks go to the Texas A&M University Supercomputing Facilities for their valuable computation resources and support on this research. I also want to extend my gratitude to Annie Zhang, Jiaxi Hu, Yuan Wang, Yang Nan, Ryan Zamora, Yun Lin, and Yanjun Guo who provided support and valuable comments throughout the course of data analysis and thesis writing.

Finally, I deeply appreciate my parents for their encouragement and support of my studying abroad.

TABLE OF CONTENTS

Page

LIST OF FIGURES

Page

LIST OF TABLES

Page

1. INTRODUCTION AND LITERATURE REVIEW

1.1 ATMOSPHERIC AEROSOLS

According to the fifth assessment of the Intergovernmental Panel on Climate Change (IPCC AR5), the impacts of aerosols and clouds on regional and global climate remain to be the largest uncertainty in climate predictions, due to the complexity on the aerosol-cloud interactions. Figure 1.1 summarizes the direct, semi-direct, and indirect effects of aerosols on the hydrological cycles and climate, and the feedbacks through cloud, precipitation, and large-scale circulations. Aerosols influence the Earth's radiative budget by absorbing and scattering solar radiation, therefore reducing the radiation reaching the ground and leading to surface cooling (the direct effect). The aerosol optical properties also change the atmospheric temperature and alter the temperature lapse rate, thus stabilizing the lower atmosphere and suppressing the convective development (the semi-direct effect) [*Hansen et al*, 1997]. *Twomey* [1977] suggests that by serving as cloud condensation nuclei (CCN), elevated aerosols increase the cloud droplets concentration and decrease the droplet size at constant water content, hence increasing the cloud optical depth and the cloud albedo (the first indirect effect). Aerosols also influence the precipitation efficiency and further impact the hydrological cycles. A higher CCN concentration results in competitions of the available water content in clouds, leading to decreasing droplets radius, suppressing the collision and coalescence process, decreasing the precipitation efficiency, and prolonging the lifetime of clouds (the second indirect effect) [*Rosenfeld and Woodley*, 2000]. On the other hand, aerosols

may contribute to an increasing concentration of giant CCN (GCCN), which enhances the precipitation by increasing the efficiency of the collision and coalescence processes [*Yin et al.*, 2000]. Moreover, aerosols can act as Ice Nuclei (IN) that potentially changes the cloud properties. An increasing of the IN on the mid-level cloud increases the ice crystals concentration that leads to a shorter cloud lifetime and more precipitation [*DeMott et al*., 2010].

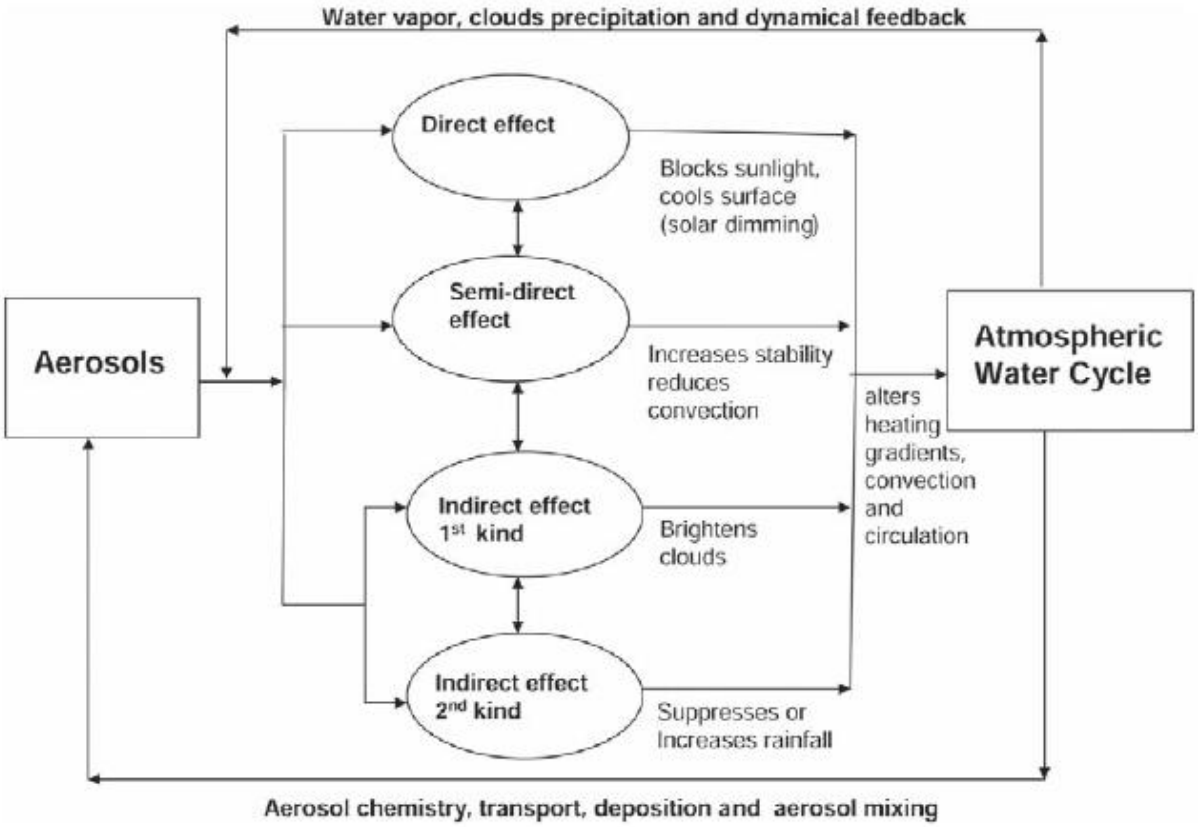

Figure 1.1: Schematic interaction pathways of the aerosols direct, semi-direct and indirect effects, and their responses; feedbacks through cloud, precipitation, and large-scale circulation; feedbacks on aerosols transport, chemistry, and deposition [*Lau et al.*, 2008].

Recently, the increase of anthropogenic aerosol loadings over East Asia has drawn great attention. *Zhang et al.* [2007] suggest that the Asian pollutant outflow is likely to increase the amount of deep convective clouds over the North Pacific. The modeling and observational works by *Wang et al.* [2014a] indicate that mid-latitude cyclones are modulated by the Asian pollution. They found invigorations of mid-latitude cyclones and intensifications of the Pacific storm tracks by anthropogenic aerosols. Moreover, *Wang et al.* [2014b] have also illustrated that the anthropogenic aerosol distinctly impacts TCs under clean to polluted maritime environments and with and without the radiative forcing. The coupled microphysical and radiative effects of the anthropogenic aerosols result in delayed development, weakened intensity, and early dissipation but an enlarged rainband and increased precipitation under polluted conditions [*Wang, et al.*, 2014b]. In addition, anthropogenic aerosols have been shown to change the energy balance of the regional climate system [*Ramanathan, et al.*, 2001]. Also, high concentration of absorbing aerosols perturbs the water cycle and dynamics of the monsoon systems by affecting the cloud and precipitation [*Lau and Kim*, 2006]. Though many studies have contributed to the aerosols-cloud interaction, the nonlinear or non-monotonic nature of the aerosol-cloud-precipitation interaction continue posing large challenges on quantifications of the aerosol effects on cloud systems [*Li et al.*, 2008]. The uncertainties on local productions and long-range transport of aerosols also complicate its chemical composition and lifetimes.

Dust, as one of the major natural aerosol species, has broad impacts on air quality, climate, and biosphere systems. Dust storms and dust plumes are the most prominent,

persistent and widespread aerosol features commonly identified in visible satellite images. Dust is injected into the atmosphere through the saltation bombardment process, which is disaggregated and ejected of the clay-sized (D < 2.5 μm) and silt-sized (2.5 μm < D < 60 μm) particles by saltating sand-sized particles (D > 60 μm) [*Alfaro and Gomes,* 2001; *Grini et al.*, 2002]. *Prospero* [1999] found that the size of a substantial fraction of wind-borne soil dust (Aeolian dust) is less than 2.5μm in diameter, and those particles can be efficiently transported thousands of kilometers horizontally and several kilometers vertically. *Prospero and Carlson* [1970] used Radon-222 as a tracer to measure the long-range transport of dust across the Atlantic Ocean within a period of a week. The dust concentration inside a dust-loaded layer is sufficiently high to cause haze in the Caribbean region. *Prospero* [1999] also observed high concentrations of Saharan dust over the peninsula of Florida, with daily concentration ranging from $10\mu m/m^3$ to $100\mu m/m^3$. Dust loading has a strong seasonal cycle that is the strongest in the summer and the minimum in the winter. The "bio-available" iron component in the Aeolian dust is an important micronutrient that determines the productivity of ocean phytoplankton. Phytoplankton absorbs CO_2 through its photosynthesis process that contributes to the fluctuation of CO_2 concentration on climatic timescales, therefore contributing to the climate variation [*Martin et al.,* 1991]. Moreover, the long-range transported African dust imports Phosphorus (P) and other micronutrients to the Amazon forest, which are important nutrients that determine the forest's health [*Okin et al.,* 2004].

The major dust source regions range from Northwest Africa to Central Asia, in which the Middle East and North Africa (MENA) region contributes more than 50% of

the global dust emission [*Parajuli et al.*, 2014]. Of estimated 1360 million tons dust particles that are lifted annually from the Saharan desert, approximately 60 to 200 million tons are transported westward to the Atlantic Ocean [*Prospero and Lamb*, 2003; *Shao et al.*, 2011]. The factors that affect the dust emission have been explored in field campaigns, laboratory measurements, satellite observations, and model simulations. Recent field campaigns show that the dust emission depends on the interaction between sediments, soil moisture, groundwater, and vegetation. *Zender et al.* [2003a] show large spatial and temporal variations on the dust emission by a global model simulation. Dust emissions can be varied by (1) wind speed, (2) surface roughness, (3) surface soil moisture, and (4) fine sediment availability. *Mahowald et al.* [2007] illustrate that the dust emission has a significant positive correlation with the cube of the wind speed and an anti-correlation with the surface soil moisture. Moreover, *Bryant et al* [2007] demonstrated that a gross perturbation of the surface hydrology of the contemporary ephemeral lake can cause significant differences on dust emissions. Furthermore, the surface emission is sensitive to climate conditions. *Prospero and Lamb* [2003] found the change of a factor of four on the North African dust emissions between the plenty Sahel precipitation condition in the 1950s and the most intense drought condition during the 1980s. Human activities, including the cultivation, deforestation, and overgrazing activities, expose and disrupt the topsoil increases the dust emission. However, the amount of anthropogenic-induced dust emission is still highly uncertain. Estimations show that the variation of dust emission caused by anthropogenic activities ranges from less than 14% to a maximum of 60% of the current global dust emission [*Mahowald and*

Luo, 2003]. The model simulation of dust emission is still challenging, due to the lack of surface observations and the inhomogeneous spatial and temporal distributions of dust [*Reale, et al.*, 2011]. The quantification of dust emission on the regional and global models is still an important topic for further understanding on the dust impacts on the regional and global climate.

Dust can directly absorb or reflect the incoming shortwave radiation, therefore cooling the surface temperature and suppressing surface evaporation. *Lau and Kim* [2007a] compared the 2005 and 2006 hurricane seasons and found the increasing dust loading in the Atlantic Ocean accounts for 30 % to 40% of the SST change. *Wong et al.* [2008] used the Model of Atmospheric Transport and Chemistry (MATCH) and National Center Environmental Prediction (NCEP) reanalysis data to investigate the correlation between the variation in the dust emission and sea surface temperature (SST) anomaly. Their result indicates a positive feedback mechanism that the increasing (decreasing) SST induces a temperature increase (decrease) at 850hPa, which increases (decreases) the anticyclonic circulation at 700hPa through the thermal wind balance, therefore modifying the dust outflow from West African that perturbs the solar radiation at the sea surface and further changes the SST [*Wong et al.*, 2008]. The SST variation may trigger a series of feedbacks on the atmospheric-ocean system that change the large-scale circulation and regional climate [*Evan*, 2007]. For example, *Foltz and McPhaden* [2008] and *Prospero and Lamb* [2003] found an anti-correlation between the Saharan dust loading over West Africa and the current and following year's Sahel precipitation. It is possibly caused by the SST anomaly that changes the latent heat and

water vapor distribution, therefore reducing the Sahel precipitation. The decreasing of the Sahel rainfall further increases the dust emission that leads to more intense or more prolong drought [*Prospero and Lamb,* 2003].

Moreover, recent modeling studies have shown that the radiative effect of dust enhances the rainfall and cloudiness of the ITCZ over the East Atlantic and suppress it on the West Atlantic and Caribbean region [*Lau et al.,* 2009]. Furthermore, Figure 1.2 shows the schematic diagram of Saharan dust induced anomalous on the Walker-type and Hadley-type circulations [*Lau et al.,* 2009]. The heavy loading dust enhances the lifting motion, hence increasing the onshore wind and moist transport to the West African continent. The dusty layer further subsides and suppresses the convections over the West Atlantic region. The dust direct effect also shifts the Inter tropical convergence zone (ITCZ) northward to the south edge of the Saharan Air Layer (SAL), which perturbs the large-scale divergence circulations that affect the African Easterly Wave (AEW), precipitation in the West African monsoon and climate of the Atlantic [*Lau et al.,* 2009; *Kim et al.,* 2010; *Wilcox et al.* 2010], and reduces the westerly flow in the West African Monsoon [*Yoshioka et al.,* 2007]. On the other hand, dust emits the longwave radiation that cools the atmosphere and warms the surface, which offsets the cooling effect by the reflection and absorption of dust on the shortwave radiation [*Miller and Tegen*, 1998].

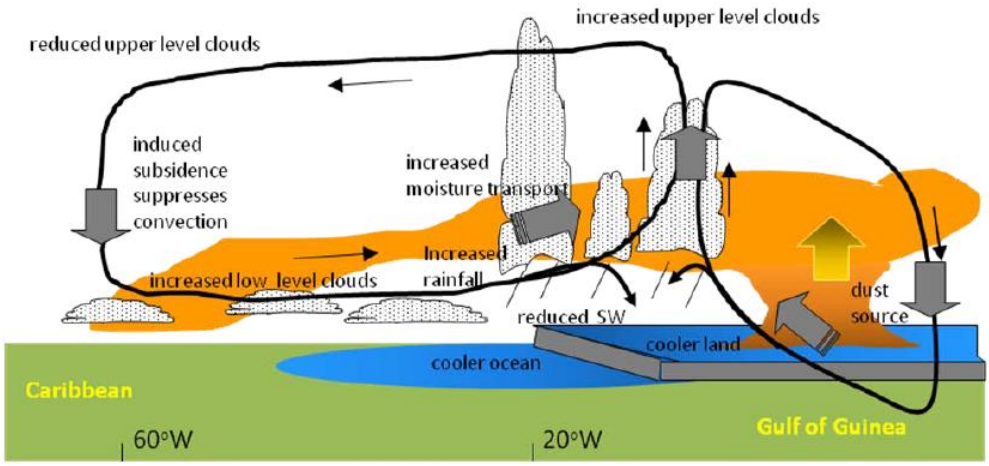

Figure 1.2: Schematic diagram for Saharan dust induced anomalous to Walker-type and Hadley-type circulation [*Lau et al.*, 2009]

Besides the dust direct effect, dust can also serve as CCN, ice nuclei (IN), and GCCN that change the cloud macro-, micro-structures, and the hydrological cycle. *Rosenfeld et al.* [2001] suggest that the Saharan desert provides large concentration of small-size range CCN, which suppresses the growth of cloud droplets, inhibits the collision and coalescence process, and restrains the precipitation formation process. Due to the large spatial and temporal extents of the Saharan dust, *Rosenfeld et al.* [2001] further proposed a climatic scale impact of dust on the clouds. On the other hand, the condensation of water vapor on CCN releases latent heat, which increases the updraft velocity in the convective system and enhances the surface precipitation efficiency, but decreases the accumulated surface precipitation [*Van den Heever, et al.*, 2006]. *Mahowald and Kiehl* [2003] suggest that the Saharan dust suppresses precipitation in the thin low-altitude cloud but enhances the high-altitude clouds over the West Africa coast. *Kaufman et al.* [2005] have linked dust with reductions in the size of cloud droplets and

with changes of cloud covers. *Hansen et al.* [1997] indicate that dust is able to decrease the high cloud cover, therefore further changing the surface and top of atmosphere (TOA) radiative budgets. Moreover, modeling and observational studies agree that dust passes through the polluted area tend to coated with sulfate and serve as GCCN, which is as important as the dust serving as CCN and IN [*Levin et al*, 1996; *Van den Heever, et al.*, 2006]. The increasing concentration of GCCN decreases the cloud's albedo and enhances the collision and coalescence process, therefore increasing the precipitation rate [*Yin et al.*, 2000; *Rosenfeld and Nirel,* 1996; *Levi and Rosenfeld*, 1996]. Furthermore, data from The Cirrus Regional Study of Tropical Anvils and Cirrus Layers-Florida Area Cirrus Experiment (CRYSTAL-FACE) campaign show that the mineral dust is a more important ice crystal residue, compared to other soluble materials such as sulfate and nitrate [*Cziczo et al.*, 2004]. *DeMott et al.* [2003] show that the IN concentration within the dust layer is two orders of magnitude higher than the typical median concentration, which could enhance the precipitation [*Levi and Rosenfeld*, 1996].

1.2 TROPICAL CYCLONES

Tropical cyclones (TCs) as a large and complex convective system are associated with enormous surface enthalpy fluxes that is one of the deadest nature phenomena and cast severe damages especially after their landfall. The frequency and sometime the intensity of the TCs are controlled by several environmental factors, including SST, vertical wind shear, environmental vorticity, and humidity of the free troposphere [*Gray*, 1979]. SST represents the energy supply to the pre-existing atmospheric disturbance on the tropical ocean and the requirement for TC formation is the SST greater than 26.5˚C

[*Shapiro and Goldenberg*, 1998]. A relative weak vertical wind shear is favorable for the development of a vertical coherent axisymmetric structure [*Lighthill et al.*, 1994]. Moreover, the environmental cyclonic vorticity induces rotations into the convective systems and increases the air spirals into the storm center, which are favorable for the development of TCs. Thus, the TC genesis region normally located at 5˚ of latitude, which brings favorable Coriolis effect into the systems. The moist mid level atmosphere avoids the dry air entraining in to the convective cloud system that maintains the updraft mixing within the eyewall. TCs are fueled by both the sensible heat flux from the warm ocean surface and the latent heat flux from phase changes of water in the rainband that sufficient moist in the mid atmosphere will continue the energy supply to the convective systems. When all factors favor the formation of TCs, the environmental-induced, asymmetric, and lower-tropospheric wind surge becomes a vital factor in determining the genesis of TCs [*Gray*, 1998]. *Gray* [1998] further explains the larger inward radial wind that provides sufficient moisture and heat supply are likely to favor the development of TCs. Moreover, some natural variability is possibly affected the TC intensity and frequency, for example the strong El Niño increases the vertical wind shear across the Atlantic Ocean, hence decreasing the TC activities [*Gray*, 1984]. Though the formation of TCs has been investigated in many observations and numerical studies, TC genesis remains unsolved due to the complexity in both physical and dynamical processes.

The scientific community has heatedly discussed the physics behind the genesis of TCs since the 1950s. The most famous theory of tropical cyclone formation is the

conditional instability of the second kind (CISK), which shows a feedback loop on the tropical cyclone genesis [*Ooyama*, 1964; *Charney and Elliason*, 1964]. The low level convergence associated with the tropical disturbance lifts the moist air, which in consequence enhances the condensation and releases latent heat. Subsequently, this process increases the ambient temperature, decreases the surface pressure, and strengthens the low level convergence that favors the tropical cyclone genesis. In the mid-1980s, an alternate formation theory began to emerge, which is known as the wind-induced surface heat exchange (WISHE) model [*Emanuel*, 1986]. The WISHE model indicates that the TC genesis is under a neutrally stable rather than convective unstable atmospheric condition, and the surface wind flux is not necessarily perturbs the temperature and induces the pressure variation. Moreover, TCs can maintain a steady state without any contribution from the ambient conditional instability. The major difference between WISHE and CISK is the relationship between the relating convective warming and the intensity of the cyclone vortex. A numerical experiment by *Craig and Gray* [1996] shows the intensification of numerically simulated TCs, which are better represented using the WISHE model rather than the CISK theory.

The research of aerosol impacts on the TCs is originated with the STORMFURY project that hypothesized the silver iodide seeding into the Atlantic hurricanes would disrupt the inner structure of the hurricane [*Willoughby, et al.*, 1985]. Although the STORMFURY project was inconclusive due to the limit amount of supercooled water in the TCs, the project reveals that the aerosol microphysics effects can alter the development of TCs. *Rosenfeld et al.* [2012] have shown that aerosols are able to

strengthen the downdraft in the outer rainband of TCs, which potentially cuts off air spirals into the center of TCs. These processes invigorate the convections in the outer rainband but break down the thermodynamic structure of the inner TCs [*Rosenfeld et al.*, 2012]. *Zhang et al.* [2007] used the regional atmospheric model system (RAMS) to simulate the influence of dust in the Saharan air layer (SAL) as CCN on the development of an idealized TC. The dust-polluted case (1000 cm^{-3}) and double polluted case (2000 cm^{-3}) concentration shows a 25hPa higher Mean Sea Level Pressure (MSLP) and a 25 m/s lower maximum surface wind speed at the TC's peak intensity compared to the clean case. *Zhang et al.* [2007] conclude that dust particles induce changes on the cloud hydrometeor properties, which modify the storm diabatic heating distribution and thermodynamic structure, and weaken the intensification of TCs through the dynamical responses. Furthermore, *Rosenfeld et al.* [2007] propose the suppression of the warm rain at the periphery enhances the evaporation and cools the lower level; therefore weakening the TCs. Subsequently, *Zhang et al.* [2009] conducted modeling studies on the dust impacts as CCN on matured TCs, which simulates the intervention of dust in the SAL on the TCs. It agrees on the invigoration of the rainband precipitation and the suppression of TCs intensity. Dust as CCN modifies the convective intensity in the periphery and weaken the airflow into the eyewall, therefore indirectly affecting the intensity of TCs. On the other hand, the dust radiative effect increases the static stability of the atmosphere and reduces the upward moisture flux in the low and mid troposphere, leading to a less conductive atmosphere for the genesis of tropical cyclones [*Reale, et al.*, 2014]. Similarly, *Bretl et al.* [2015], using ECHAM6, show an increase of wind

shear, a decrease of moisture in the SAL region, and a more stabilized atmospheric condition under the radiative dust condition, therefore inhibiting the TC genesis. Simulations also show that dust enhances the vertical circulation associated with the AEJ, which favors the development of deep convections on the south edge of the SAL, consequently facilitating a favorable condition for the development of TCs. However, studies of the dust radiative effects on TCs still need further studies with the comprehensive coupled atmospheric and ocean model.

The Saharan dust not only impacts the TCs from its direct and indirect effects, but also associated with other dynamical features influences the genesis and intensification of the TCs. The SAL, that always contains high concentrations of Saharan dust, is defined as a warm and dusty layer that and ranges from 1.5km to 4km in the vertical and can extend thousands of kilometers horizontally, which can reach as far as the U.S. The potential impacts of the SAL on weather systems over the tropical Atlantic have been contemplated since the early 1970s [*Carlson and Prospero*, 1972]. *Evan et al.* [2006] suggest that the scattering and absorption of the dust in the SAL may perturb the Accumulated Cyclone Energy (ACE) and weaken TCs' intensity. They found that intense SAL activities in 1983 and 1985 produce a less conductive environment for the formation of TCs. *Dunion and Velden* [2004] explain that SAL may inhibit the formation and intensification of TCs through three mechanisms: 1) introducing dry air into the TCs, 2) increasing the vertical wind shear in the presence of a mid-level easterly jet (MLEJ) of SAL, and 3) stabilizing the atmospheric environment by the dust radiative effect that heats up the mid-troposphere. *Wong and Dessler* [2005] investigated the

thermodynamic structure of the SAL and found that the largest temperature increase is located on 850hPa. This thermo anomaly indicates the lifting of the condensation and free convection level, which increases the energy barrier to convection, leads to reductions of deep convections in the SAL. The Geostationary Operational Environmental Satellite (GOES) SAL-tracking imagery shows when both TCs and African Easterly Waves (AEWs) are engulfed by the SAL, much of the convection dissipated. *Sippel et al.* [2011] used an ensemble forecast model to investigate the Tropical Storm Debby (2006). They found that the dry SAL interfered with the TC and delayed its intensification in the early stage, but did not disturb the intensity of the storm, as it became stronger. They also concluded that the SST plays a more important role on the TC intensity than that of SAL. Furthermore, *Braun* [2010] reevaluated the SAL impacts on TCs using the National Center for Environmental Prediction (NCEP) data from 41 storms in the Atlantic Basin. He claimed that most of the previous studies are based on false assumptions and found no significant differences in the intensity of the SAL between the intensified and weakened tropical storms. He suggests that SAL is not the determining factor on the intensity of tropical storms, but the large-scale subsidence may inhibit the development of TCs. On the other hand, *Karyampudi and Pierce* [2002] investigated the dynamical impacts of SAL on the genesis of TCs and showed that the SAL induces a horizontal temperature gradient on the mid-level atmosphere to sustain the MLEJ through the thermal wind balance. MLEJ further invigorates the disturbances on the southern and the leading edge of the jet, which potentially favors the formation of TCs. Moreover, *Karyampudi and Carlson* [1988] claimed that SAL outbreaks are

important for the initialization of the African Easterly Waves (AEWs), which contributes to 50% of the tropical storms genesis in the Atlantic basin. Because of the limit representation of aerosols and SAL in the general circulation model, the quantitative impacts of SAL on the TC genesis remain an open issue [*Pratt and Evans,* 2009].

The hurricane season in 2005 was one of the most active on record. Twenty-eight storms occurred, including twenty-seven tropical storms (TSs) and one subtropical storm (Figure 1.3a). Seven of the TSs became major hurricanes, including the deadly hurricane Katrina [*Beven, et al.,* 2008]. Several factors may contribute to the severe hurricane season: warmth of SST in both the Tropical Atlantic Ocean and Caribbean Sea, geopotential anomaly in the mid-troposphere, and tropical waves. Similarly, at the beginning of the hurricane season in 2006, the warm and relatively low shear atmospheric conditions were favorable for an active hurricane season. However, the 2006 Atlantic hurricane season in the end was just near average with ten tropical storms, in which five of them became hurricanes (Figure 1.3b) [*Franklin, et al.,* 2008]. This is the first hurricane season since 2001 that no landfall had happened in the U.S. The reason as to how nature foiled the conductive condition in the 2006 hurricane season has been widely discussed. *Lau and Kim* [2007a] show a positive anomaly of dust loading over the Atlantic Ocean in 2006 that induced solar attenuation and accounted for 30% to 40% of the SST change in 2006. The SST anomaly triggered series of atmospheric responses, which possibly includes the suppression of hurricane activities. Moreover, *Franklin et al.* [2008] also mentioned that the development of El Niño in the late summer of 2006 was likely to reinforce the subsidence over the western Atlantic Basin

and increase the vertical wind shear, which is not favorable for the genesis of TCs. However, *Lau and Kim* [2007b] compared the long-term El Niño-induced and dust-induced SST anomalies and found the 2006 SST anomaly was similar to the dust-induced pattern. *Lau and Kim* [2007a] also expressed that the change of SST seems to be phase-locked with dust events, with a two to three weeks delay. What causes the variation of the hurricane activities in 2005 and 2006? In order to answer the above question, a careful investigation on the July, August, and September (JAS) of 2005 and 2006 could provide insights on the variation of dust loading on hurricane activities.

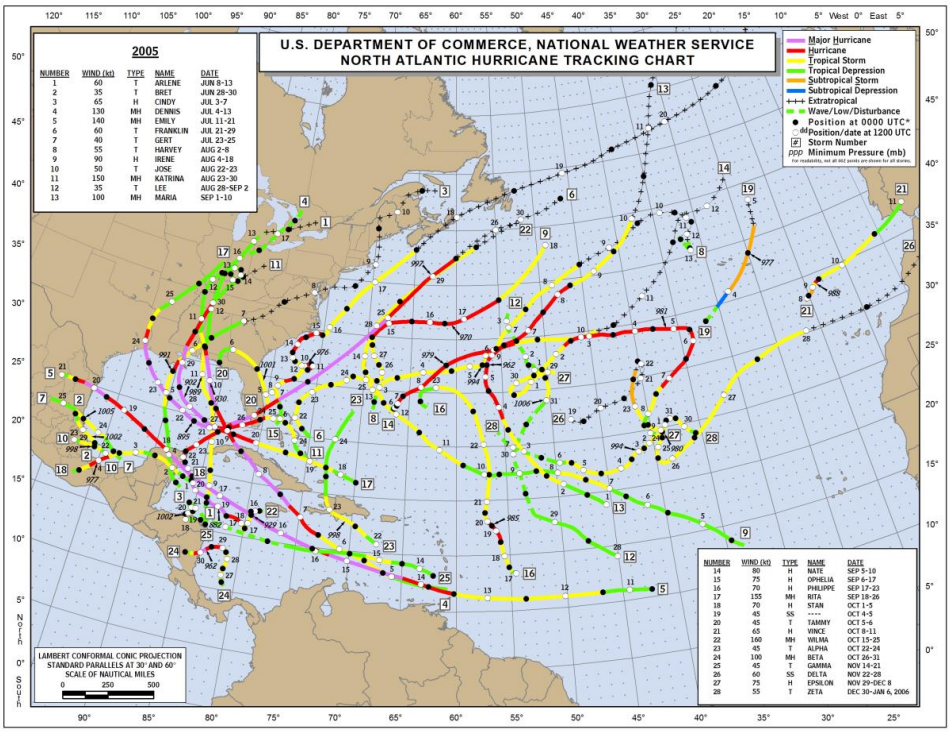

(a)

Figure 1.3: National Hurricane Center (NHC) report in 2005 (a) and 2006 (b)

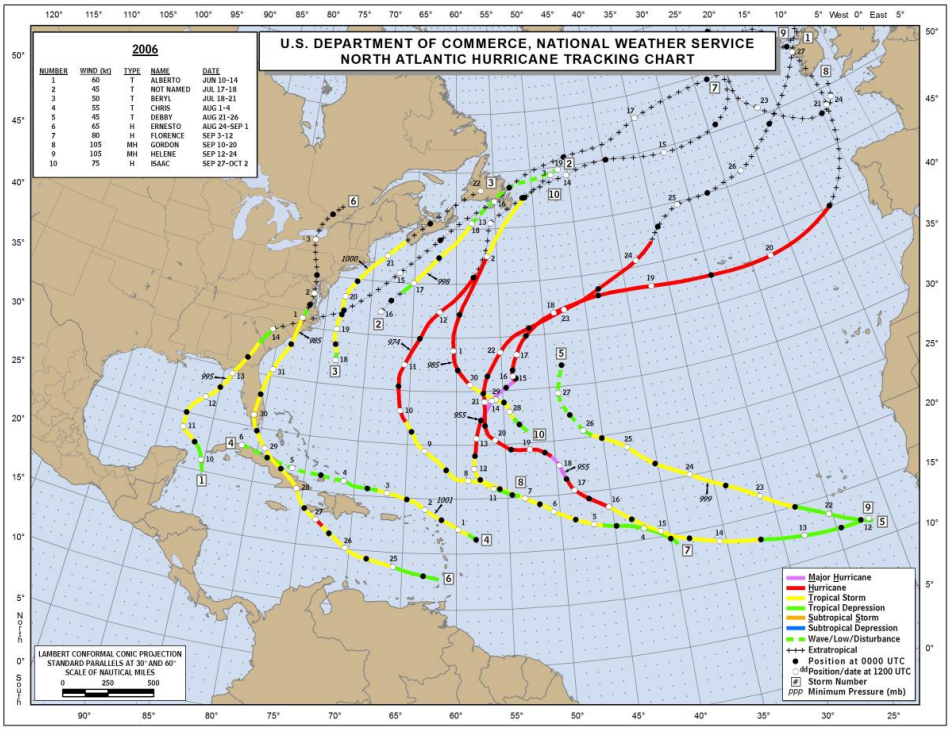

(b)

Figure 1.3: Continued

1.3 OUTLINE OF THE THESIS

The outline of the thesis is organized as follows. In Section 2, the data for model validation and statistical method will be introduced. A brief introduction of CAM5 physics and its dust emission module will also be presented in Section 2. In Section 3, the main content is the validation of the model output on aerosol optical depth, precipitation rate, and temperature field. In the Section 4, I analyze the dust impacts on the regional climate by investigating precipitation, cloud fraction, radiation and other meteorological variables by comparing the dust and non-dust scenarios. Moreover, detailed analysis of TC-genesis-related variables is presented in Section 4. Section 5 contains the conclusion and the discussion for future works.

2. DATA AND METHOD

2.1 OBSERVATION AND REANALYSIS

The Moderate Resolution Image Spectroradiometer (MODIS) that is carried by Aqua and Terra satellites provides extensive remote sensing data on aerosol, cloud, and etc. since 2002. It contains 36 spectral bands between 0.415 to 14.235 micron with spatial resolution of 250m (2 bands), 500m (5 bands) and 1000m (29 bands). The MOD08_M3 is a global level-3 MODIS Atmospheric Monthly Product collected on Terra with 1 x 1 degree spatial resolution. The data from July to September in 2005 and 2006 will be used to validate the CAM5.1 aerosol optical depth (AOD) monthly output. The monthly average is calculated from the average of unfilled daily AOD (MOD04_L2). Each grid is weighted by pixel count method that excludes those pixel counts smaller than six. The Enhanced Deep Blue retrieval algorithm assesses the reflectance over the bright dust surfaces in the blue channel [*Hsu et al.*, 2004] and has been applied over the land where the standard AOD retrieval mechanism failed. The enhanced deep blue products have been widely validated against field and Aerosol Robotic Network measurements that provide useful information on the AOD over bright land surfaces such as deserts. The MODIS AOD shows the measured extinctions from multiple aerosols species, including dust, maritime aerosol, and biomass burning aerosol in the North Atlantic Ocean.

The Global Precipitation Climatology Project (GPCP) version 2 [*Adler et al.,* 2003] is a globally monthly analysis of surface precipitation at 2.5*2.5 resolution, which is available since January 1979. GPCP incorporates precipitation estimates from low-orbit

satellite microwave data, geosynchronous-orbit satellite infrared data, and surface rain gauge observations. The higher accuracy of the low-orbit microwave observations is used to calibrate, or adjust, the more frequent geosynchronous infrared observations. And, the combined satellite-based product is adjusted by the rain gauge analysis. The monthly precipitation rate from July, August, and September of 2005 and 2006 will be used for the validation of model output.

The ERA-Interim reanalysis data from European Centre for Medium-Range Weather Forecasts (ECMWF) [*Dee et al.,* 2003] will be used for the verification of the CESM model. The ECMWF provides the global atmospheric and surface meteorological parameters from January, 1979 to present with a T255 (~80km) horizontal, 60 vertical resolutions, and 12-hour time interval. The ERA-Interim monthly temperature will be used to evaluate the model temperature output.

2.2 STATISTICAL METHOD

The Welch's T-test will be used to test the hypothesis of the means between two scenarios, i.e. dust and non-dust. The two-tail t-test with $\alpha = 0.05$(95% of confident level) rejection interval is used. The null hypothesis for the t-test is that there is no difference between the dust scenarios ($\bar{x}$) and the non-dust scenarios ($\bar{y}$). The dots region in the graph represents the region that rejects the null hypothesis, i.e. there are significant differences between dust and non-dust scenarios.

$$T = \frac{\bar{x}-\bar{y}}{\sqrt{\frac{sx^2}{nx}+\frac{sy^2}{ny}}}$$

The aim of this test is to exclude the internal model variation effects in the model results. Several caveats are required to be considered using this statistical test, i.e. $\bar{x}$ and $\bar{y}$ follow the normal distribution. Welch's t-test is more robust compared to the Student's t-test and maintains the type-I error rate when comparing unequal variance data. However, more ensembles are preferred for detections of the robust dust-induced anomalies. Due to the limit of computational resources, five ensembles from each scenario will contribute to the Welch's t-test.

2.3 MODEL DESCRIPTION

The National Center for Atmospheric Research's (NCAR) Community Earth System Model (CESM) will be used to simulate the atmospheric condition on July, August, and September on 2005 and 2006. CESM is composed of atmosphere (atm), ocean (ocn), land (lnd), and land-ice (ice) models that work simultaneously through the central coupler (cpl). Simulations will be conducted using F_AMIP_CAM5 compset, which represents the stand-alone version of the Community Atmosphere Model (CAM5.1.1) coupled with an active land model (CLM), a thermodynamic only sea-ice model (CICE), and a data ocean model (DOCN) with the climatological SST from 1850 to 2008 [*Conley et al.*, 2012]. It has a 1.9 x 2.5 horizontal resolution with 30 vertical layers (f19_f19) and 30-minute time step. The current experiment set-up does not include the SST variations, which allow us to solely focus on the dust impacts on land and atmosphere. Although previous studies have shown the variations of SST in 2005 and 2006 [*Lau and Kim*, 2007a, 2007b], changes caused by the dust direct effect maybe small [*Foltz and McPhaden*, 2008]. Table 2.1 shows the model physics schemes.

Physics process	CAM5.1.1
Shallow convection	*Park et al.* [2009]
Deep convection	*Neale et al.* [2008]
Microphysics	*Morrison and Gettelman* [2008]
Macrophysics	*Park et al.* [2014]
Radiation	*Iacono et al.* [2008]
Aerosols	*Ghan et al*. [2012]
Dynamics	Finite Volume

Table 2.1: CAM5.1.1 physics schemes

2.3.1 Aerosol module

The Modal Aerosol Module 3 (MAM3) was applied to the current CAM5 configuration. All the aerosols are divided into three modes according to their lognormal size distribution: accumulation, Aitkin, and coarse mode, shows in Figure 2.1. MAM3 assumes that the aerosols are internally mixed in each mode and externally mixed among modes, which simplifies the aerosol size distribution in CAM5 and significantly optimizes the computational time. The mass and the number mixing ratio of internal-mixed aerosols are predicted from the cloud microphysics scheme. CAM5 is capable to simulate all important aerosol processes including aerosol nucleation, coagulation, condensational growth, gas and liquid phase chemistry, emission, dry deposition, and wet deposition [*Liu, et al.,* 2012]. The aerosol-cloud interactions including the activation of cloud droplets, precipitation processes due to particle size

dependent behavior, and explicit radiative interaction of cloud particles [*Conley, et al.*, 2012].

The anthropogenic aerosol initial conditions, including industrial, domestic and agriculture activities sources are from the IPCC AR5 emission dataset. The CO_2 volume mixing ratio in 2005 and 2006 is the same as 379ppm. However, there are large uncertainties remaining in the aerosols emissions, including emission sizes, flux rates of sea salt and mineral dust, and etc. [*Liu et al*., 2012].

Dust with the sea salt is merged into the accumulation and coarse modes in the aerosol modal. Particularly, when the dust is coated with sulfate and organic spices, dust is more soluble and readily absorbs water and can activate as CCN. It can be easily removed by the wet deposition process. The simulated dust emission is 2900-3100 Tg/yr, which is 60% higher than the multi-model mean (~1870 Tg/yr) and 2.6-3.1 days lifetime [*Liu et al.*, 2012].

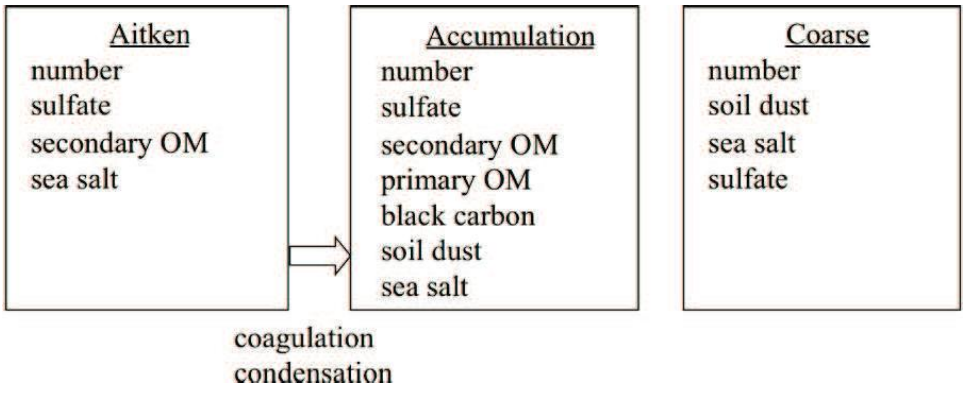

Figure 2.1: Predicted aerosols species in each mode of the MAM3

2.3.2 Dust model

The dust model consists of three major components: (1) emission, (2) vertical transport, wet and dry deposition, and (3) radiative effects [*Albani, et al.*, 2014]. Dust emission is simulated by the Dust Entrainment and Deposition Module (DEAD) [*Zender, et al.*, 2003a], which is implemented in the Community Land Model (CLM). It is based on a saltation-sandblasting process depends on the modeled wind friction velocity, soil moisture, and vegetation/lake/snow cover [*Zender, et al.*, 2003a]. The model friction wind velocity is determined by the drag process, Owen effect and soil moisture. Only the erodible fraction of the surface is able to emit dust into the atmosphere. The surface topography lows are normally hot spots for dust emission [*Zender et al.*, 2003b]. Dust is ejected from the surface whenever the friction velocity exceeds the threshold friction velocity of dust. It is accelerated by the fluid velocity and dragged by the gravitational force. Some of dust particles especially the large ones drag to the surface and blast fine particles. This process is named as saltation bombardment, which is the generation process for most dust plumes and storms. It is simulated using the following equation in the model.

$$F_j = TA_m S\alpha Q_s \sum_{i=1}^{I} M_{i,j}$$

The total vertical mass flux of dust (kg m^{-2} s^{-1}) in the transported bin j, $F_{j,}$ has transferred i bins of particles emission. T is a global tuning factor that is equal to 5*10^-4 in the CLM. S is the source erodibility factor that is sets to 1 as a placeholder, which would include the impacts of different soil size and texture. A_m is the dust

mobilization factor that represents the exposure of the bare soil in the grid cell. It is determined by the coverage of lake, wetland, snow and vegetation. Q_s represents the horizontal dust mass flux, which is only determined by the friction wind speed and the threshold friction wind speed of the particle. α is the sandblasting mass efficient that converts the horizontal mass flux to the vertical mass flux. It is determined by the mass fraction of clay in the soil. $M_{i,j}$ is the mass fraction ratio of the tri-modal source mode to four-bin transport mode. The DEAD output, i.e. the dust vertical saltation flux, is implemented into the CAM and controls by the meteorological field for the transportation of dust and other atmospheric trace species. Dust deposition processes include dry gravitational settling, turbulent dry deposition and wet deposition. Wet depositional processes are parameterized within CAM5 and the dust is settled down as long as it reaches the threshold of the gravitational velocity and turbulence velocity. However, the wet deposition is the dominant process for dust removal from the atmosphere. Dust is able to go through four processes: 1) nucleation scavenging, 2) sub-cloud scavenging in convective and stratiform clouds respectively. The model also accounts for the re-evaporation processes that emit dust back into the atmosphere.

Above all, the CAM5 uses the MAM3 as the aerosol representation mode. Dust is partitioned into the accumulation (0.1 to 1.0 micron) and coarse (1.0 to 10 micron) modes. Both number and mass concentration are predicted in each mode. Moreover, the dust particles are hygroscopic and can undergo the equilibrium Kohler theory.

2.3.3 Cloud

Four kinds of clouds are treated respectively in each level of the model, i.e. liquid and ice stratus, shallow and deep cumulus. The treatment of convective clouds physics follows *Zhang and McFarlane* [1995] and has been modified by *Neale et al.* [2008]. The cumulus cloud microphysics follows the single moment scheme, which the size distribution of cloud droplets is either followed the droplets distribution in the stratiform clouds or as a set constant number. Therefore, the model is not able to simulate the aerosol indirect effect to cumulus clouds. On the other hand, CAM5.1.1 uses a two-moment bulk microphysics [*Morrison and Gettelman,* 2008] scheme on the simulation of stratiform clouds. The cloud droplets size distribution follows the gamma distribution and the model predicts the number and mixing ratio of the cloud droplets and ice crystals. A prognostic ice crystal number concentration and an ice nucleation scheme are implemented in the CAM5.1.1 [*Liu et al.*, 2007]. Dust particles are generally non-soluble, therefore acting as contact IN [*Lohmann* ,2002] and deposition/condensation IN [*Demott et al.*, 2003].

The total cloud fraction is determined by the horizontal and vertical overlaps of four kinds of clouds. Horizontally, the deep and shallow cumulus clouds are non-overlapping due to different physical bases, whereas the liquid and ice stratus clouds are maximum overlapping. Moreover, the stratus clouds are only located at the region without cumulus clouds [*Park et al.,* 2014]. The overlapping algorithm modifies the radiative flux and the precipitation. According to the International Satellite Cloud Climatology Project (ISCCP), CAM categorized the cloud into three types by their cloud-top pressure (CTP),

i.e. high clouds (CTP <440hPa), middle clouds (440hPa<CTP<680hPa), and low clouds (CTP> 680hPa) (Figure 2.2)

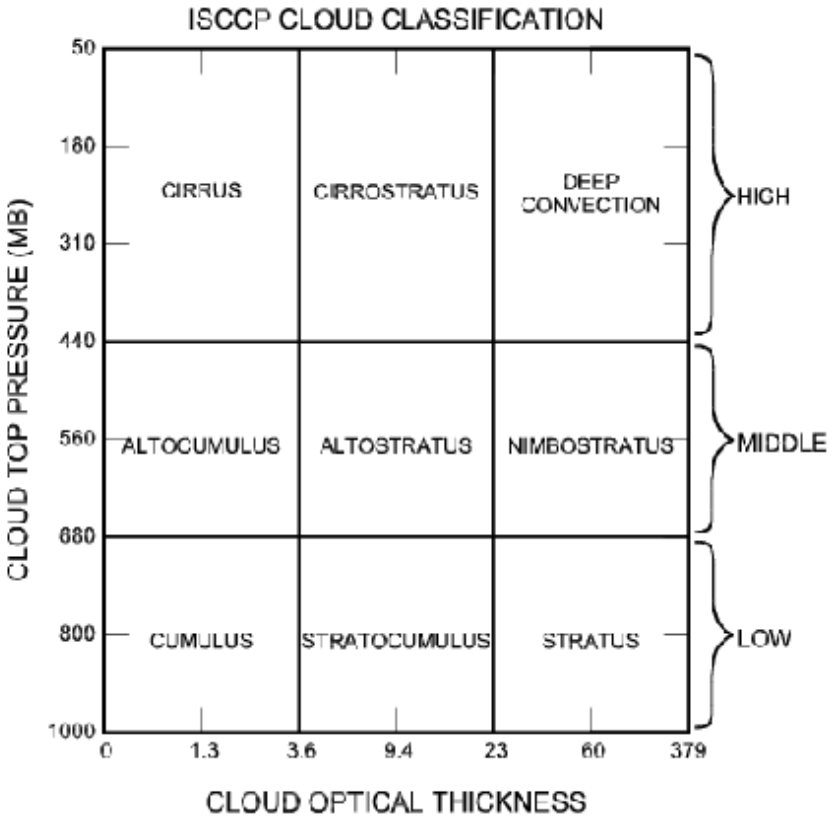

Figure 2.2: Cloud categories in CAM5 from *ISCCP (http://isccp.giss.nasa.gov/cloudtypes.html*)

2.3.4 Radiation model

The model radiative transfer uses the Rapid Radiative Transfer Model for General Circulation Models (RRTMG), that is a broadband *k*-distribution radiation model [*Iacono et al.*, 2003]. Aerosol optical properties follow the parameterizations by the *Ghan and Zaveri* [2007], which accounts for the hygroscopic growth of aerosol components following the Kohler theory and calculates the single scattering albedo,

extinction factors, and refraction indices by looking into the wet refractive index and wet surface mode radius [*Ghan and Zaveri,* 2007]. The dust radiative forcing only considers the absorption of the longwaves (LWs) and ignores the scattering of the LW radiation.

2.3.5 Model setup

The model simulations include two scenarios, with or without the surface dust emission from continents. The dust scenario includes the online dust emission and cam5-physics, whereas, the non-dust scenario (non-dust hereafter) sets the vertical dust saltation flux in the DEAD model to zero. All simulations are integrated from 2001-01-01 to 2004-12-31 as spin-up and restart from 2005-01-01 to 2006-11-30. Each scenario has five sets of ensembles, which slightly perturbs the initial temperature field in order to eliminate the effects of the model internal variations and to evaluate the significant differences between these two scenarios.

All model simulations were performed on the TAMU EOS supercomputer, which is an IBM "iDataPlex" commodity cluster with nodes based on Intel's 64-bit Nehalem & Westmere processor. Each processor is composed of 6 head nodes, 4 storage nodes, and 362 compute nodes. Each simulation conducts 32 processors and 36-hour wall time.

2.4 REGION OF INTEREST

The major hurricane development region is defined as the region between 10°N and 20°N and 20°W to 85°W, where 60% of Atlantic named storms and 85% of major African wave forming hurricanes are originated here [*Goldenberg et al.,* 2001; *Evan et al.,* 2006]. In order to quantify the dust impacts on Atlantic hurricanes specifically on the southern edge of the SAL, the hurricane genesis region (GNR) is defined within the

Main Develop Region from 50ºW to 20ºW and from 5ºN to 15ºN [*Lau and Kim* ,2007a] (Figure 2.3). The other region of interest, hurricane intensification region (ITR), is located on the front edge of the SAL from 70ºW to 40ºW and from 15ºN to 30ºN, which covers the front edge of the SAL, another convective active region.

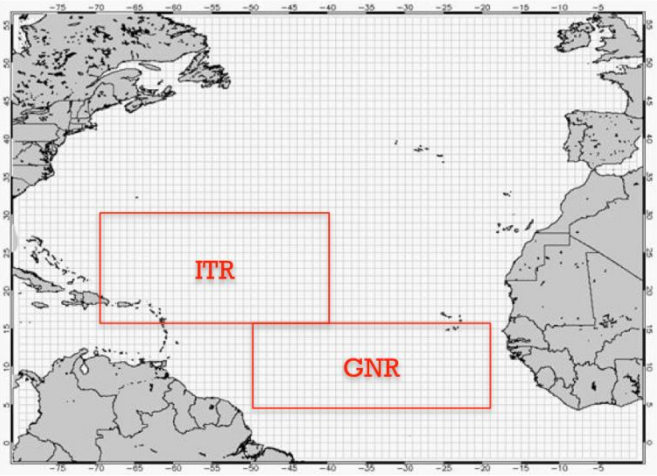

Figure 2.3: Regions of interests: hurricane genesis region (GNR): 50º-20ºW, 5º-15ºN; hurricane intensification region (ITR): 70º- 40ºW, 15º-30ºN [*Lau and Kim*, 2007a]

3. MODEL VALIDATION

3.1 AEROSOL OPTICAL DEPTH

The dominant aerosol species over the West Africa and East Atlantic region during the boreal summer is the mineral dust. Thus, the value of aerosol optical depth (AOD) can directly represent the amount of dust loading over West African to the Mid Atlantic Ocean. The model-simulated monthly AOD at 550nm is compared with the MODIS global monthly AOD, both qualitatively and quantitatively. Figure 3.1 shows the MODIS monthly AOD (left) and CAM AOD (right) on August of 2005 and 2006. The high AOD (0.5-1.0) area is located between 10N and 25N and extended from the African Continent to the Atlantic Ocean. This high AOD region corresponds to dust sources and high concentration of long-range transported mineral dust. The model successfully captured the heavy dust loading. Moreover, for the daily analysis of August 21 to 27, 2006 (Figure 3.2), the model reproduces the dust episode on a weekly basis, whereas fails to generate the right timing of the dust event. As show in Figure 3.2, the high AOD region is located just off the West African continent at [15W, 27N] on August 26, while the simulated maximum AOD spots on the African Continent which represents the beginning of a dust episode.

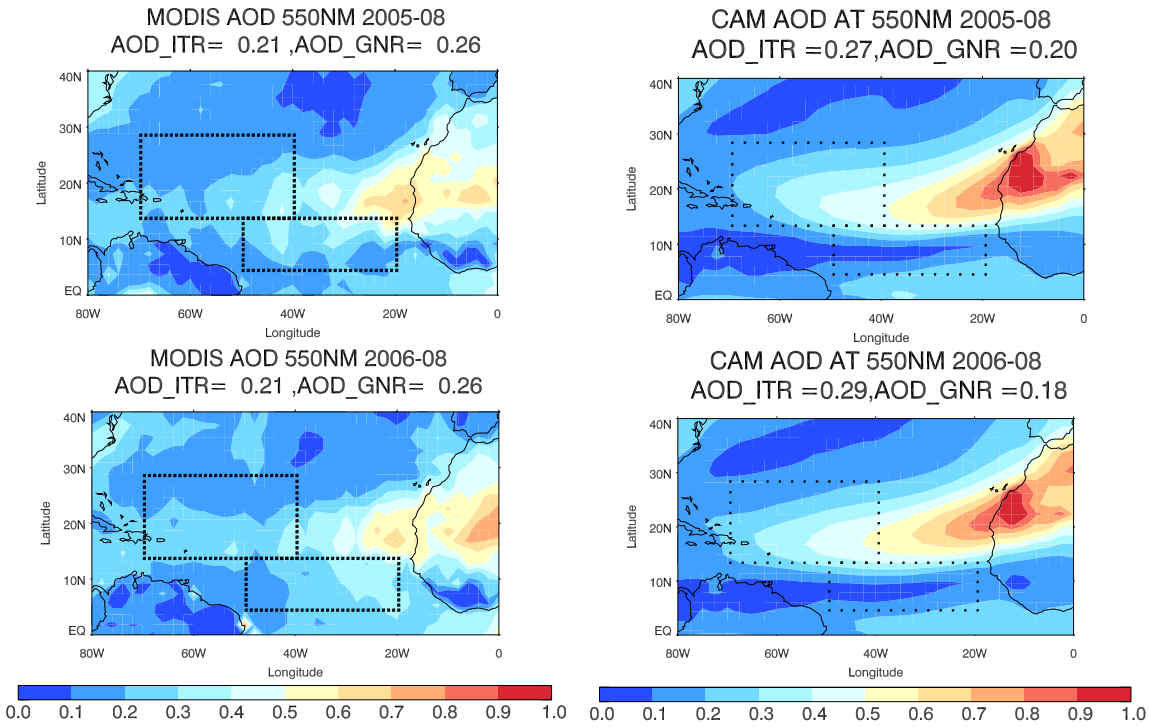

Figure 3.1: MODIS AOD (left) and CAM output AOD (right) in August 2005 and August 2006

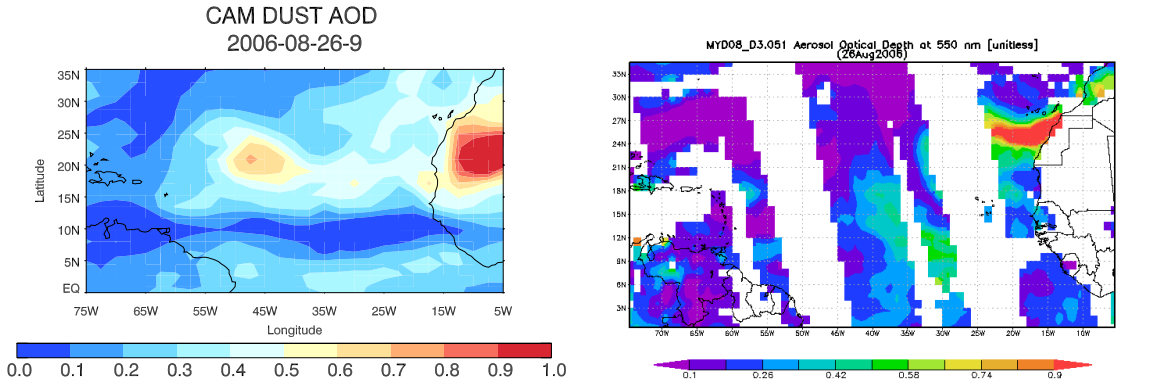

Figure 3.2: Daily AOD comparison between CAM and MODIS output on August 26 and 27 in 2006

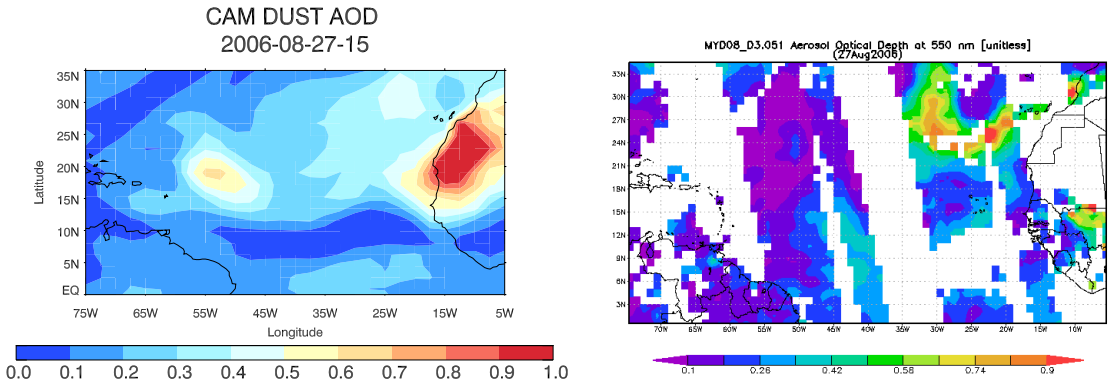

Figure 3.2: Continued

The major inconsistencies between CAM and MODIS AOD are on the Saharan Desert, i.e. the dust source region, which potentially cause by the uncertainties on the MODIS deep blue algorithm and the overestimation of dust emission in CAM5 [*Liu et al.*, 2012]. Moreover, the overestimation of AOD in the mid Atlantic Ocean is because of the overestimation of the dust emission and the inefficient dry deposition of small particles [*Zender et al.*, 2003a]. CAM5 underestimates the AOD (i.e. dust loading) over the heavy precipitation region at 10N and the AOD over GNR, due to the overestimation of aerosols wet deposition rate in the model (Figure 3.3). Above all, the model overestimates the AOD over the Saharan Desert and ITR (16%) and underestimates AOD in the GNR (29%). It also biases on the temporal and spatial distribution of the daily maximum AOD. These inconsistencies could potentially induce bias on the aerosol direct and indirect effects. Overall, CAM is able to capture the heavy dust outflow trend in the AOD, especially over the ocean.

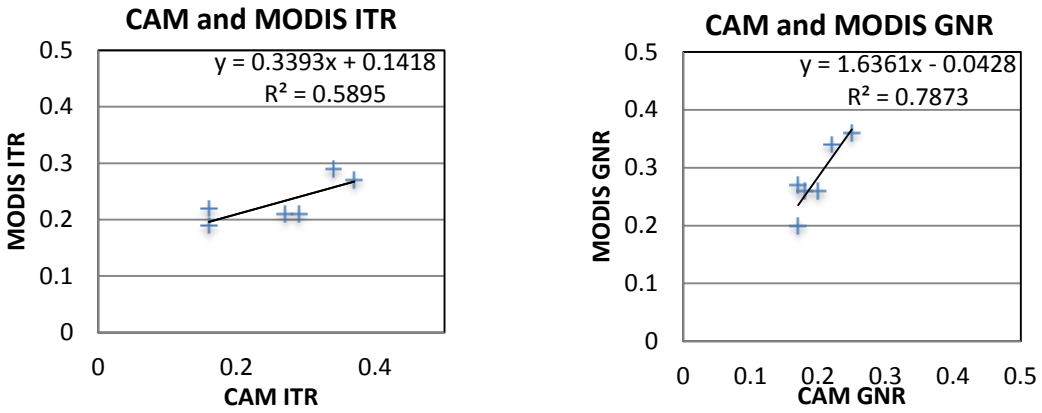

(a) (b)

Figure 3.3: CAM and MODIS AOD scatter plot on JAS of 2005 and 2006 (a) ITR (b) GNR

3.2 PRECIPITATION

GPCP monthly precipitation rate has been compared with the model-simulated precipitation rate (Figure 3.4). The maximum precipitation area at 10N corresponds to the ITCZ, in which CAM simulates the maximum at 20mm/day on the West African coast and GPCP observed a maximum precipitation of 16-18mm/day at [37W, 10N]. Moreover, the spatial average of the precipitation rate in GNR is significantly higher in the model simulation (8.72mm/day) than that of the GPCP observations (4.38mm/day). This is because of CAM overestimates deep convective cloud frequency over land during the boreal summer [*Park et al.*, 2014], therefore overestimating the convective precipitation that is the major contributor to the total precipitation in the tropical region. Above all, the model successfully captures the major precipitation trend qualitatively.

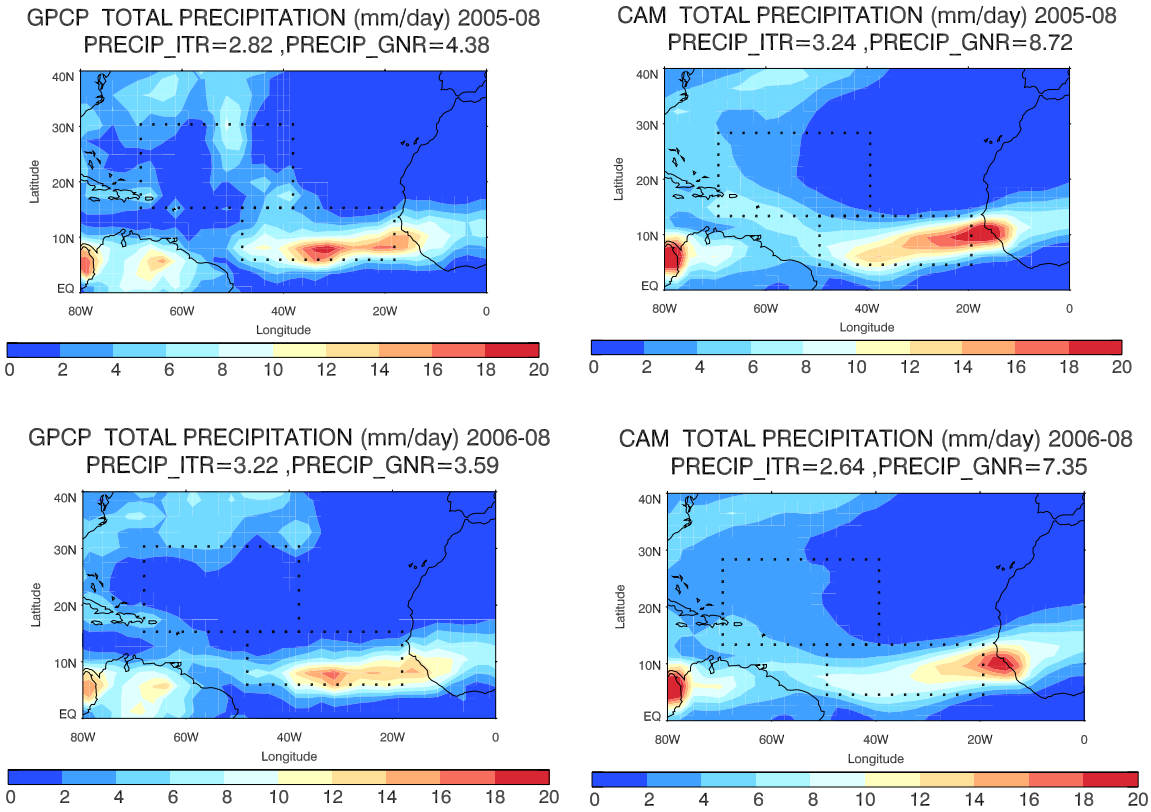

Figure 3.4: GPCP (left) and CAM (right) precipitation rate comparison in August 2005 and August 2006

3.3 TEMPERATURE

Figure 3.5 shows the temperature cross-sections at 20N and 20W from the ERA-Interim (left) and CAM5 (right) in August 2005. In the 20N temperature cross-section map, the maximum temperature is above 320K at the surface of the West African continent in the ERA-Interim, where CAM5 has a slightly lower temperature. This is possibly because of the model overestimation on the dust emission that blocks the incoming solar radiation and cools the surface. CAM5 also simulates a warm tongue from 20W to 40W at around 850hPa that corresponds to temperature inversion caused by the SAL while the ERA-Interim does not observe this figure, since the model maybe

oversensitive on the dust radiative impacts on the temperature field. For the cross section map along 20W, there is a warm core on 900hPa at 20N in the ERA-Interim whereas in the CAM5 on a higher level at 22N. This is possibly because of the bias in large-scale circulation between the ERA-Interim and CAM5. Overall, CAM5 captures the thermo structure of the atmosphere over the West African to Mid Atlantic region, with a slightly underestimation on surface temperature.

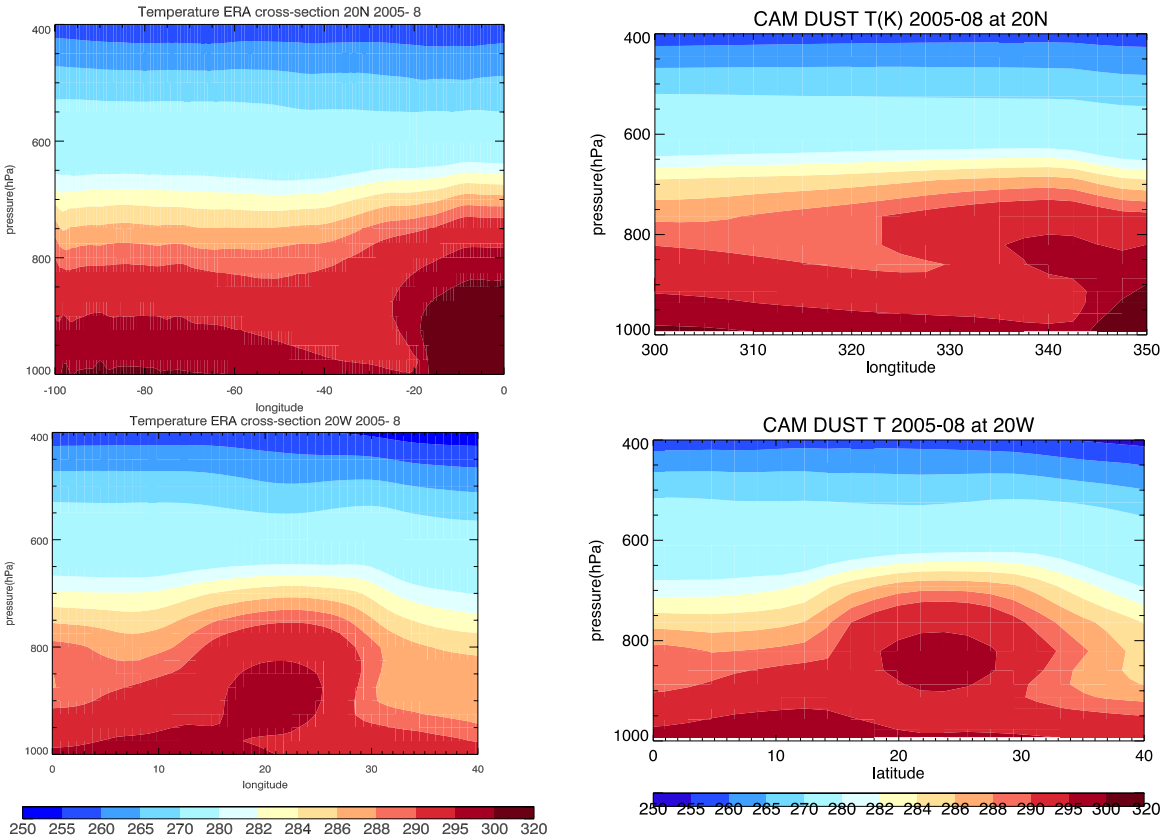

Figure 3.5: Temperature cross section along 20N (top) and 20W (bottom) between the ERA-Interim reanalysis (left) and CAM5 output (right) on August 2005

4. RESULTS

In this section, the model simulations on the dust and non-dust scenarios in August 2005(left) and August 2006(right) will be analyzed. Each column panel consists of three figures in which the top and middle ones are the average of five ensembles on the dust and non-dust scenarios respectively and the bottom figure shows the differences between two cases. The dotted region in the difference map represents the significant differences between two scenarios in a 95% confident level (two-tails t-test, details in the Statistical method section in Section 2).

4.1 DUST DISTRIBUTION

Dust optical depth (DOD) illustrates the extinction of solar beams in the column by dust particles, which represents the amount of dust loading in the atmosphere. CAM5 uses the MAM3 aerosol module, which divides aerosols into Aitkin, accumulation and coarse modes based on their size. The long-range transported dust is categorized into the accumulation (mode 1) and coarse (mode 3) modes. Figure 4.1 shows the average of the five dust ensembles on the DOD (top) and the dust mixing ratio at 821hPa (bottom). The high DOD region is located on the north of 15N where the Saharan Desert is located and further extends to the mid Atlantic Ocean. The maximum DOD can reach the maximum value of 1.0 over West Sahara, which is known as the “hot spot” that contains the favorable characteristics for dust emission. As mentioned in section 2.3.2, the surface soil texture in this region loosely coheres the dust to the surface. As long as the wind friction velocity exceeds the threshold wind friction velocity, the dust is blasted from the

surface and emitted into the atmosphere. During the African summer, dust is able to transport long distance from the African continent to the Atlantic Ocean under the dominant easterly wind. The long-range transported dust can reach as far as the West Atlantic or even the Caribbean region. The ITR has a higher dust loading compared to that of the GNR. The dust mixing ratio at 820hPa is well correlated with the high DOD region and reaches the maximum dust mixing ratio at 2.4*10^-4 g/kg over the African continent. The dust emission was turned off over the continents in the non-dust scenario, therefore the DOD and the dust mixing ratio are zero (not show here).

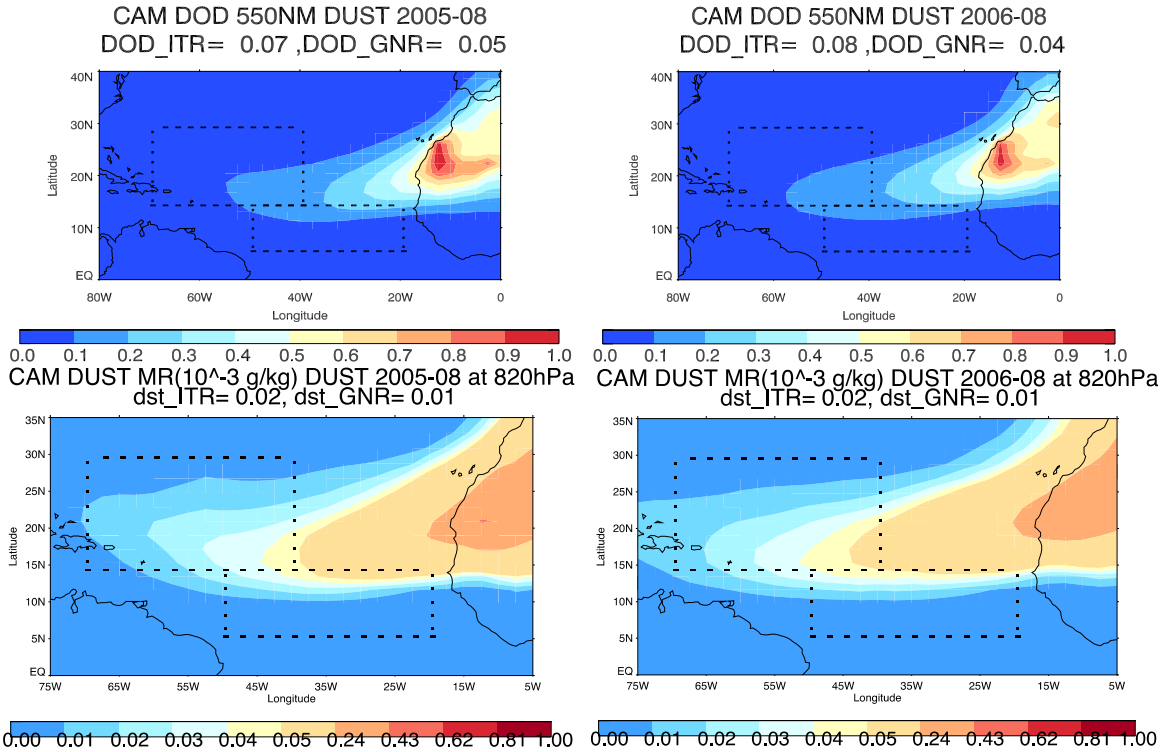

Figure 4.1: DOD (top) and dust mixing ratio (bottom) in August 2005 (left) and August 2006 (right)

The vertical dust distribution is represented by the dust mixing ratio at 10W (top) and 22N (bottom) in August of 2005 and 2006, shown in Figure 4.2. The maximum dust mixing ratio (1.35*10^-3 g/kg) is located at the surface of 30N (Figure 4.2a, b). The dust plume can transport vertically up to 600hPa and horizontally to 70W (Figure 4.2c, d). The dust mixing ratio can be as high as 1.45 * 10^-4 g/kg in 500hPa (c, d). The dust mixing ratio at the meridional cross section of 20W and 40W (figures not shown here) show that the maximum dust loading are 2*10^-4 g/kg and 7.5*10^-5 g/kg respectively at 700hPa. Moreover, the long-range transported dust concentration reaches the maximum at 700hPa.

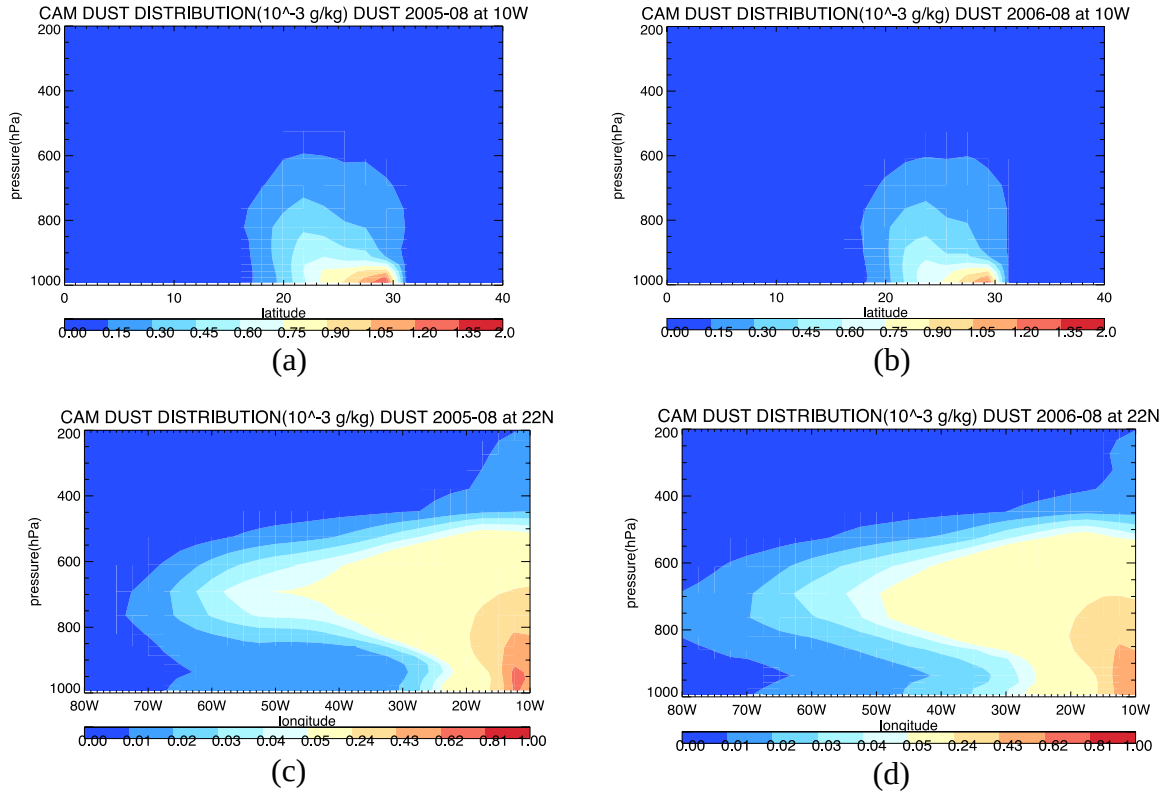

Figure 4.2: Meridional dust mixing ratio at 10W (top) and zonal dust mixing ratio at 22N (bottom) in August 2005 (left) and August 2006 (right)

The dust mixing ratio in the accumulation (as_1) and coarse (as_3) modes are compared respectively in Figure 4.3. Dust mixing ratio in the accumulation mode is an order of magnitude lower than that of the coarse mode. Dust in the accumulation mode, that contains smaller particles compared to the coarse mode, can transport long distance and reach 75W at 2*10^-6 g/kg (10% of maximum accumulation dust mixing ratio), whereas the coarse dust only transports to 50W with 4*10^-5 g/kg which is10% of the original dust mixing ratio in coarse mode. This is due to significant gravitational settling and wet removal of the large dust particles. Based on the assumption of internal mixing in each mode, the removal of dust particles in the non-dust scenario may cause significant changes on both size and mass distribution of aerosols.

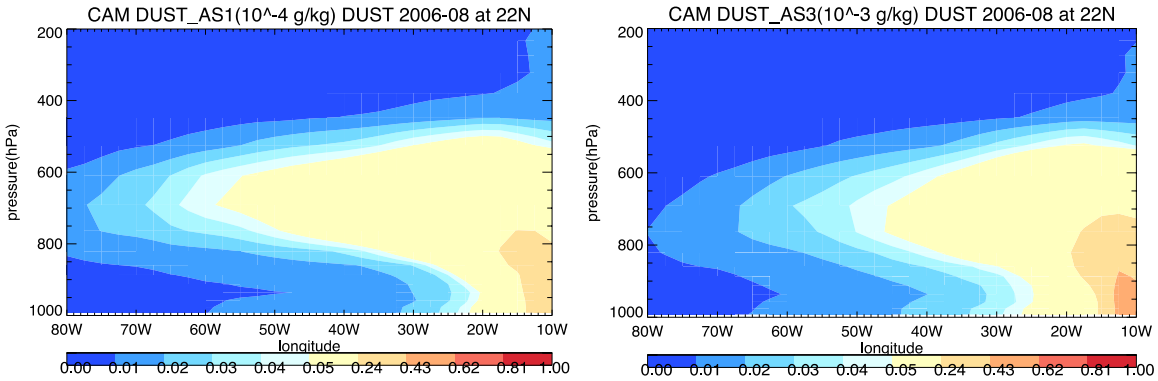

Figure 4.3: Dust mixing ratio (g/kg) at 22N in the accumulation mode (as1, left) and in the coarse mode (as3, right) in August 2006

Lau and Kim [2007a] conclude that the dust emission in 2006 is significantly higher than that of 2005. However, the model fails to capture the interannual variability of dust emission in 2005 and 2006, since the 10m wind speed, which is a dominant factor on the surface dust emission, in 2005 is higher than that of 2006 on the African Continent

(shown in Figure 4.4). Moreover, CAM5 tends to underestimate the interannual variability in a year-to-year base.

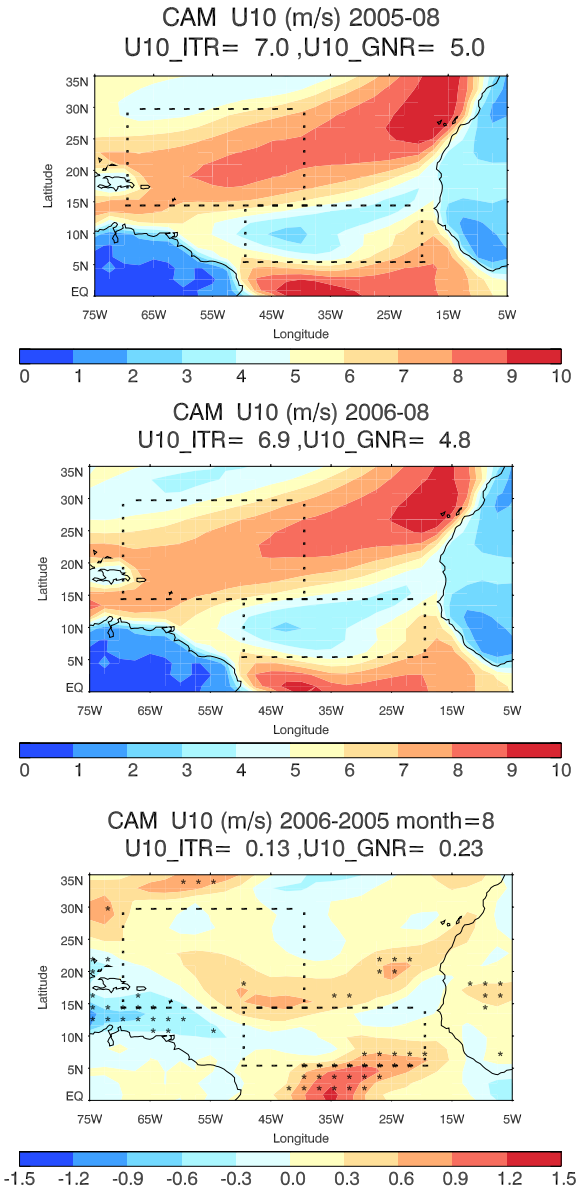

Figure 4.4: 10m wind speed (m/s) in August 2005 (top), 2006 (mid) and the difference between 2006 and 2005 (bottom)

4.2 TOTAL PRECIPITATION RATE

The total precipitation is composed of convective precipitation and large-scale precipitation. Convective precipitation is heavier compared to the large-scale precipitation in the tropical region. They will be analyzed respectively in the following section.

4.2.1 Convective precipitation rate

Figure 4.5 shows the convective precipitation (shaded) over-plotted with the 827hPa wind in August 2005 (left) and August 2006 (right). The ITCZ is located between 5N and 15N with the maximum precipitation rate at 18-22mm/day in August 2005 and 14-18mm/day in August 2006 along the West African coast. The heavy rain band extends westward across the North Atlantic Ocean with a decreasing trend to the west. Based on the difference map (bottom), the ITCZ shifts to the south in the non-dust scenario, resulting in a dipole structure near the African Continent. Compared to the dust scenario, non-dust scenario has more precipitation (1.6-2.4mm/day) in the downstream region near the South America continent.

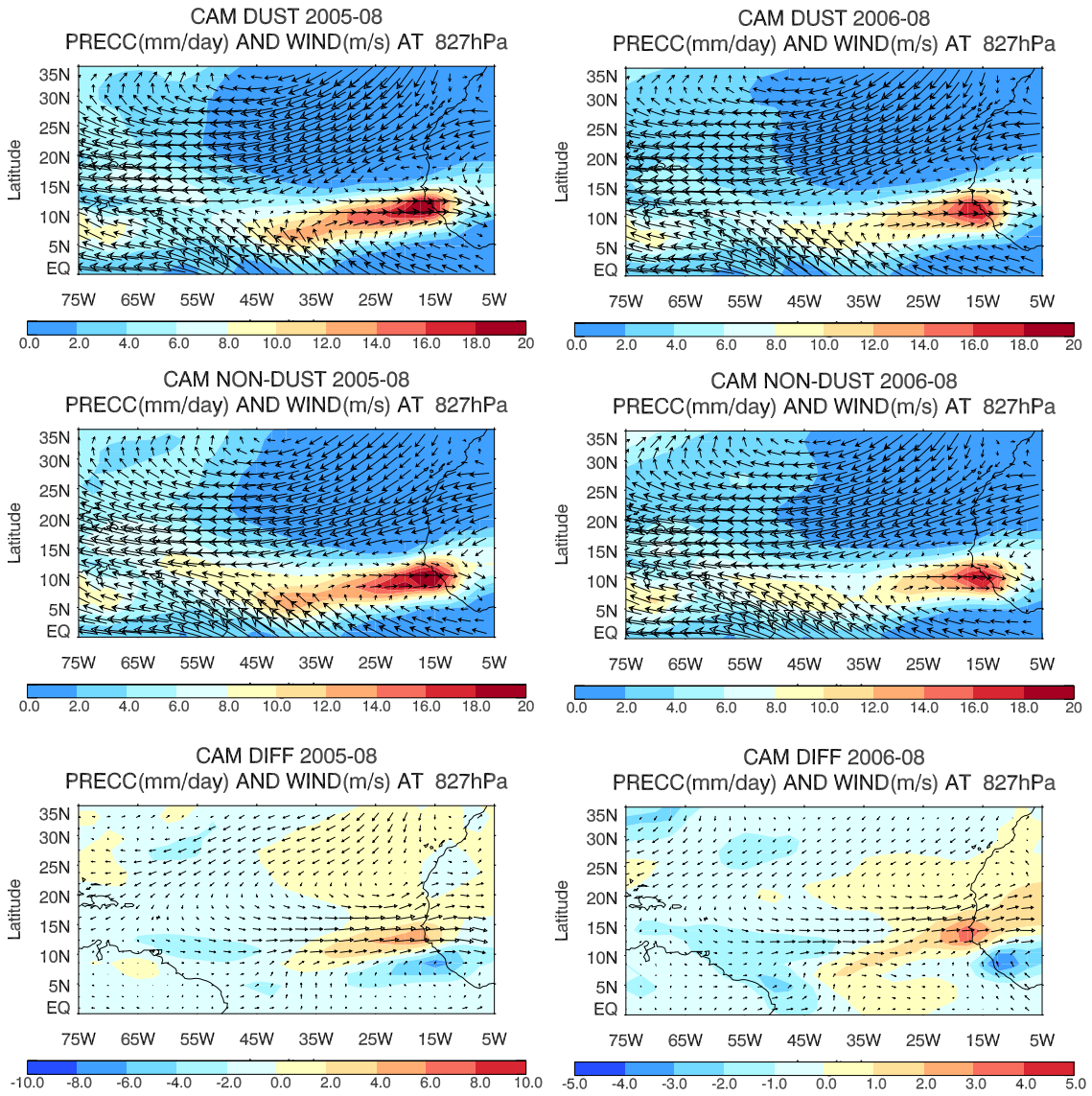

Figure 4.5: Convective precipitation rate (mm/day) and wind (m/s) at 827hPa in August 2005 (left) and August 2006 (right)

CAM5 follows the single moment cloud microphysics scheme for the simulation of convective clouds. Thus, dust indirect effect on clouds does not directly affect the convective precipitation rate. However, dust radiative effect can change the vertical temperature profile and the moisture distribution, thus changing the regional circulation.

Surface pressure at the same time period shows that dust enhances the low pressure over the Saharan desert (Saharan Heat Low). The enhancement of the Saharan Heat Low increases the pressure gradient between the African continent and the Atlantic Ocean, therefore increasing the moist advection and pushing the ITCZ northwards. Moreover, the 827hPa wind indicates the dominant westerly wind in the West African monsoon, which transports the moist air from the mid Atlantic to West Africa. The difference map shows that dust moves the westerly wind belt northward, which also enhances the moist supply to the ITCZ. Moreover, dust also strengthens the northwesterly wind along the West African coast, induces cyclonic anomaly on the north of 20N over the East Atlantic Ocean, which agrees with *Wong et al.* [2008] conclusion on the dust modifications on the upper level circulations. These modify the vertical circulation and precipitations rate in that region. The suppression of convective precipitation near the South America continent is possibly because of the decreasing westerly wind, which suppresses the moist supply to the precipitation zone near the South America continent. Above all, dust perturbs the regional circulation that shifts the ITCZ northward by enhancing the Saharan Heat Low and suppresses the convective precipitation rate near the South America continent.

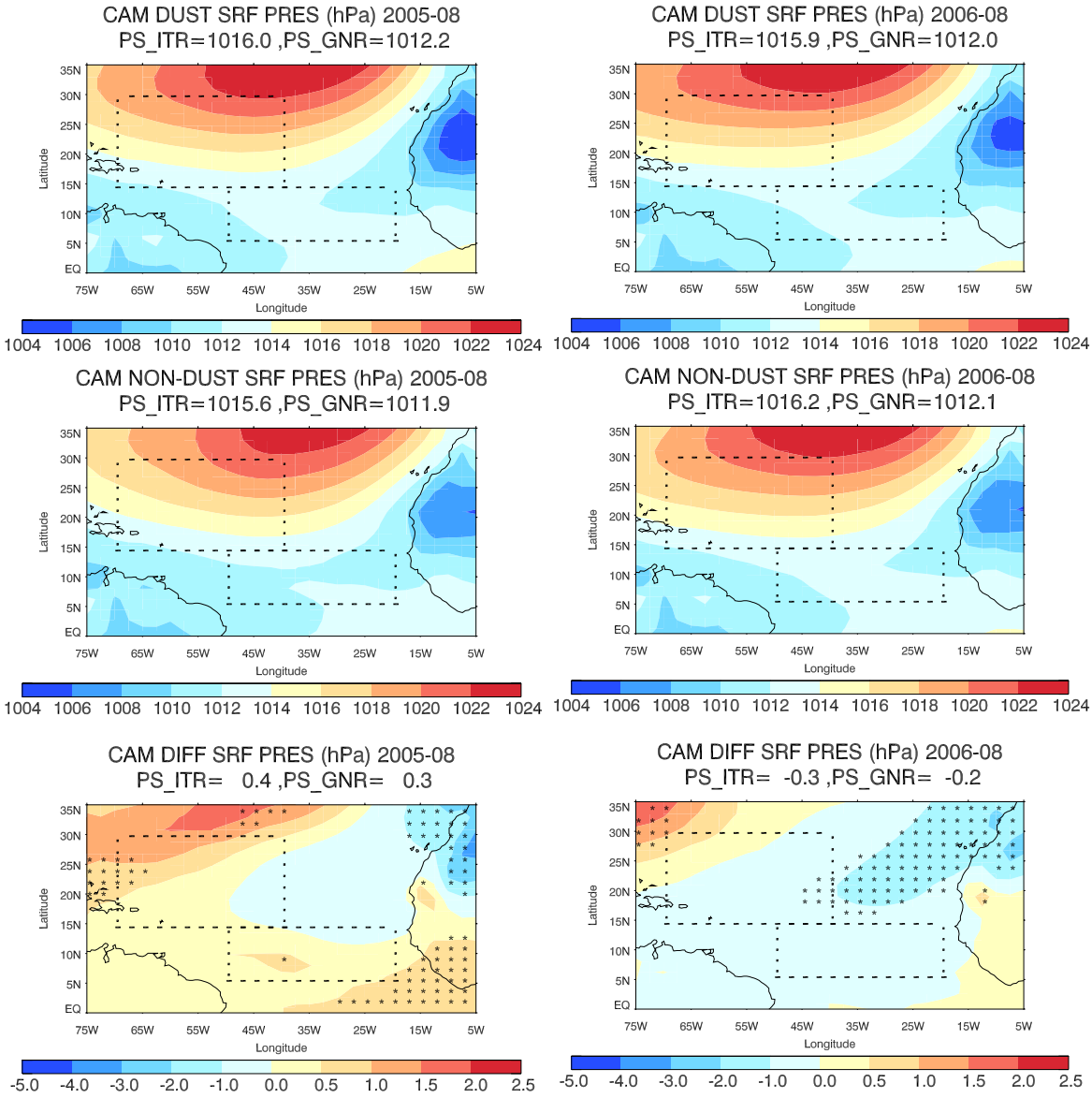

Figure 4.6: Surface pressure (hPa) in August 2005 (left) and August 2006 (right)

4.2.2 Large-scale precipitation rate

The large-scale precipitation includes both liquid and ice stratiform precipitation, which is shown in Figure 4.7. In both scenarios, the large-scale precipitation is highly concentrated on the West African with the maximum precipitation rate at 2.8mm/day at

10N on West African coast. According to the difference map, the non-dust large-scale precipitation rates are 0.8-1.0 mm/day (2005) and 0.6-0.8 mm/day (2006) less than that of the maximum large-scale precipitation in the dust scenario.

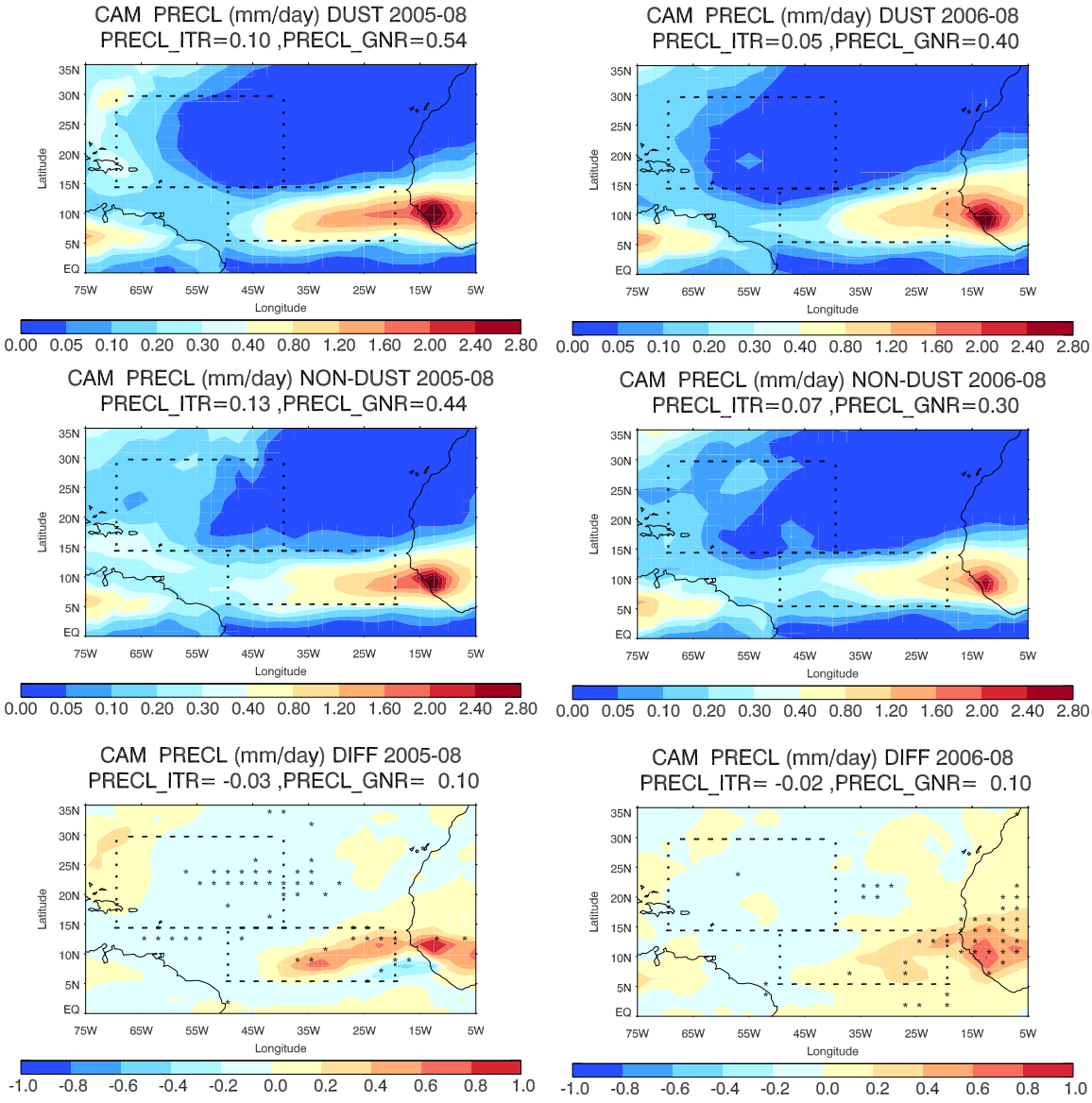

Figure 4.7: Large-scale precipitation (mm/day) in August 2005 (left) and 2006 (right)

CAM5 is able to simulate the aerosol indirect effect on the stratiform clouds using the two-moment bulk cloud microphysics scheme [*Morrison and Gettelman*, 2008]. The maximum large-scale precipitation belt overlaps with the southern edge of major dust emission region (Figure 4.1). Dust increases the CCN concentration in the liquid stratus clouds over the West African continent. Moreover, because of the increasing moist supply from the mid Atlantic Ocean, CCN has sufficient water content and are able to increases the effective radius of droplets at 827hPa for 3 microns at 10N compared to the non-dust scenario (Figure 4.8). The increasing of droplets effective radius and the CCN concentration potentially invigorates the collision and coalescence process, therefore increasing the large-scale precipitation rate between 10N and 15N in the dust scenario. Moreover, the large-scale precipitation is determined by the accretion rate of the water content, which is calculated by the sub-grid cloud water mixing ratio, rain mixing ratio, and cloud fraction. Increasing of the cloud droplet radius is likely to increase the cloud water mixing ratio, change the cloud fraction, therefore further increasing the large-scale precipitation rate.

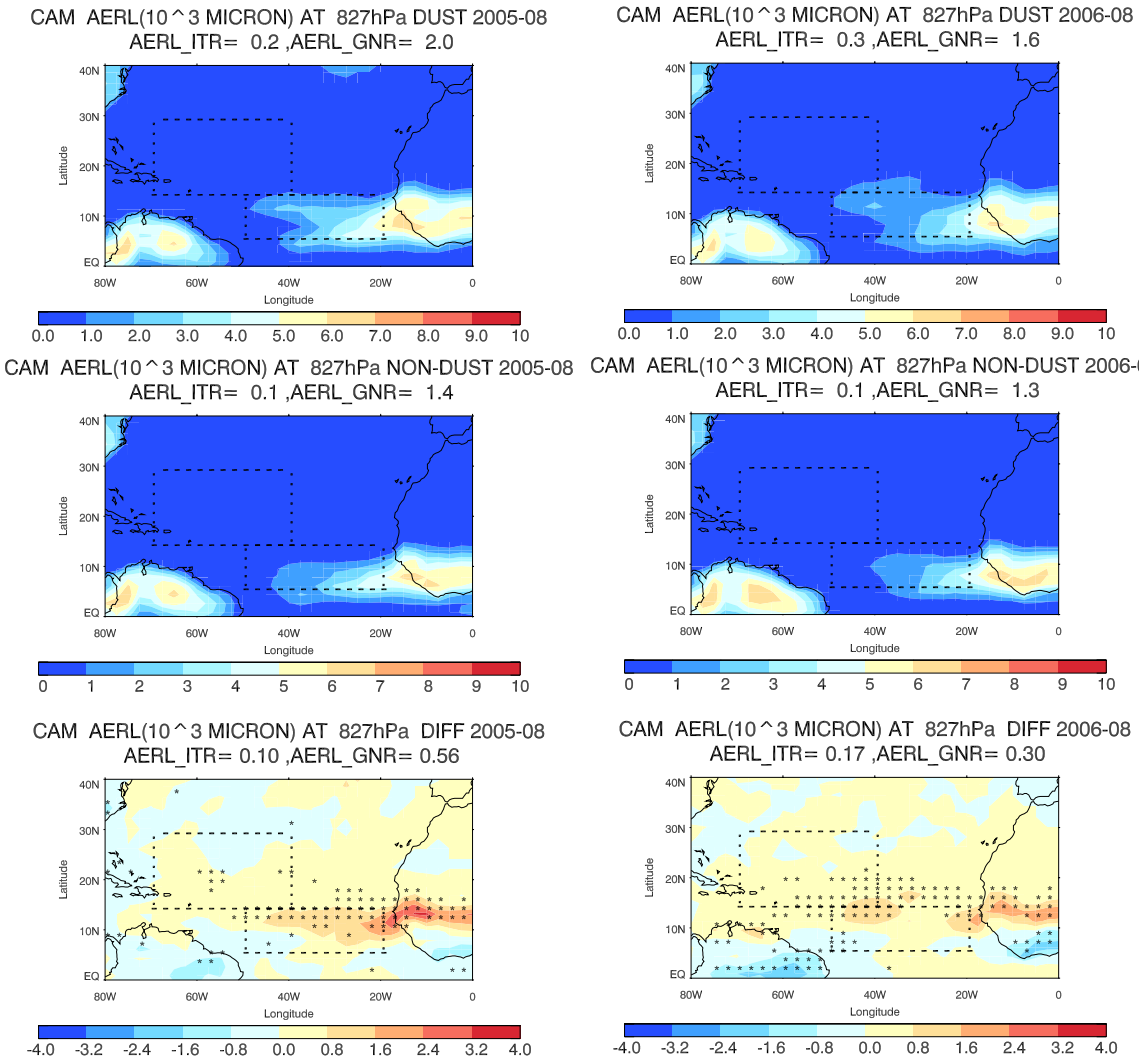

Figure 4.8: Average droplets effective radius (micron) at 827hPa in August 2005 (left) and August 2006 (right)

It is worth mentioning that the convective precipitation rate is an order of magnitude higher than that of large-scale precipitation rate in the tropical region. Therefore, the total precipitation rate (Figure 4.9) follows the convective precipitation trend and is mainly determined by the large-scale circulations. In conclusion, dust shifts the heavy precipitation band, i.e. ITCZ, northward by increasing the moist advection to West

African continent and enhancing the moist supply by increasing the mid-level westerly wind. Moreover, dust increases the large-scale precipitation rate by increasing the dust effective radius hence increasing the collision and coalesces processes. Dust decreases the precipitation rate in the downstream region by decreasing the moist supply from the ocean.

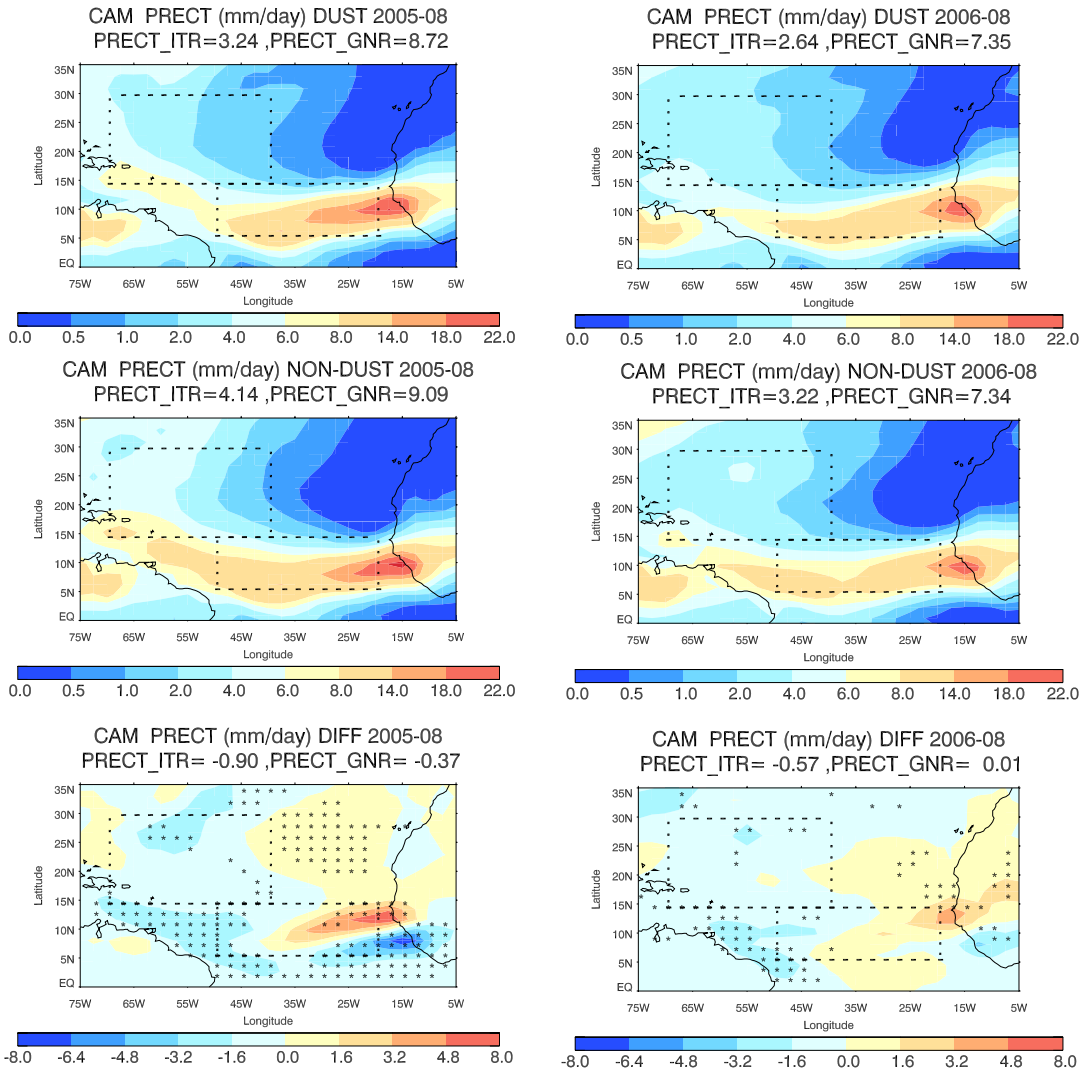

Figure 4.9: Total precipitation rate (mm/day) in August 2005 (left) and August 2006 (right)

4.2.3 Total precipitable water

The total precipitable water (TMQ, Figure 4.10) is defined as the total atmospheric water vapor in the column within a unit cross-area. Similar to the convective precipitation rate trend, the maximum TMQ (60kg/m^2) is located at 10N, which is correlated with the ITCZ. It is associated with air convergence and rising motion, which not only transports moisture into the convergence zone but also saturates the air parcel through the rising motion, therefore increasing the TMQ in the convergence zone. Moreover, dust increases the West African monsoon that contributes to the moisture supply to the West African continent, therefore increasing the maximum TMQ value near the West African coast in the dust scenario. The large-scale subsidence over the subtropical region (north of 25N on the East Atlantic) results in a relative low TMQ value region. The maximum TMQ region also moves along with the ITCZ to the north in the dust scenario.

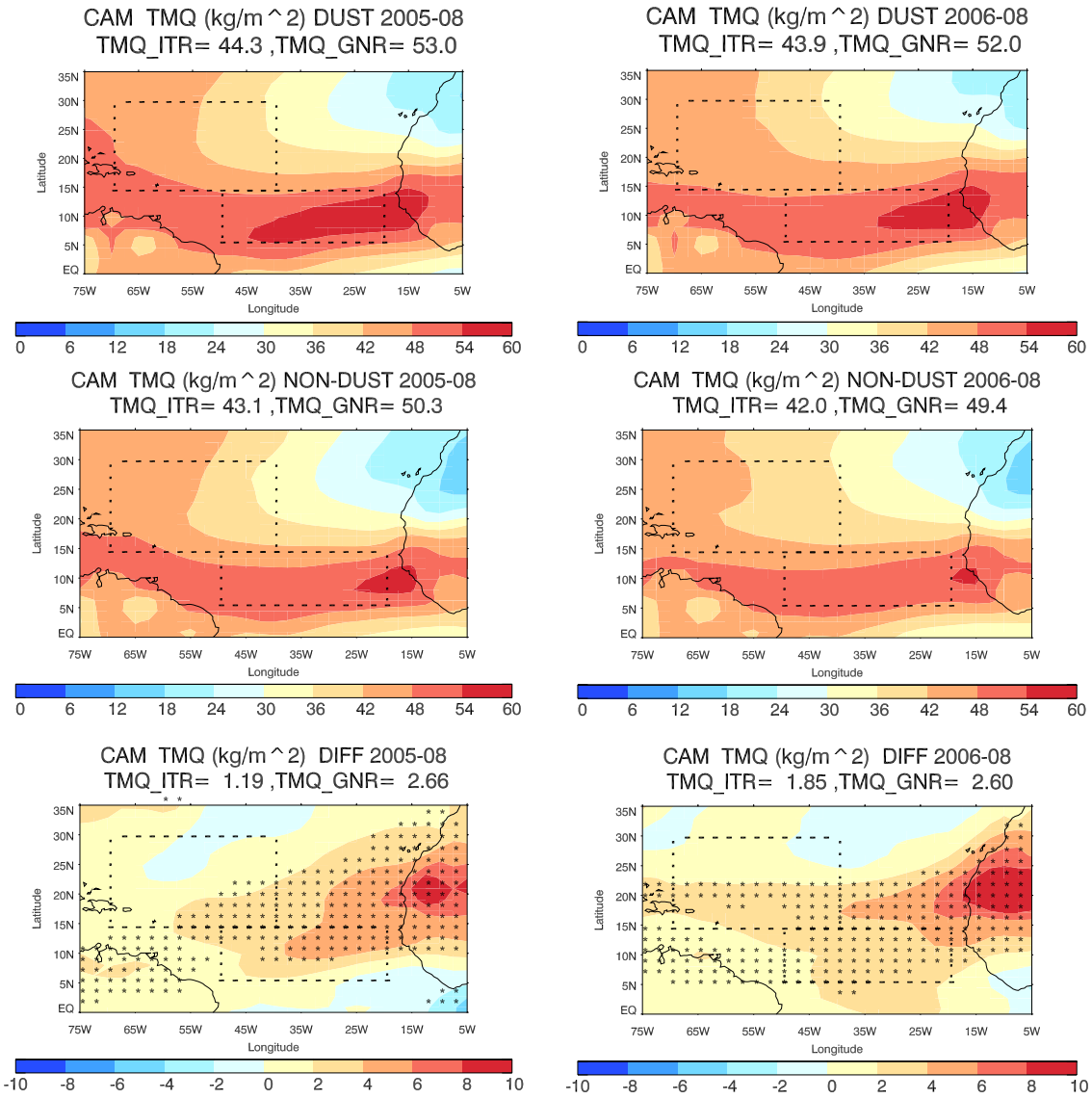

Figure 4.10: Total precipitable water (kg/m^2) in August 2005 (left) and August 2006 (right)

Figure 4.11 shows the specific humidity (Q) along 10W overplotted with the meridional (v) and vertical (w) wind. The maximum Q (0.016-0.018 g/kg) is collocated with the maximum TMQ between10N and 20N, which is associated with the low level convergence. The difference map in Figure 4.11 shows that dust enhances the surface

convergence near 20N that lifts and saturates the air parcel, hence increasing the moisture content in such region. Moreover, there is significant enhancement of the low level westerly wind in 20N (figures not shown here) that potentially transport the maritime moist air to the African continent, thus increasing the TMQ along 20N.

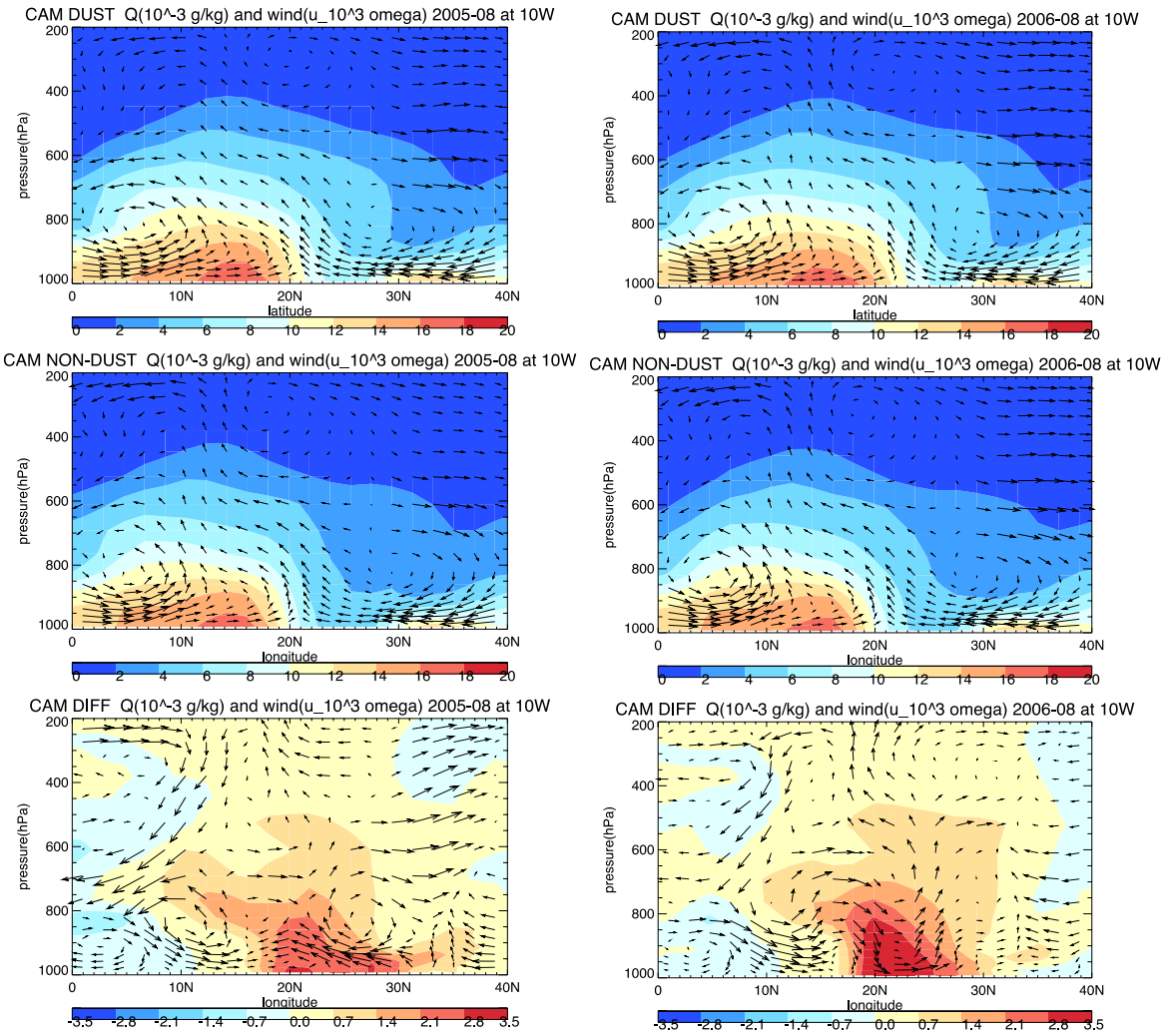

Figure 4.11: Specific humidity cross section at 10W overplotted with wind (v-10^3 omega) in August 2005 (left) and August 2006 (right)

Above all, dust shifts the ITCZ northward, which redistributes the atmospheric water content. Moreover, dust perturbs the local circulation that enhances the low-level convergence and westerly wind near 20N, hence increasing the TMQ in such region. This is mostly due to the dust-induced local circulation anomaly that perturbs the TMQ distribution.

4.3 DUST IMPACTS ON CLOUDS

Cloud has broad impacts on the climate system by perturbations of the hydrological cycle and radiative budget. Low clouds cool the earth-atmosphere system by reflecting incoming shortwave radiation, whereas high clouds warm the atmosphere by trapping the longwave emission from the surface. However, cloud simulation remains to be the largest uncertainty in the global climate model, because of the various scales and complexities on the cloud macrophysics and microphysics processes. To increase the efficiency of the model calculation and to best represent the cloud, CAM5 divides all clouds into four categories: shallow and deep cumulus, ice and liquid stratus. The deep convective clouds, liquid and ice stratus dominates the ITCZ. The shallow cumulus cloud covers most of the ocean, and the liquid stratus cloud covers the West African coast. The model defines the high, med and low clouds according to the International Satellite Cloud Climatology Project (ISCCP, details in section 2.3.3). Dust can change both the cloud fraction and cloud properties through changing the vertical heat and moisture distributions. Dust impacts on the different cloud levels will be explained in the following section.

4.3.1 Low cloud fraction

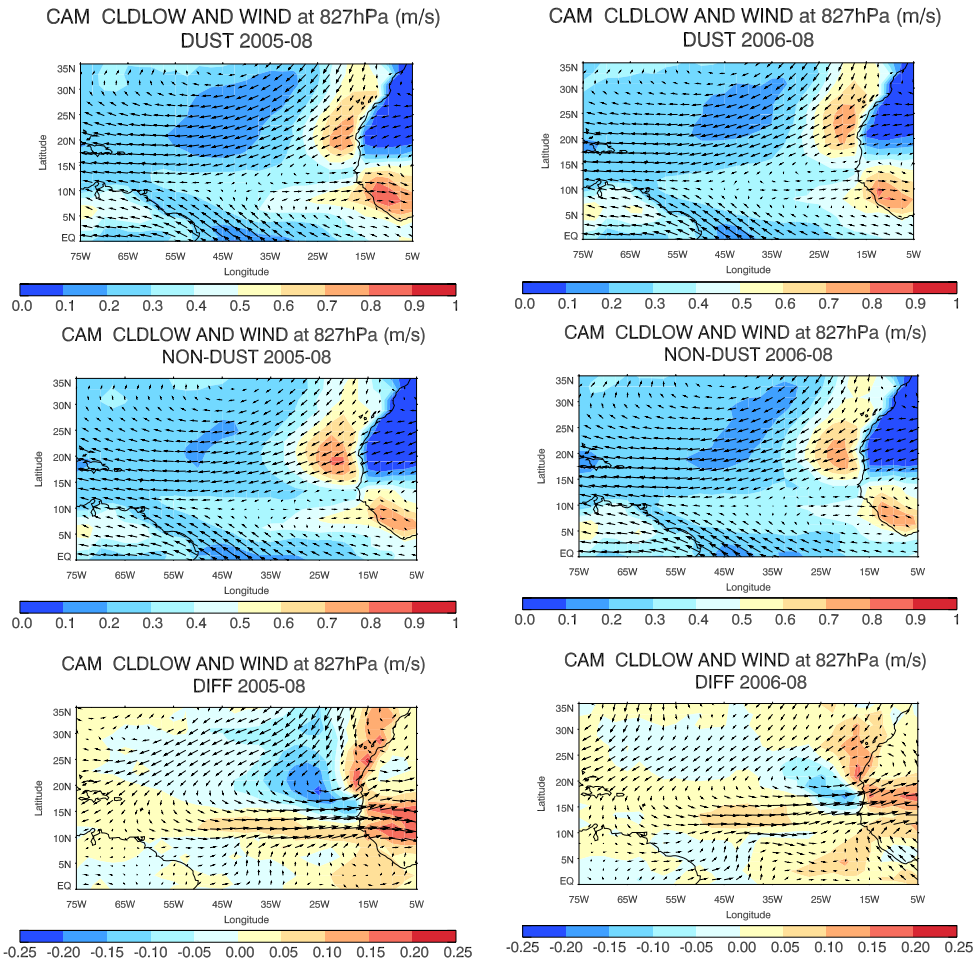

Figure 4.12: Low cloud fraction overplotted with 827hPa wind in August 2005 (left) and August 2006 (right)

Low clouds include cumulus, stratus and stratocumulus clouds, which corresponds to shallow cumulus over the ocean and liquid stratus near West African. The minimum low cloud fraction is on the north of 20N over the Saharan Desert (Figure 4.12), because of the large-scale subsidence and the dry atmospheric condition. The maximum low cloud fraction (greater than 0.7) region is located on the north of the 15N along the West

African Coast, which is dominated with maritime stratus clouds. The other maximum low cloud coverage region (greater than 0.8) is at 10N near West African, corresponding to the stratus deck over the West Africa and the low level clouds associated with the ITCZ.

The low cloud fraction is affected by the large-scale circulation and the moisture distribution. Over the East Atlantic Ocean, the low clouds are under the influence of northeasterly-dominated wind in the dust case, whereas it is under the ENE wind in the non-dust scenario. These result in the westerly and northwesterly anomalies on the wind field that pushes the low clouds toward the West African coast in the dust scenario. Moreover, dust enhances the Saharan heat low (Figure 4.6) that increases the onshore wind, which increases the low cloud fraction near the African coast and decreases the low cloud coverage in the mid Atlantic Ocean (difference map in Figure 4.12). For the region over the West African continent at 10N, the increasing of the low cloud fraction is due to the increasing of westerly wind, which transports the moist air into the West African continent.

4.3.2 Middle cloud fraction

The middle clouds include the altostratus, nimbostratus, and altocumulus that are located from 2km to 7km, which possibly intervene with the heavy dust-loaded layer on the north of 15N. Figure 4.13 shows the middle cloud fraction in August 2005 (left) and August 2006 (right). The maximum cloud cover (greater than 0.5) region is along the 10N and crosses the Atlantic Ocean, which is correlated with the ITCZ. Comparing to

the non-dust scenario, dust scenario has a significantly higher mid cloud fraction on the east of 50W at 10N, but a lower mid cloud fraction near South America.

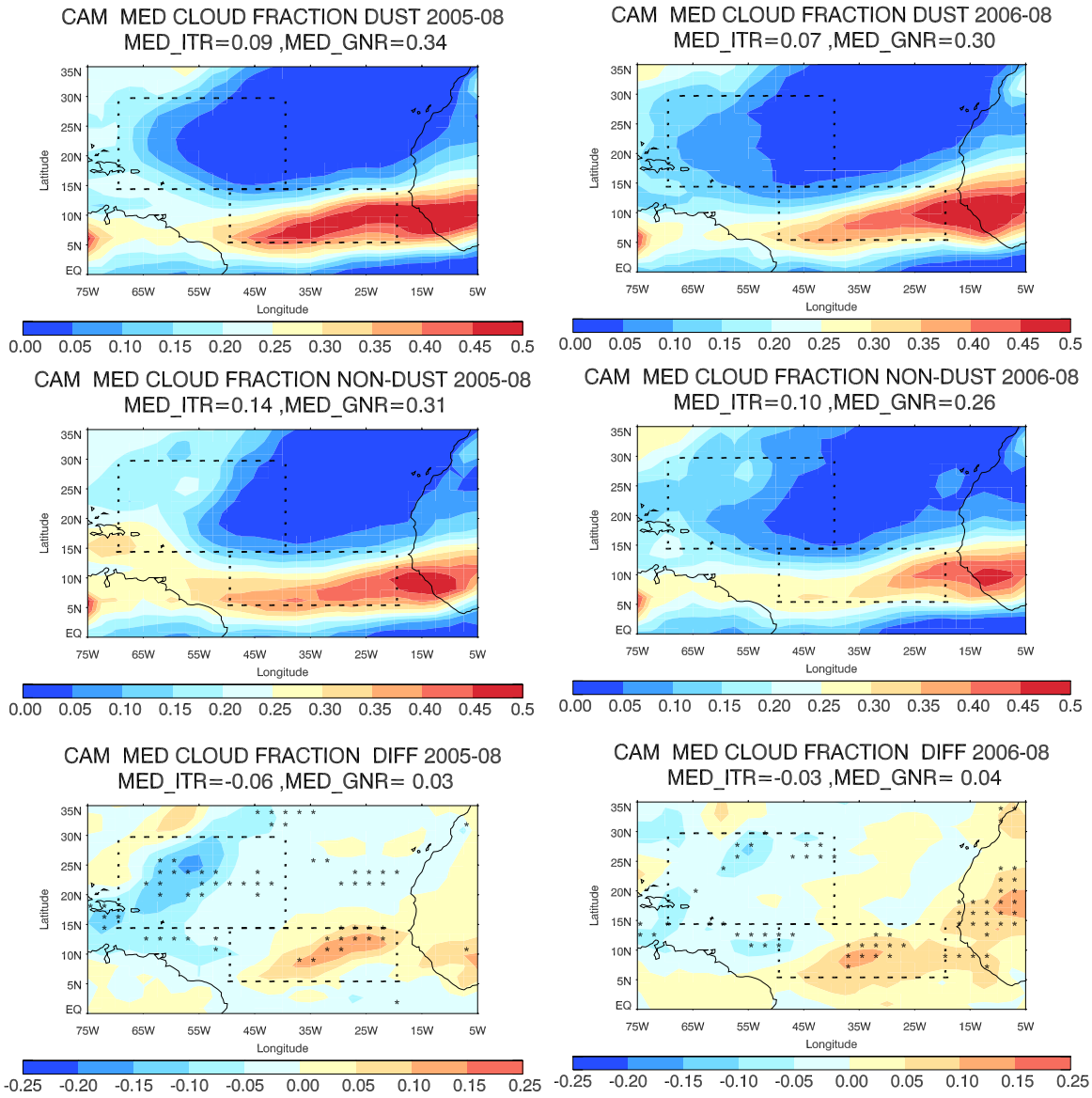

Figure 4.13: Middle cloud fraction in August 2005 (left) and August 2006 (right)

The dust direct effect slightly increases the temperature above the dust-loading layer over 800hPa (Figure 4.13) where most of the middle clouds are located. This potentially increases the saturation vapor pressure, hence decreasing the relative humidity near the heavy dust-loaded region on the north of 15N (figure not shown here). Moreover, the large-scale subsidence at this region also suppresses the formation of middle clouds. This corresponds to the minimum middle cloud fraction over the East Atlantic Ocean on the north of 15N. The middle cloud fraction is correlated with the ascending motion at 522hPa, as shown in Figure 4.14. Based on the difference map (Figure 4.14 bottom), there are significant increases of the vertical velocity north of 10N that corresponds to the increase of middle level cloud fraction. The vertical velocity anomaly is possibly caused by the northward shift of the ITCZ.

In conclusion, dust perturbs the middle cloud fraction by increasing the mid-level atmospheric temperature on the north of 15N and increasing the vertical velocity along 10N.

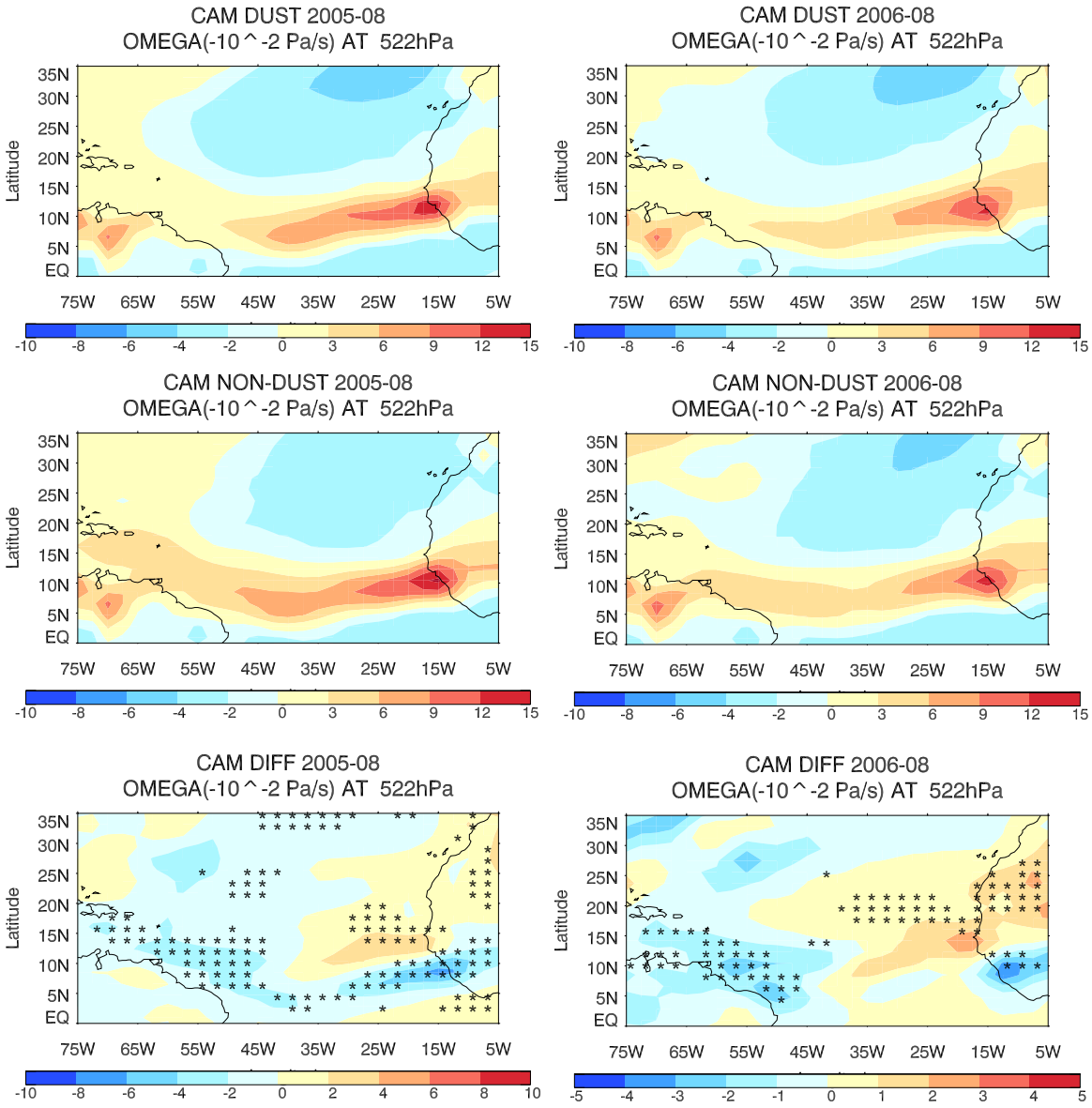

Figure 4.14: Omega (-10^-2 Pa/s) at 522hPa in August 2005 (left) and August 2006 (right)

4.3.3 High cloud fraction

Cirrus, cirrostratus, and deep convective clouds are categorized as high cloud. The maximum high cloud fraction (greater than 0.9) is along 10N, which corresponds to the deep convective clouds and maximum convective precipitation region (Figure 4.5). In

Figure 4.15, the high cloud band further extends westward to South America with a decreasing trend. With the existence of dust, the high cloud has an expanded coverage along 10N, which results in the increase of high cloud coverage on 20N and decrease on 10N in the difference map. Moreover, the maximum high cloud coverage is 0.2-0.3 higher in the non-dust scenario than that of the dust scenario at [20W, 10N].

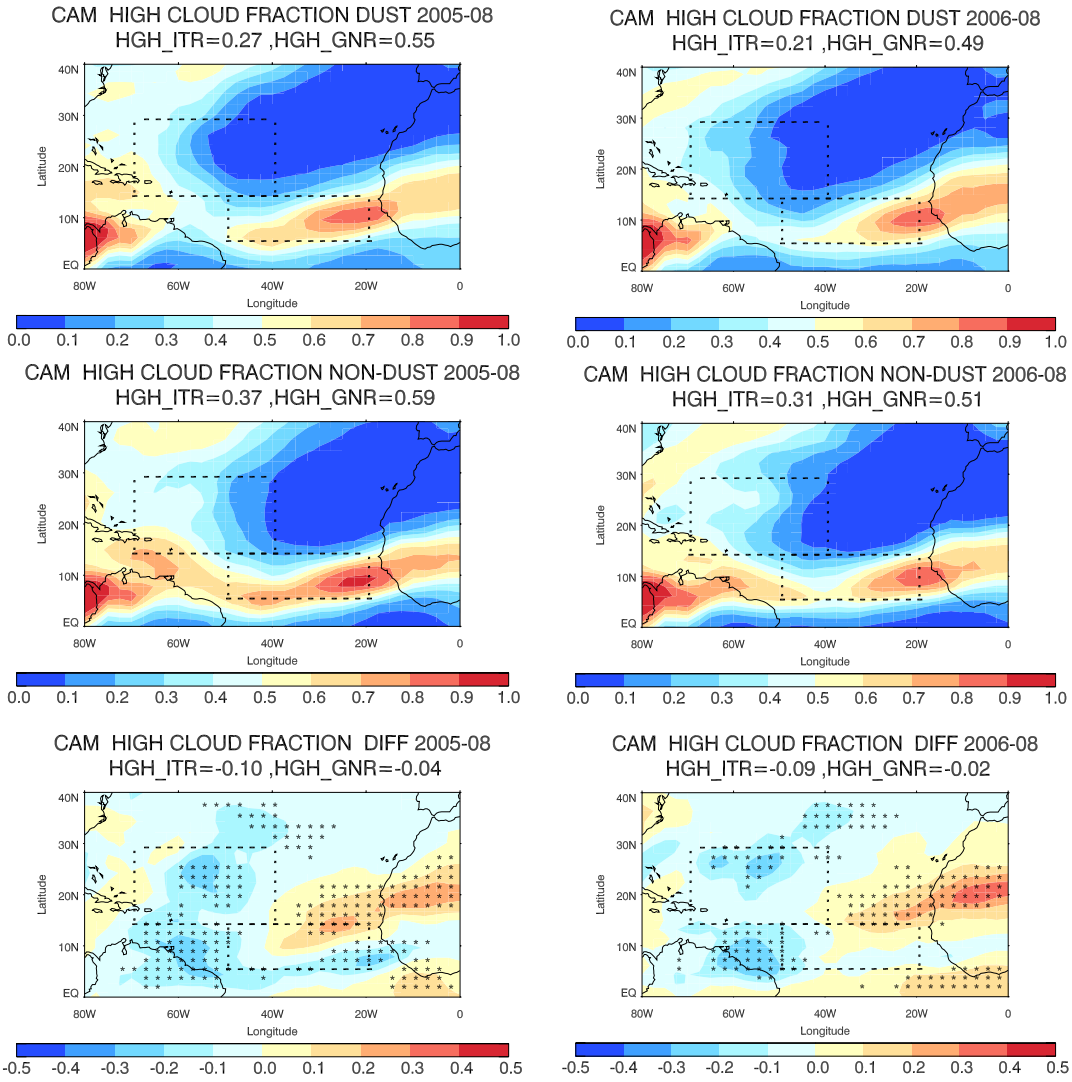

Figure 4.15: High cloud fractions in August 2005 (left) and August 2006 (right)

CAM5 is not able to simulate the aerosol indirect effect on the deep convective clouds. Therefore, the major factors that determine the deep convective cloud coverage are the large-scale circulation and the moisture distribution. There is an increase and expansion of the specific humidity at 315hPa in the dust scenario at the maximum convective region (figures not shown here). On the other hand, the maximum upper level divergence at 200hPa is along 10N, which is associated with the ITCZ and the maximum vertical velocity (Figure 4.16). The increase of the upper level divergence in the non-dust scenario results in the increase of high cloud fraction. The convergence region over the East to Mid Atlantic Ocean on the north of 15N represents the large-scale subsidence that is associated with the subsidence branch of the Hadley Cell and the direct circulation of the AEJ. Dust enhances the temperature contrast between the African continent and ocean, therefore moving the AEJ northward and enhancing the upper level divergence on the north of 10N, which results in a positive anomaly in the difference map.

Overall, dust perturbs both the moist distribution and the large-scale circulation, in which the large-scale circulation is the determinant factor on the high cloud coverage. It shifts the high cloud northward and broadens the high cloud cover in the deep convective clouds along 10N.

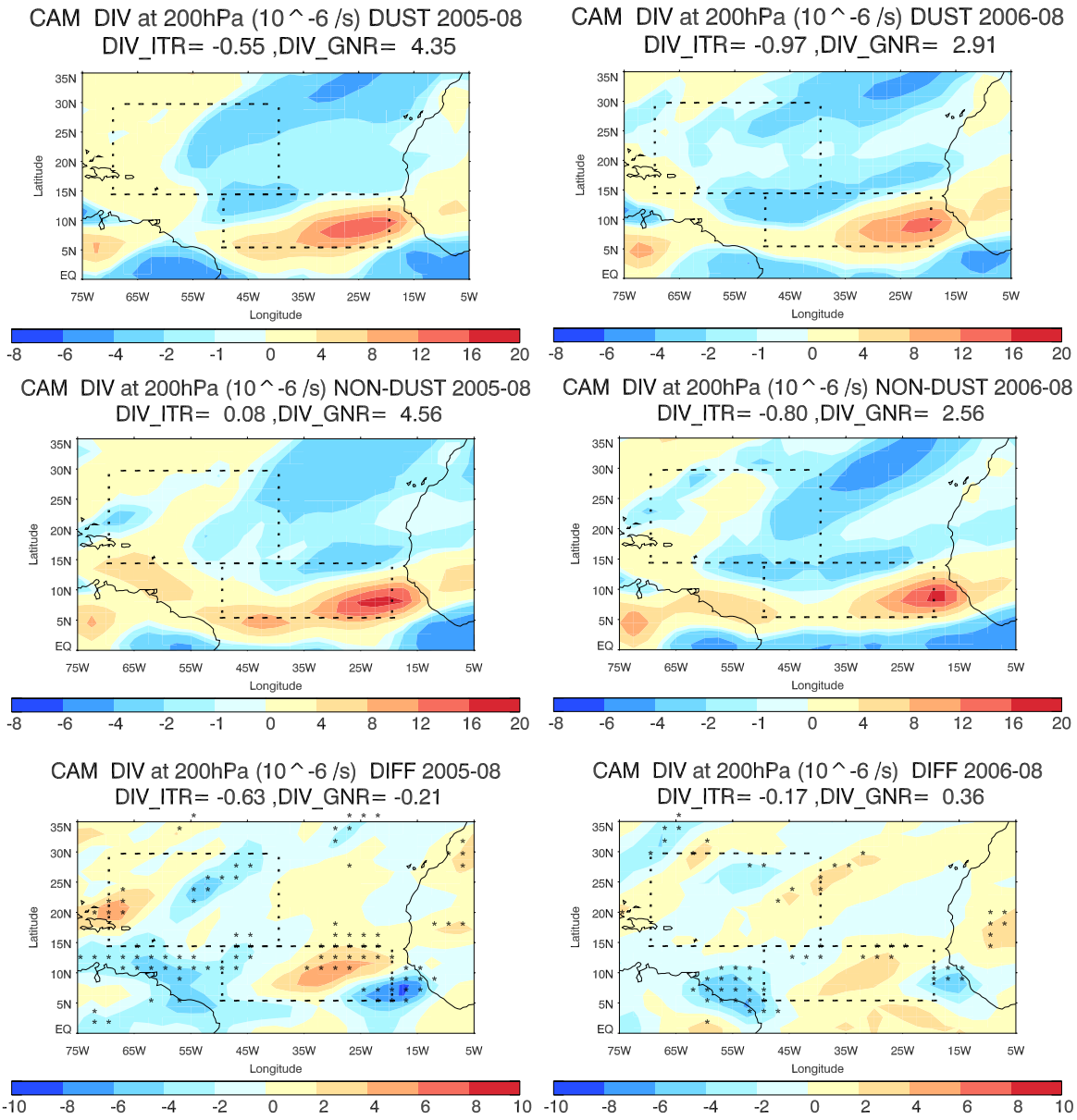

Figure 4.16: Upper level divergence at 200hPa in August 2005 (left) and August 2006 (right)

4.4 DUST IMPACTS ON RADIATION

Dust absorbs and reflects the shortwave radiation (direct effect) and perturbs the longwave radiation by trapping the longwave emission from surface and atmosphere,

and changing the atmospheric water vapor distribution, cloud fraction and temperature profiles, therefore perturbing the radiation budget. The dust impacts on the radiative budget are analyzed in the following section.

4.4.1 Net surface radiative flux

The net surface radiative flux (SRFRAD) in Figure 4.17 shows the subtraction between the incoming solar radiation (incoming energy) and the longwave radiation (outgoing energy) at the surface. The maximum surface radiative flux are at 700W/m^2 for both cases in the mid Atlantic Ocean at the ITR, where there is less cloud coverage, less dust intervention, and low reflectivity. The minimum surface fluxes are 475W/m^2 and 500W/m^2 at 10N on the African continent in dust and non-dust scenarios respectively. Another low surface radiative flux region, 550W/m^2 for dust scenario and 575W/m^2 for non-dust scenario, is along the West African coast on the north of 15N. The minimum net radiative flux regions are correlated with the low cloud fraction regions (Figure 4.12).

The shortwave radiation, that is four times higher than that of the longwave radiation, plays a vital role in determinations of the net surface radiative flux. Low clouds reflect the solar radiation and decrease the surface net flux. Thus, the maximum low cloud coverage (Figure 4.12) is correlated with the minimum surface radiative flux. Dust enhances the onshore flow and pushes the low cloud fraction toward the West African continent, therefore reducing the surface radiative flux (bottom) for up to 60W/m^2. Moreover, the increasing of the moist supply increases the low cloud cover at

10N on West African. Above all, dust perturbs the surface net radiative flux at the GNR for 8W/m^2, which is sensitive to changes of the low cloud cover.

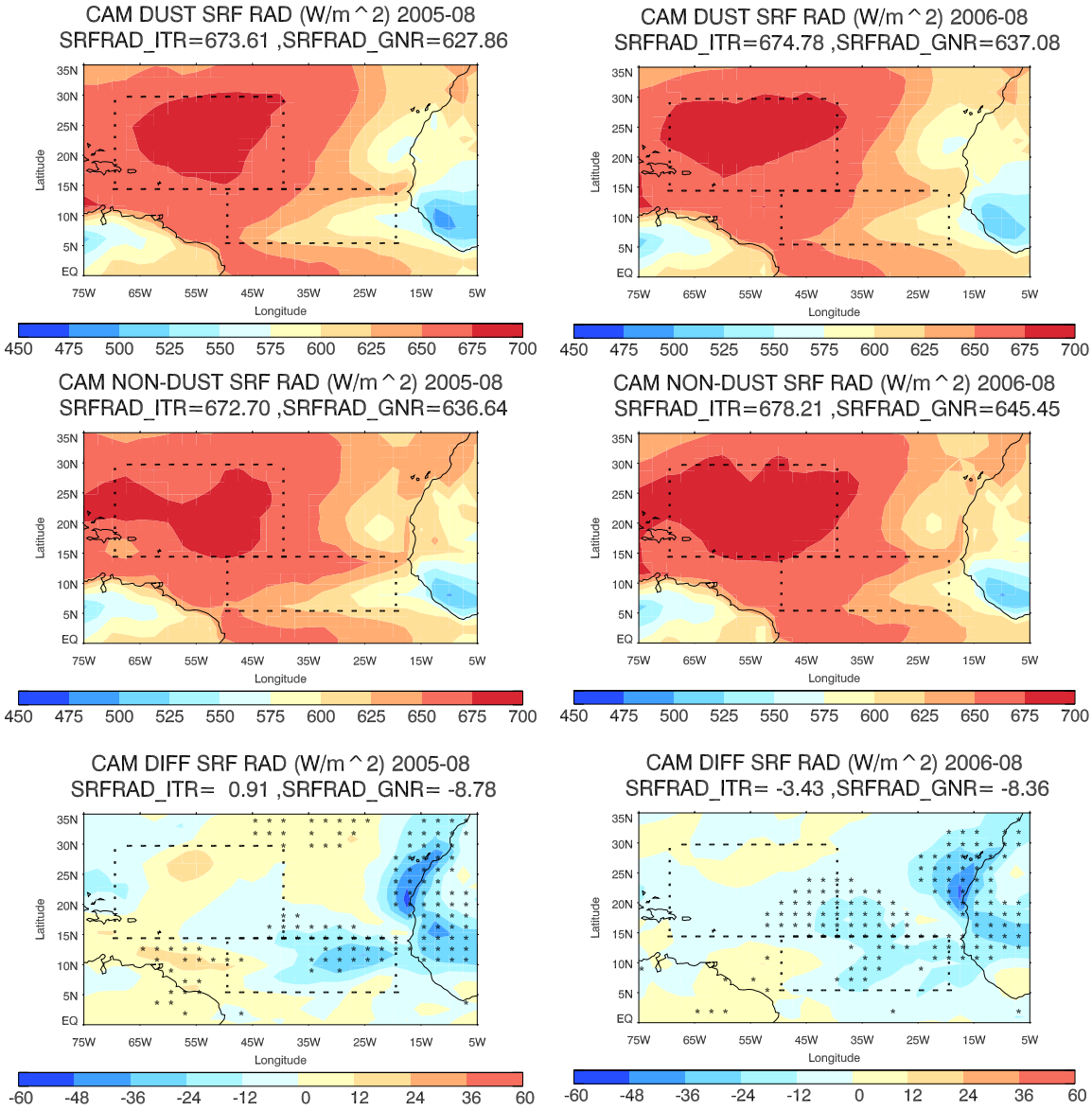

Figure 4.17: Net surface radiative flux in August 2005 (left) and 2006 (right)

4.4.2 Clear sky net solar flux on TOA

Figure 4.18 shows the net solar flux (downward minus upward solar radiation) at top of the atmosphere (TOA) under clear sky condition. This condition allows us to solely focus on the dust direct effect on the radiative budget. The lowest solar flux at TOA is 280W/m^2 for both dust and non-dust scenarios on the West African continent. The maximum value (395-400W/m^2) is located over the Western Atlantic Ocean near the Caribbean Sea. From the difference map, the removal of dust decreases the net solar flux at TOA, i.e. increases the upward radiation, for 25W/m^2 over the African continent. On the other hand, the dust removal increases the net solar flux, i.e. decreases the upward radiation, over the Atlantic Ocean for 15W/m^2, therefore warms the regional climate by trapping more solar radiation in the atmosphere. Moreover, the net solar flux at TOA over the ocean is greater than that of the continental area due to the low albedo over the ocean.

Dust both absorbs and reflects the solar radiation, but the dominant factor varies from different surface conditions. Dust is more reflective over the low albedo region, such as the ocean, but more absorptive over the high albedo region, such as the Saharan desert. Therefore, the removal of dust has difference effects over the continent and the ocean. Dust decreases the shortwave radiation for 3.5W/m^2 at the ITR and 1W/m^2 at the GNR.

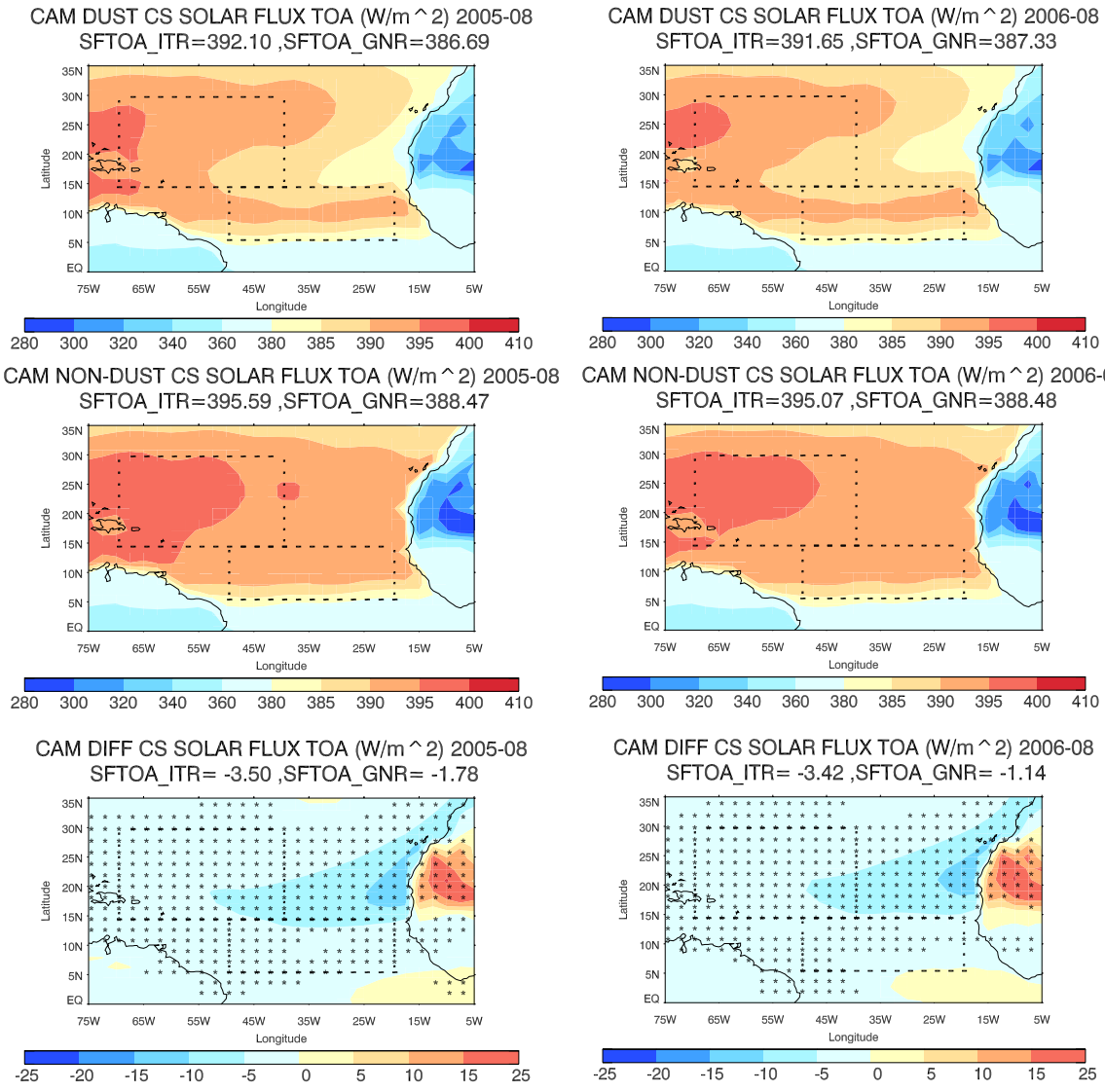

Figure 4.18: Clear sky solar radiative flux at TOA in August 2005 (left) and August 2006 (right)

4.4.3 Longwave cloud forcing

The cloud forcing (Figure 4.19) is defined as the difference between all sky and clear sky conditions of the net downward radiation [*Park, et al.*, 2014]. The positive (negative) cloud forcing indicates the warming (cooling) of the atmosphere below the cloud as well as the surface. The maximum longwave cloud forcing is 80W/m^2 in the

dust scenario and 70W/m^2 in the non-dust scenario at 10N near the West African coast. The longwave cloud forcing has a decreasing trend westward along 10N to the South America continent.

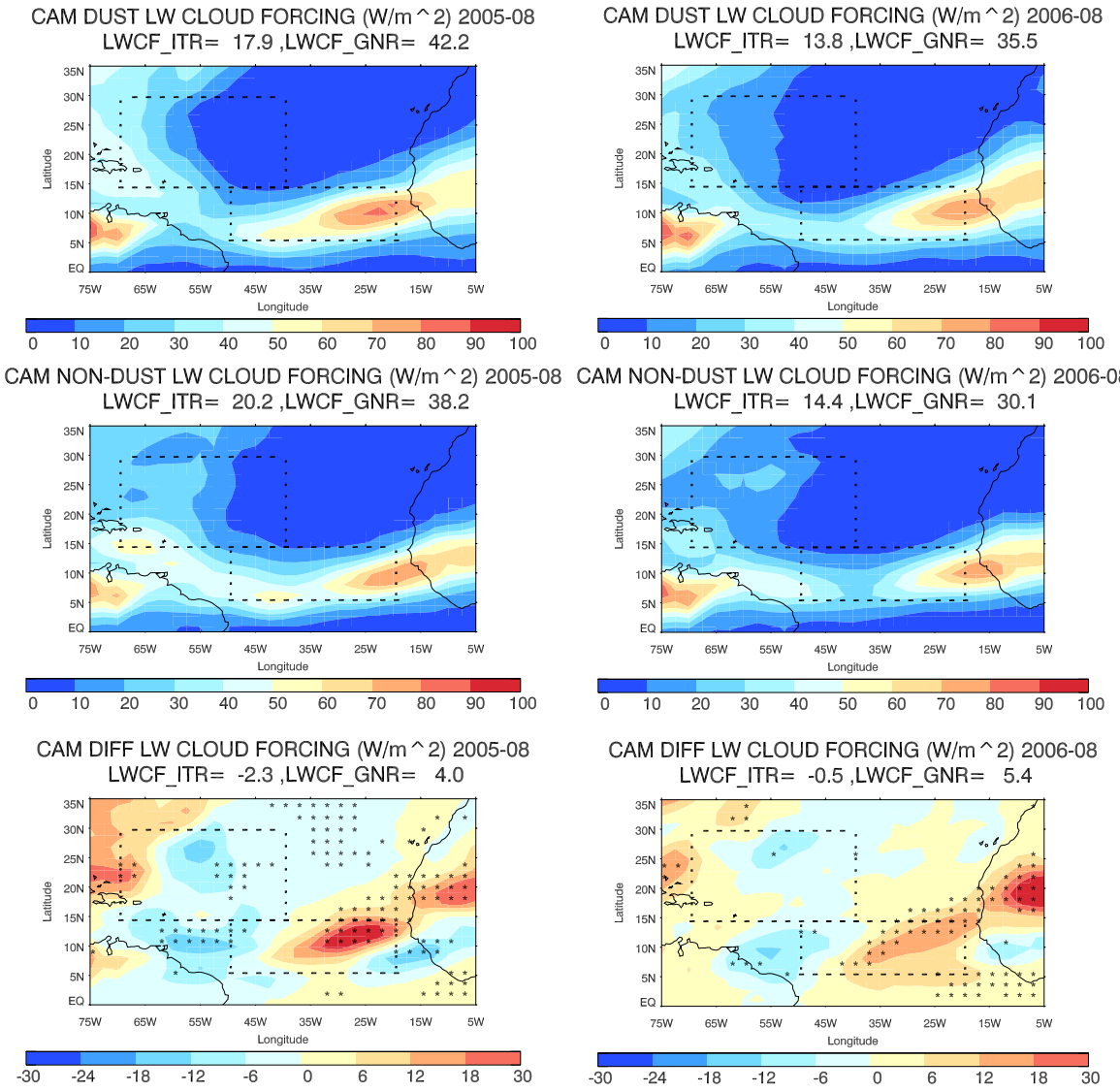

Figure 4.19: Longwave cloud forcing in August 2005 (left) and August 2006 (right)

The longwave cloud forcing follows the similar trend as the high cloud fraction, since the high cloud traps the longwave emission from the lower atmosphere. The dipole shape of the cloud forcing indicates a northward shift of the longwave radiation band, which is correlated with the northward shift of high cloud in the dust scenario (Figure 4.15). The difference map (bottom) shows an increase of 30W/m^2 on the north of 10N and a decrease of 18W/m^2 on the south of 10N. In conclusion, dust changes the longwave radiation by perturbing the high cloud cover. Dust increases the longwave cloud forcing in the GNR for 5W/m^2 and decreases the cloud forcing in the ITR.

4.4.4 Net longwave radiation at the surface

Figure 4.20 shows the net longwave radiation at the surface that is the difference between the upward and downward longwave radiations (upward-downward longwave), which shows the dust impacts on cloud and moist distribution. The maximum longwave radiative flux is 150W/m^2 over the Saharan desert. The minimum longwave radiative flux is 15W/m^2 at 10N over the West African continent and on the north of 15N along the West African coast. The minimum longwave radiative trend is similar to the distribution of low cloud, since the low cloud increases the downward longwave radiation, therefore decreasing the net longwave radiation at the surface. Moreover, dust heats the atmosphere in the heavy dust loading region, which is located on the north of 15N from West Africa to the mid Atlantic, hence increasing the downward longwave radiation in the heavy dust loading region. This decreases the surface net longwave radiation over the Saharan region for as large as 50W/m^2.

In conclusion, dust changes the surface longwave radiation through the modification of the low cloud fraction. It also increases the temperature in the heavy dust-loading region, thus decreasing the net longwave radiation. Dust decreases the net longwave radiation in the ITR for 2W/m^2 and decreases for 3W/m^2 in the GNR.

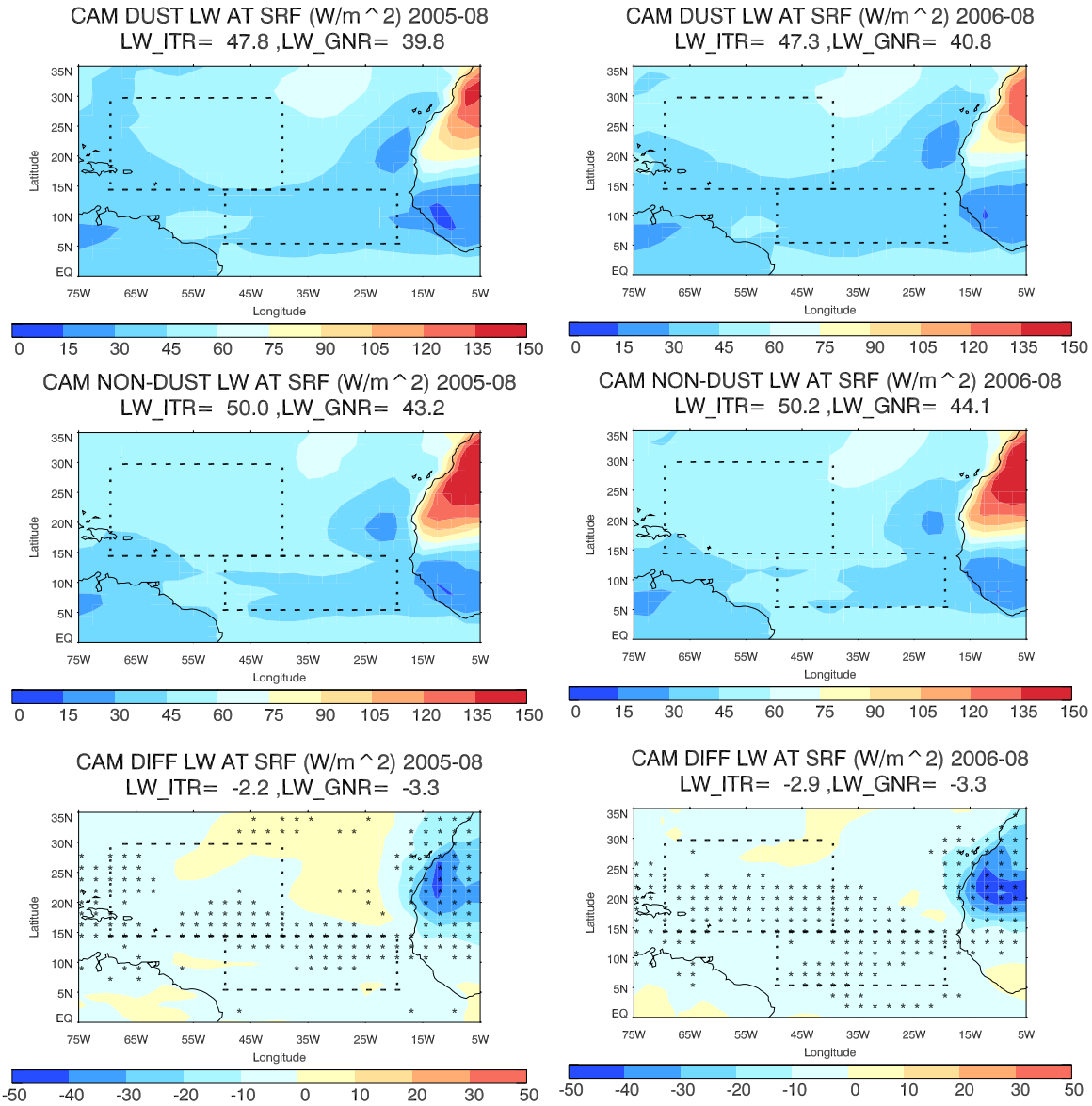

Figure 4.20: Net longwave radiation at the surface in August 2005 (left) and August 2006 (right)

4.4.5 Net radiation at TOM

The net radiation at the top of the model (TOM) is the summation of the shortwave and longwave radiations, which represents the total energy remaining in the Earth System. Positive (negative) net TOM radiation represents the radiative surplus (deficit) in the Earth System. In Figure 4.21, the maximum net radiative flux (90-100 W/m^2) is on the West Atlantic Ocean, where there is less cloud coverage and dust intervention. The minimum net radiative flux is (-40 to -50W/m^2) at 10N over the West African continent, where there is maximum low cloud coverage. The other relative low net flux region (-10 to -20W/m^2) is over the Saharan desert, where the desert surface reflects the shortwave radiation thus has less net radiative flux compared to ocean surface. Based on the difference map, dust decreases the net radiative flux at 10N over the West African, due to the increasing of low cloud cover (Figure 4.12). The decreasing of the TOM radiation on the north of 25N along the West Africa coast for 40W/m^2 and on south of 15N over the African continent for 30W/m^2 are also related to the increasing low cloud coverage. Moreover, dust increases the net radiative flux on the north of 15N in the mid Atlantic Ocean, corresponding to the decrease of low cloud cover, which decreases the upward shortwave radiation and increases the net radiation at TOM. On the other hand, dust absorbs the solar radiation in the Saharan desert and eliminates the upward shortwave radiative flux to the TOM, results in an increase of the net radiation for 50W/m^2.

Overall, dust perturbs the net radiative flux at the TOM mostly by changing of the low cloud coverage.

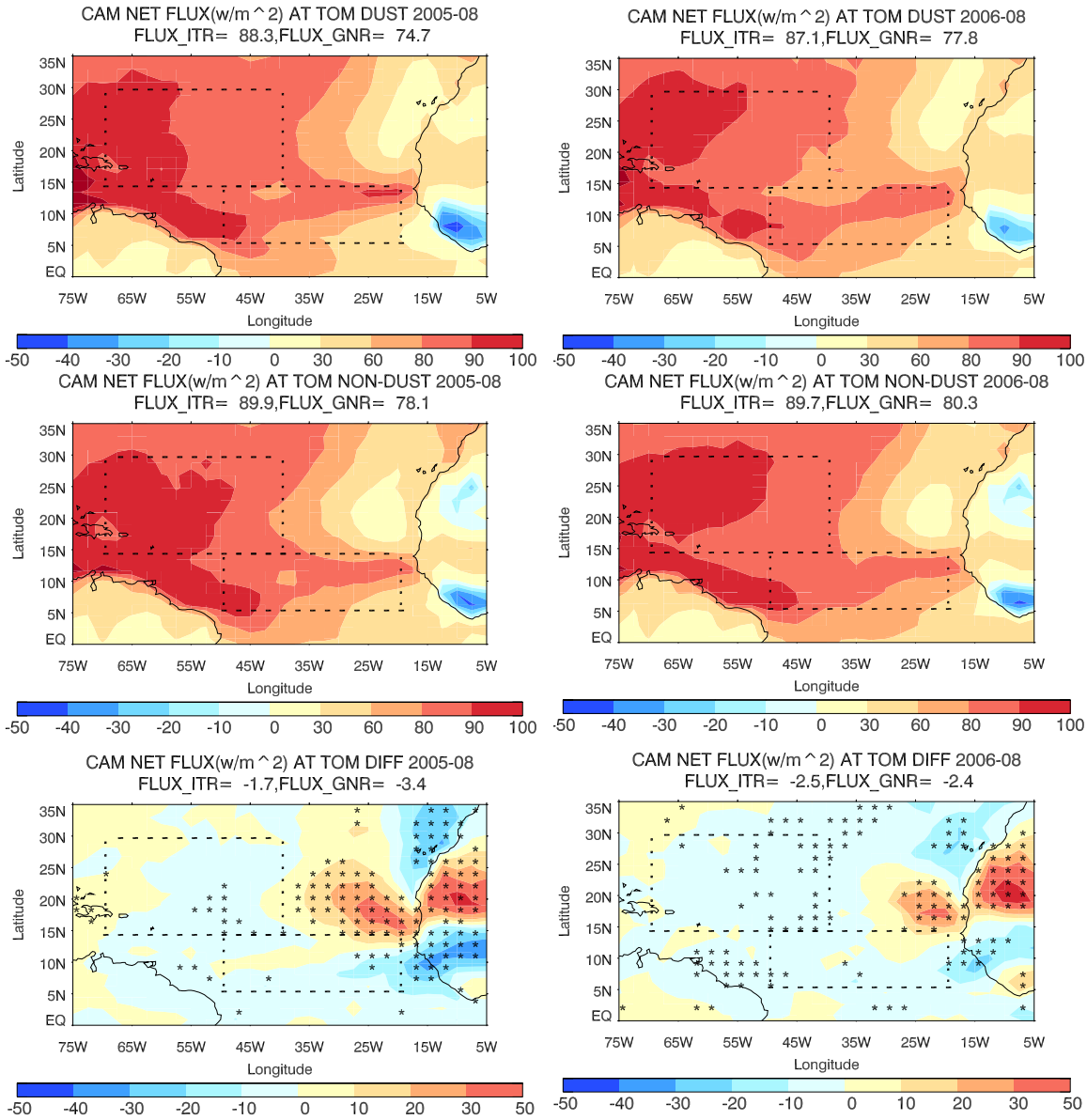

Figure 4.21: Net radiative flux at TOM in August 2005 (left) and August 2006 (right)

In conclusion, dust perturbs the radiative budget through several pathways, 1) absorbing and reflecting the incoming shortwave radiation, 2) changing the low cloud coverage, 3) changing the high cloud fractions. Under the clear-sky condition, dust absorption dominates over the bright surface, whereas the reflection of dust dominates

over the low albedo region. Moreover, dust increases the downward longwave radiation by heating the mid atmosphere. Under the all-sky condition, dust perturbs the radiative budgets induces changes on cloud fractions that further. The increasing low cloud coverage reflects the solar radiation, hence decreasing the surface solar flux and increasing the upward shortwave radiation at TOA. The increasing of high cloud fractions traps the longwave radiation in the atmosphere and decreases the upward longwave radiation to the TOA, therefore warming the regional climate.

4.5 DUST IMPACTS ON TROPICAL CYCLONE GENESIS

In this section, dust impacts on the favorability of tropical cyclogenesis are investigated by interpreting several vital parameters, including the low level vorticity, mid-level wind shear, entropy deficit [*Emanuel, et al.*, 2004], and potential intensity [*Bister and Emanuel*, 2002].

4.5.1 Low level relative vorticity

$$\zeta = \frac{\partial v}{\partial x} - \frac{\partial u}{\partial y} = \frac{v_{i+1,j-} v_{i,j}}{\Delta x} - \frac{u_{i,j+1-} u_{i,j}}{\Delta y}$$

The Z-component of the relative vorticity is used to evaluate the environmental low-level vorticity, since the X and Y components are normally an order of magnitude smaller than that of the Z component. It is calculated by the above equation, where i and j represent the grid index and Δx and Δy are the grid space in x and y direction respectively. The low-level vorticity induces rotation to the convective systems and increases the air spirals into the storm center. A positive (negative) vorticity represents the cyclonic (anticyclonic) motion, which is (not) favorable for the TC formation. The positive vorticity field is located on the north edge of the ITCZ and on the south of the

AEJ (Figure 4.22). Dust intensifies the Saharan Heat Low, therefore increasing the low level vorticity over the West Africa. As mentioned in the previous section, dust perturbs the large-scale circulation and moves the ITCZ northward. Due to the shift of the convergence zone in the difference map, the low level vorticity significantly decreases in the GNR but increases in the ITR, therefore possibly suppressing the genesis of the TCs in the GNR and moving the possible region for TC genesis northward.

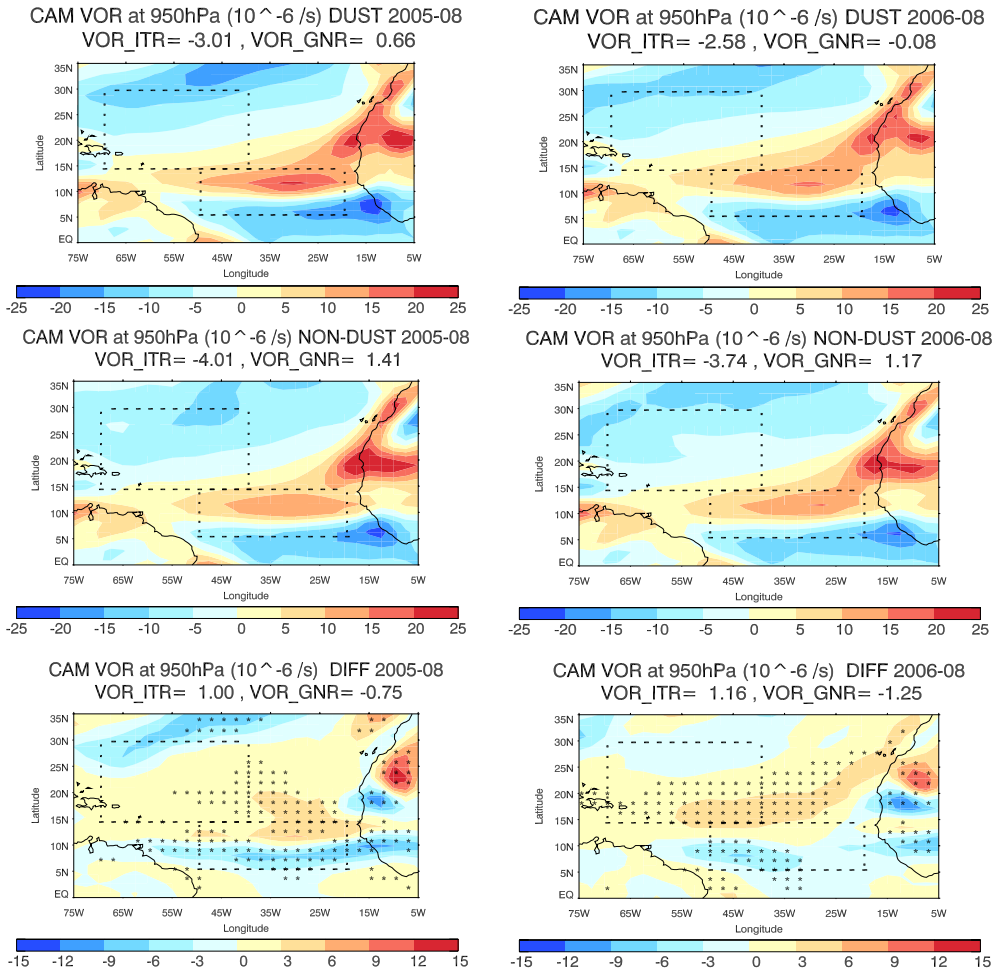

Figure 4.22: Low level vorticity at 950hPa in August 2005 (left) and August 2006 (right)

4.5.2 Vertical wind shear

The vertical wind shear is the absolute differences of the wind vector between 850hPa and 200hPa. *Dunion and Velden* [2004] suggest that the SAL increases the mid level easterly jet, therefore increasing the vertical wind shear and suppressing the development of tropical cyclones. *Bracken and Bosart* [2000] conclude that a relative weak vertical wind shear (10-15 m/s) could enable the development of vortices. The maximum wind shear in Figure 4.23 shows a zonal distribution of the high wind shears (21 - 24 m/s) along 10N over the African coast, which is correlated with the Tropical Easterly Jet (TEJ) at 100hPa to 200hPa level. Another maximum wind shear region is located on the north of 25N along the West African coast is associated with the Azore High, which has a cyclonic circulation in the upper level but an anticyclonic circulation in the lower atmosphere. Based on the difference map, there is an increase of the vertical wind shear (6-9m/s) between 5N and 15N on the east of 50W, possibly due to the northward movement of the ITCZ and an increasing of the TEJ in 200hPa and an enhanced westerly monsoon in the lower level as mentioned in the previous section. The wind shear increases for 2-3 m/s in the GNR, potentially suppressing TC genesis in such region.

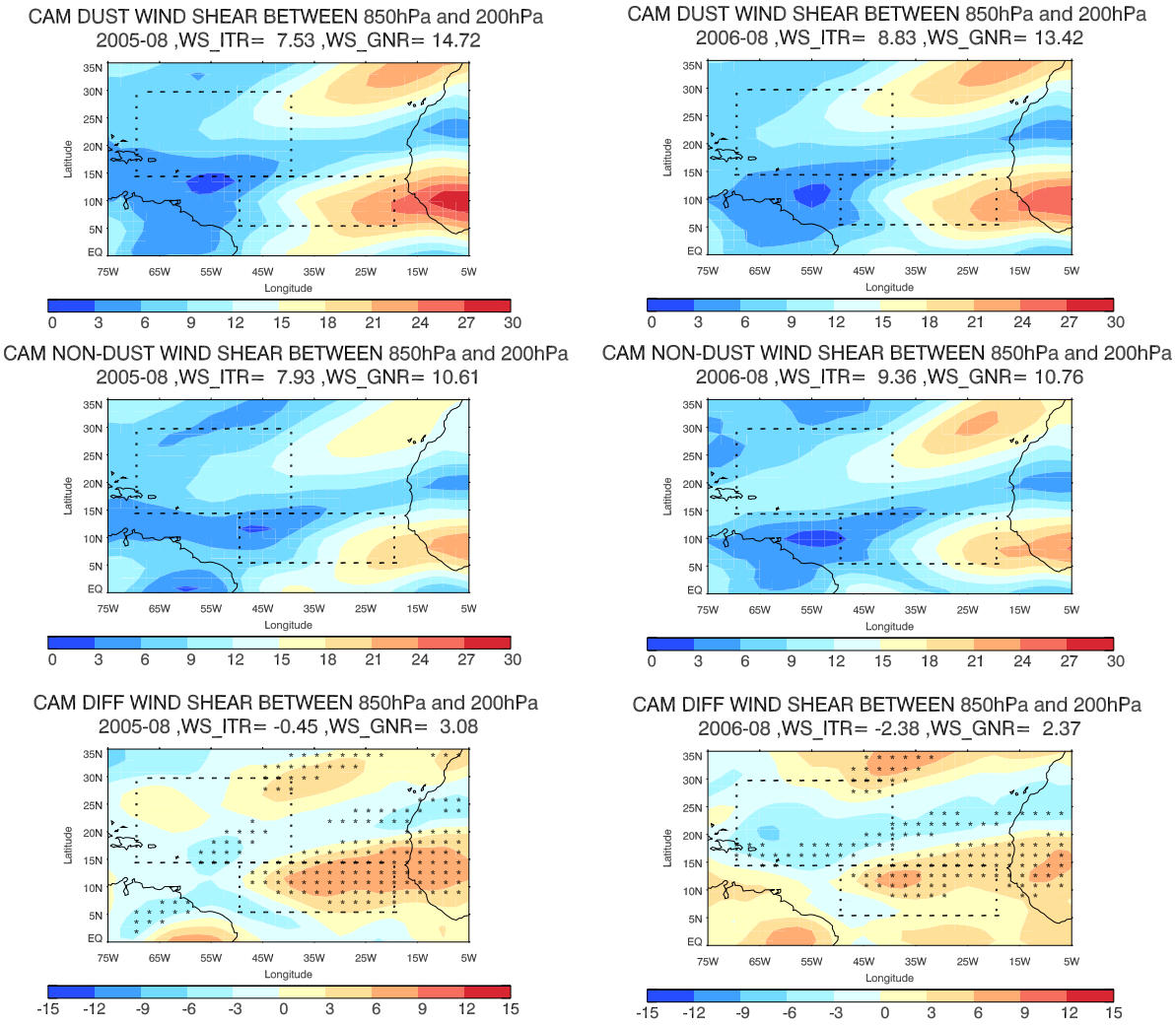

Figure 4.23: Vertical wind shear between 850hPa and 200hPa in August 2005 (left) and August 2006 (right)

4.5.3 Mid level moisture

The low to mid level moisture indicates the amount of moisture and, to some extent, energy supplies for TC formation and intensification. Figure 4.24 shows the relative humidity at 700hPa. The maximum RH reaches 80 to 90% between the equator and 15N, which corresponds to the moisture inside the ITCZ. The minimum RH (10-20%) is located on the north of 25N along the West African coast, where the dominant

subsidence motion is located, which dries and warms the atmosphere and decreases the RH.

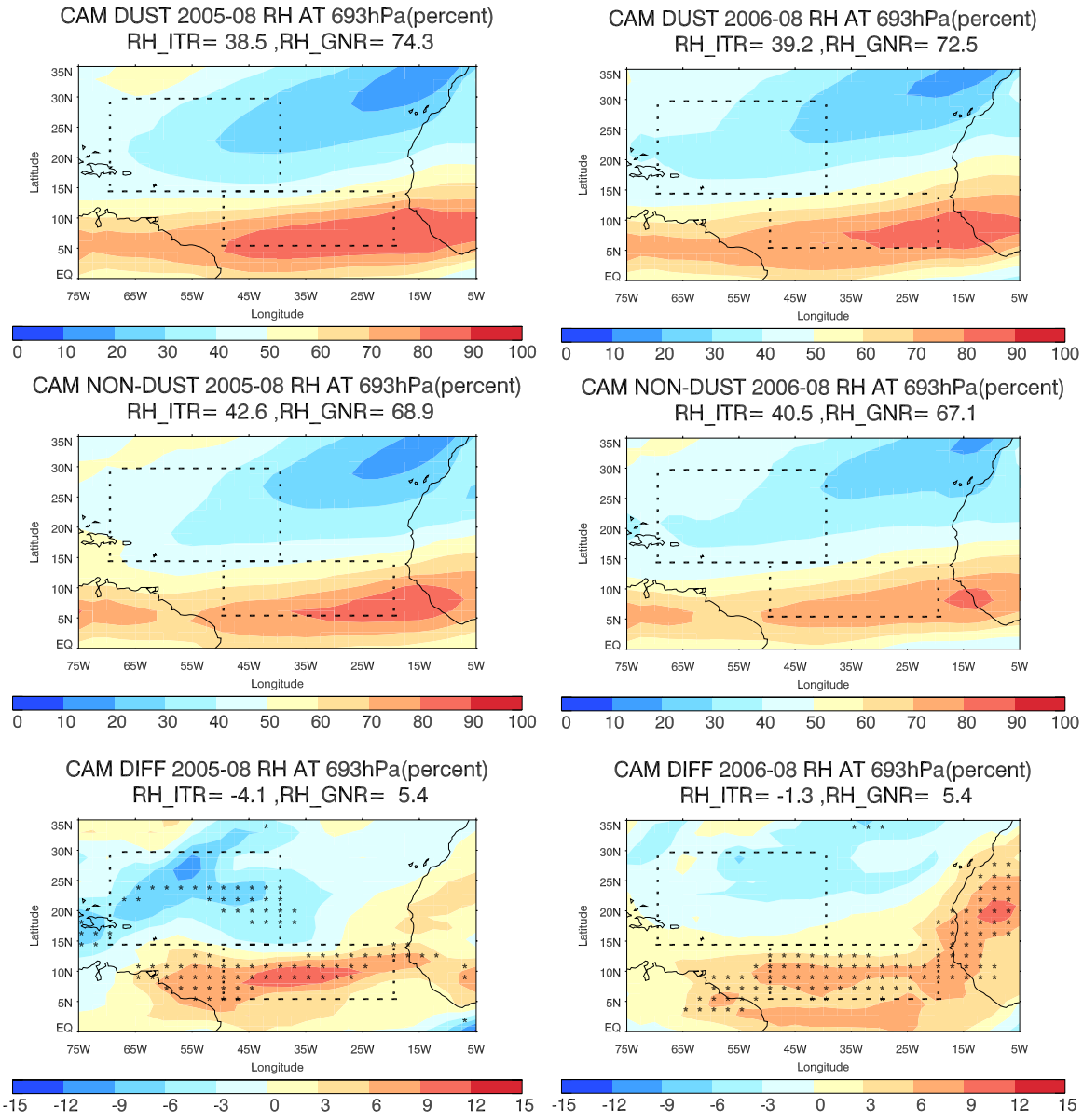

Figure 4.24: RH in the 693hPa in August 2005 (left) and August 2006 (right)

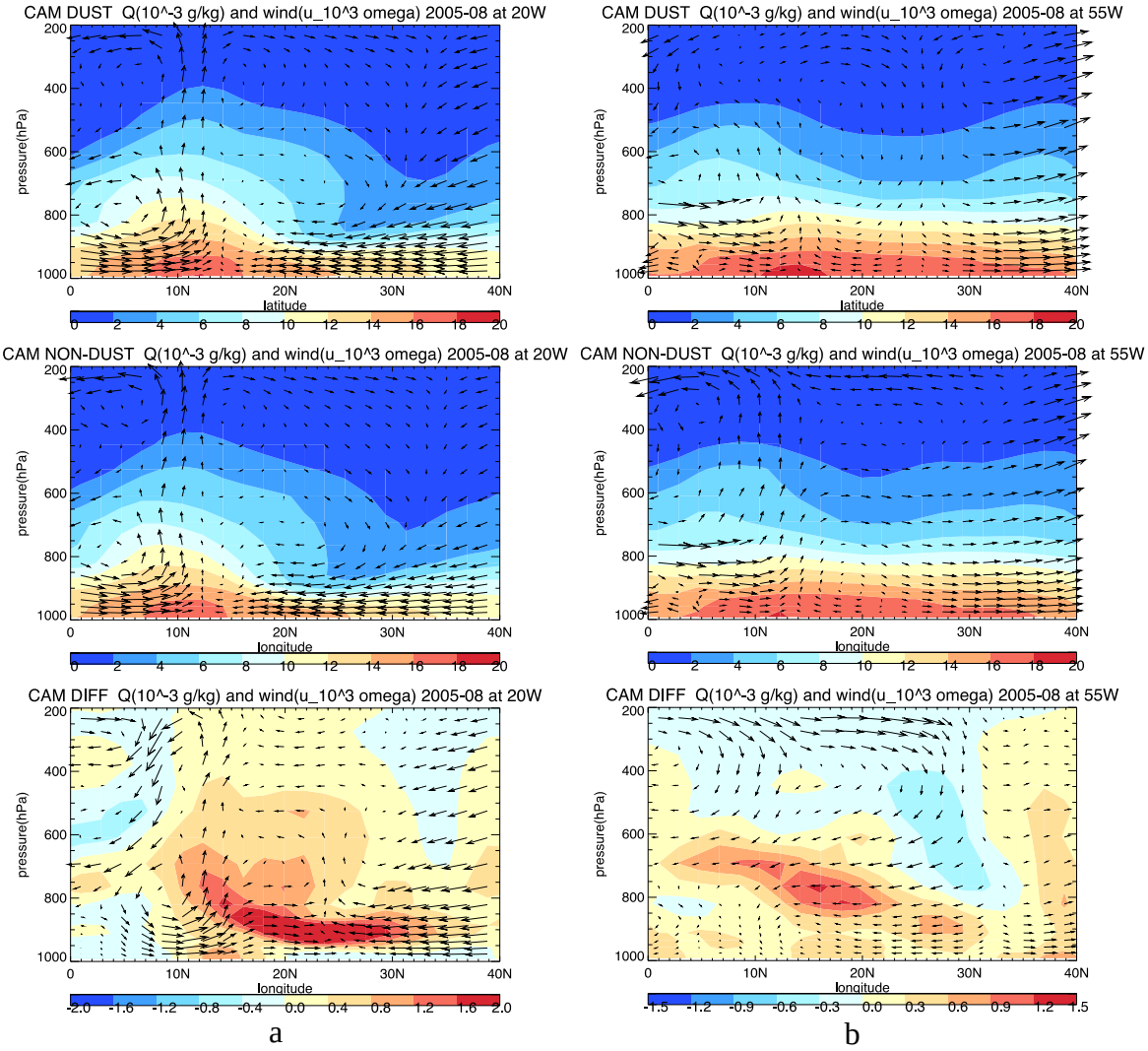

Figure 4.25: Cross-section of SH overplotted with wind at 20W (a) and 55W (b) in August 2005

Based on the dust and non-dust comparison, dust increases the RH on the south of 15N by increasing the lifting motion that enhances the condensation in the ITCZ therefore increasing the mid level RH. Moreover, the cross section of specific humidity (SH) at 20W overplotted by the meridional and vertical wind (Figure 4.25a) shows that dust increases the SH in the lower atmosphere, due to the enhancement of the West

African monsoon that transport moist air from the ocean to the West African continent. It decreases the RH on the north of 15N especially over the ITR for 9%, possibly due to the stronger subsidence in the dust scenarios compared to the non-dust cases at 700hPa (Figure 4.25b). The 9-12% increases of RH in the GNR may contribute to the moist instability that favors the convective development.

4.5.4 Entropy deficit

The entropy deficit is a non-dimensional variable that is calculated using the following equation [*Tang and Emanuel*, 2012]

$$X_m = \frac{S_m^* - S_m}{S_{SST}^* - S_b}$$

S_m^* is the saturation entropy in the mid level atmosphere (600hPa) whereas S_m is the environmental entropy at the same level. S_{SST}^* is the saturation entropy at the sea surface temperature and S_b is the entropy of the boundary layer. The denominator of the entropy deficit represents the air-sea entropy gradient that represents the potential of entropy flux to the convective system. The nominator illustrates the mid-level moisture by comparing between the saturated and environmental entropy. Thus, a large the energy deficit reflects a less possibility of a TC formation, since there are/is less energy supply and/or a dry mid atmosphere.

S represents the entropy of the system, which is defined as the unavailability of the system energy converting into kinetic energy and also represents the disorder of the system. It is calculated using the following equation [*Bryan*, 2008].

$$s = c_p \log(T) - R_d \log(p_d) + \frac{L_{v0} r_v}{T} - R_v r_v \log(H)$$

C_p is the specific heat constant for dry air under constant pressure. R_d is the gas constant for dry air. L_{v0} is the latent heat for vaporization. R_v is the gas constant for vapor, whereas r_v is the vapor mixing ratio. H is the relative humidity.

In Figure 4.26, the minimum entropy deficit is located along 10N, which is correlated with the ITCZ, since there is a moist mid atmosphere and sufficient energy supply to the convection active region. The other minimum region is along the West African coast on the north of 15N, where the warm and dry Saharan air just moves off the West African coast. The dry and warm air undercuts with cold and moist ocean surface, resulting in a significant entropy gradient between the saturated sea surface and boundary layer. Based on the difference map, dust increases the entropy deficit on the north of 10N significantly by increasing convergence and mid level moisture. On the other hand, there is slightly decrease along 10N, which corresponds to the increasing of the moist supply by dust in the mid Atlantic region. Overall, the spatial average of the deficit at the GNR slightly increases, therefore decreasing the possibility of TC genesis.

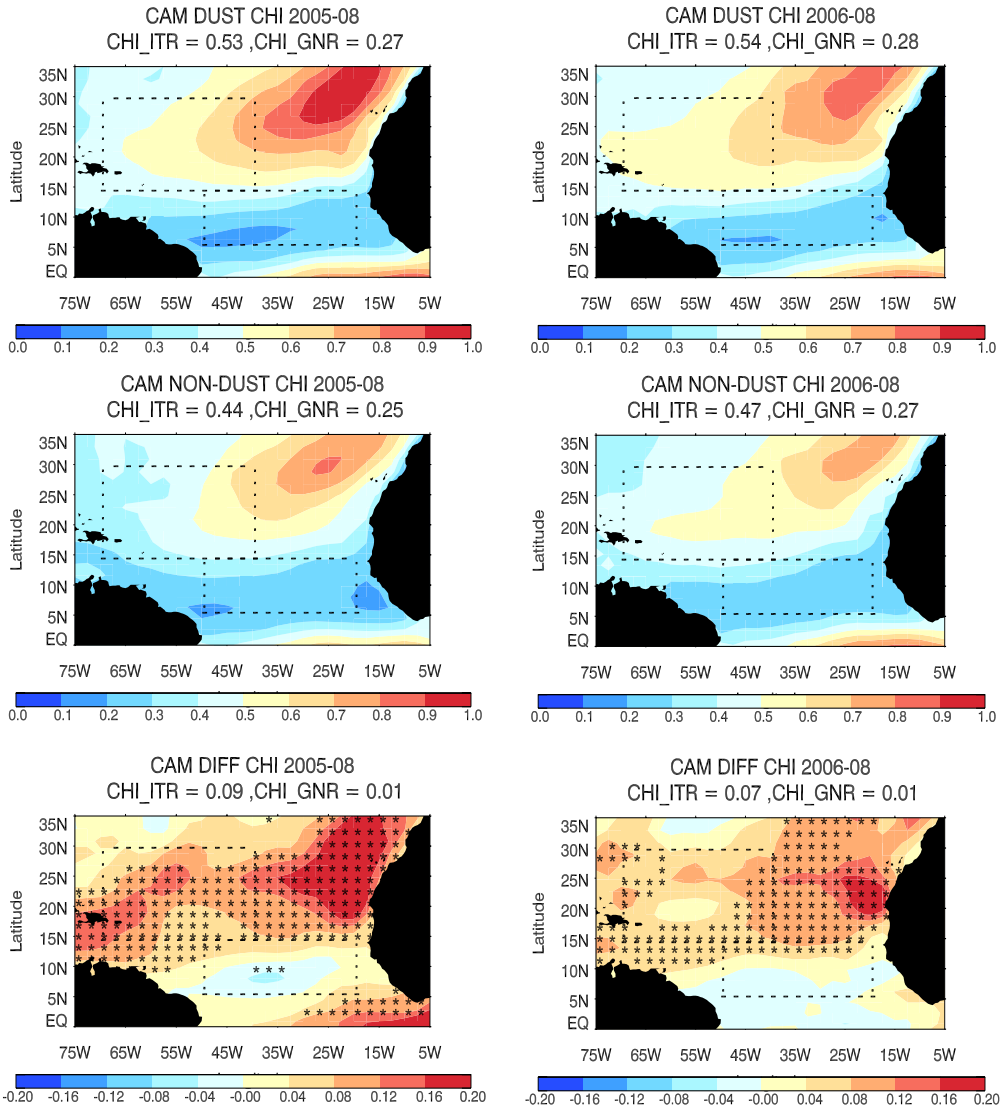

Figure 4.26: Entropy deficit in August 2005 (left) and August 2006 (right)

Above all, dust has various impacts on TC genesis from both the thermodynamics and dynamical perspectives. It decreases the favorability of TC genesis in the GNR by increasing the entropy deficit, increasing wind shear, and decreasing the low level vorticity. On the other hand, the increasing of mid level moisture by dust favors the TC formation especially over the GNR.

5. CONCLUSION AND DISCUSSION

This study investigates the Saharan dust impacts on the regional climate and the genesis of tropical cyclones in the Atlantic hurricane seasons of 2005 and 2006. The stand-alone version of the Community Earth System Model version 1.0.4, CAM5.1, is shown to be capable of simulating the dust emissions from Saharan desert and the long-range dust transport to the mid Atlantic region. Comparison with the MODIS products shows that the aerosol optical depth (AOD) from the model simulations is underestimated in the GNR (29%) but overestimated in ITR (16%). Moreover, CAM5.1 overestimates the precipitation rate near the West African coast, similarly to most of the General Circulation Models (GCMs). The model reproduces the major climate features such as the African Easterly Jet (AEJ), the Intertropical convergence zone (ITCZ), West African Monsoon, and etc. Comparison of the dust and non-dust simulations reveals that dust plays a substantial role in changing the climate in the West African and North Atlantic region. The influence of dust includes intensifying the Saharan Heat Low over heavy dust-loaded region (north of 15N) and shifting the ITCZ northward by enhancing the West African Monsoon. The perturbation of large-scale circulation further leads to changes of high clouds in the ITCZ and draws low clouds closer to the West African coastline. The redistribution of high (low) clouds is responsible for the modification of radiative fluxes, especially the longwave (shortwave) radiation on the surface and at TOA. In terms of the direct effect, dust absorbs the shortwave radiation over the bright

surface but reflects over the dark surface. Overall, dust decreases the regional radiative energy in the atmosphere, thus providing less energetics for the genesis of TCs.

To elucidate the dust impacts on the large-scale environments for tropical cyclogenesis, several dynamical and thermodynamical parameters have been analyzed including mid-level wind shear, low-level vorticity, mid-level moisture, and the entropy deficit. In particular, the spatial average of each parameter in the ITR and the GNR has been compared. Dust favors the genesis of TCs from the thermodynamic perspective by increasing the mid-level moisture in the GNR. On the other hand, the TC formation is suppressed by dust through increased wind shear, increased entropy deficit, and decreased low-level vorticity in the GNR. It is likely that the region of TC genesis shifts northward because of the northward movement of the convergence zone.

The results of this study provide evidence for direct and indirect effects of dust on the tropical precipitation and radiation, without the consideration of the forcing feedback from the ocean. It is possible that using the prescribed SST rather than a coupled global climate model introduces bias on the dust impacts on the Atlantic Tropical Cyclogenesis. For example, *Miller and Tegan* [1998] have investigated the differences between the coupled General Circulation Model (GCM) and the uncoupled Atmospheric General Circulation Model (AGCM), showing significant differences in precipitations over the West Atlantic Ocean, due to the suppression of latent heat flux and moisture supply to the atmosphere in the GCM. By using an uncoupled model in this study, dust mainly disturbs the vertical temperature on the north of 15N over the African continent and the East Atlantic Ocean, while maintaining the surface temperature undisturbed over the

ocean. The upper level temperature changes increase the inversion and stabilize the atmosphere, hence trapping the evaporated moisture in the lower atmosphere. For the non-dust scenario, the removal of both the radiative and microphysical effects of dust likely corresponds to an increasing of SST, therefore increasing the moisture supply and invigorating convective developments. Also, the unchanged SST eliminates the variation in latent heat flux. Therefore, future studies are needed to investigate the dust impacts on the SST using the atmosphere and ocean coupled model.

This study promotes the strength of the Global Climate Models (GCMs) in the physical-based large-scale circulation and real time climatology of the SST and sea-ice. The preliminary results proved the significant effects of dust on the Atlantic regional climate. Furthermore, dust impacts on tropical cyclones remain an open question and require future study. In order to simulate the realistic tropical cyclone structure, a both vertically and horizontally high-resolution model configuration is required. Moreover, due to the computational limit, the current model resolution is approximately 250km * 190km, which is incapable to generate realistic tropical cyclone structures and investigate the aerosol impacts on the intensity or frequency of the TCs. For future assessment of the dust impacts on the tropical cyclones, a finer resolution model preferably 0.25 degree would be necessary to investigate the dust microphysical interaction with the tropical cyclones.

6. REFERENCES

Adler, R.F., G.J. Huffman, A. Chang, R. Ferraro, P. Xie, J. Janowiak, B. Rudolf, U. Schneider, S. Curtis, D. Bolvin, A. Gruber, J. Susskind, and P. Arkin (2003): The Version 2 Global Precipitation Climatology Project (GPCP) Monthly Precipitation Analysis (1979-Present). *J. Hydrometeor.*, 4,1147-1167.

Albani, S., N. Mahowald, A. Perry, R. Scanza, C. Zender, N. Heavens, V. Maggi, J. Kok, and B. Otto-Bliesner (2014), Improved dust representation in the Community Atmosphere Model, *Journal of Advances in Modeling Earth Systems*, *6*(3), 541-570.

Alfaro, S. C., and L. Gomes (2001), Modeling mineral aerosol production by wind erosion: Emission intensities and aerosol size distributions in source areas, *J. Geophys. Res.*, 106, 18,075–18,084.

Beven-II, J., L. Avila, E. Blake, D. Brown, J. Franklin, R. Knabb, and others (2008), Annual Summary-Atlantic Hurricane Season of 2005, *Tropical Prediction Center, NOAAN/NWS/National Hurricane Center, Miami (March 2008).*

Bister, M. and K. Emanuel (2002), Low frequency variability of tropical cyclone potential intensity. 1. Interannual to interdecadal variability, *J. Geophys. Res.*, *107, 4801, doi:10.1029/2001JD000776.*

Bracken, W. E., and L. F. Bosart (2000), The role of synoptic-scale flow during tropical cyclogenesis over the North Atlantic Ocean, *Monthly weather review*, *128*(2), 353–376.

Braun, S. A. (2010), Reevaluating the role of the Saharan Air Layer in Atlantic tropical cyclogenesis and evolution., *Monthly Weather Review*, *138*(6).

Bretl, S., P. Reutter, C. C. Raible, S. Ferrachat, C. S. Poberaj, L. E. Revell, and U. Lohmann (2015), The influence of absorbed solar radiation by Saharan dust on hurricane genesis, *Journal of Geophysical Research: Atmospheres*, *120*(5), 1902-1917.

Bryan, G. (2008), On the computation of pseudoadiabatic entropy and equivalent potential temperature. *Mon. Wea. Rev., 136, 5239–5245.*

Bryant, R. G., G. R. Bigg, N. M. Mahowald, F. D. Eckardt, and S. G. Ross (2007), Dust emission response to climate in southern Africa, *Journal of Geophysical Research: Atmospheres (1984-2012)*, *112*(D9).

Carlson, T. N., and J. M. Prospero (1972), The large-scale movement of Saharan air outbreaks over the northern equatorial Atlantic, *Journal of Applied Meteorology*, *11*(2), 283–297.

Charney, J. G., and A. Eliassen (1964), On the growth of the hurricane depression, *J. Atmos. Sci., 21*, 68–75

Conley A. J., et al. (2012). Description of the NCAR Community Atmosphere Model (CAM 5.0). Retrieved from http://citeseerx.ist.psu.edu/viewdoc/download?doi=10.1.1.422.3202&rep=rep1&type=pdf

Craig, G. C., and S. L. Gray (1996), CISK or WISHE as the mechanism for tropical cyclone intensification, *Journal of the atmospheric sciences*, *53*(23), 3528–3540.

Cziczo, D., D. Murphy, P. Hudson, and D. Thomson (2004), Single particle measurements of the chemical composition of cirrus ice residue during CRYSTAL-FACE, *Journal of Geophysical Research: Atmospheres (1984-2012)*, *109*(D4).

Dee, D. P., et al. (2011), The ERA-Interim reanalysis: configuration and performance of the data assimilation system, *Q.J.R. Meteorol. Soc., 137, 553-597*

DeMott, P. J., K. Sassen, M. R. Poellot, D. Baumgardner, D. C. Rogers, S. D. Brooks, A. J. Prenni, and S. M. Kreidenweis (2003), African dust aerosols as atmospheric ice nuclei, *Geophysical Research Letters*, *30*(14).

DeMott, P., A. Prenni, X. Liu, S. Kreidenweis, M. Petters, C. Twohy, M. Richardson, T. Eidhammer, and D. Rogers (2010), Predicting global atmospheric ice nuclei distributions and their impacts on climate, *Proceedings of the National Academy of Sciences*, *107*(25), 11217–11222.

Dunion, J. P., and C. S. Velden (2004), The impact of the Saharan air layer on Atlantic tropical cyclone activity, *Bulletin of the American Meteorological Society*, *85*(3), 353–365.

Emanuel, K. A. (1986), An air-sea interaction theory for tropical cyclones. Part I: Steady-state maintenance, *Journal of the Atmospheric Sciences*, *43*(6), 585–605.

Emanuel,K. A., C. DesAutels, C. Holloway, and R. Korty (2004), Environmental control of tropical cyclone intensity. *J. Atmos. Sci., 61, 843–858.*

Evan, A. T., J. Dunion, J. A. Foley, A. K. Heidinger, and C. S. Velden (2006), New evidence for a relationship between Atlantic tropical cyclone activity and African dust outbreaks, *Geophysical Research Letters*, *33*(19).

Evan, A. (2007), Comment on "How Nature foiled the 2006 hurricane forecasts," *Eos, Transactions American Geophysical Union*, *88*(26), 271–271.

Foltz, G. R., and M. J. McPhaden (2008), Trends in Saharan dust and tropical Atlantic climate during 1980-2006, *Geophysical Research Letters*, *35*(20).

Franklin, J. L., and D. P. Brown (2008), Atlantic hurricane season of 2006, *Monthly Weather Review*, *136*(3), 1174–1200.

Ghan, S. J., X. Liu, R. C. Easter, R. Zaveri, P. J. Rasch, J.-H. Yoon, and B. Eaton (2012), Toward a minimal representation of aerosols in climate models: Comparative decomposition of aerosol direct, semidirect, and indirect radiative forcing, *Journal of Climate*, *25*(19), 6461–6476.

Ghan, S. J., and R. A. Zaveri (2007), Parameterization of optical properties for hydrated internally mixed aerosol, *J. Geophys. Res.*, *112*, D10201.

Goldenberg, S. B., C. W. Landsea, A. M. Mestas-Nuñez, and W. M. Gray (2001), The recent increase in Atlantic hurricane activity: Causes and implications, *Science*, *293*(5529), 474–479.

Gray, W. M. (1979), Hurricanes: their formation, structure, and likely role in the tropical circulation. In *Meteorology Over the Tropical Oceans*,ed. DB Shaw, 155-218.

Gray, W. M. (1984), Atlantic seasonal hurricane frequency. Part I: El Nino and 30 mb quasi-biennial oscillation influences, *Monthly Weather Review*, *112*(9), 1649- 1668.

Gray, W. M. (1998), The formation of tropical cyclones, *Meteorology andatmospheric physics*, *67*(1-4), 37–69.

Grini, A., C. S. Zender, and P. Colarco (2002), Saltation sandblasting behavior during mineral dust aerosol production, *Geophys. Res. Lett.*, 29(18), 1868, doi:10.1029/2002GL015248.

Hansen, J., M. Sato, and R. Ruedy (1997), Radiative forcing and climate response, *Journal of Geophysical Research: Atmospheres (1984-2012)*, *102*(D6), 6831- 6864.

Hsu, N. C., S.-C. Tsay, M. D. King, and J. R. Herman (2004), Aerosol properties over bright-reflecting source regions, *Geoscience and Remote Sensing, IEEE Transactions on*, *42*(3), 557–569.

Iacono, M. J., J. S. Delamere, E. J. Mlawer, M. W. Shephard, S. A. Clough, and W. D. Collins (2008), Radiative forcing by long-lived greenhouse gases: Calculations with the AER radiative transfer models, J. Geophys. Res., 113, D13103, doi:10.1029/2008JD009944.

Karyampudi, V. M., and T. N. Carlson (1988), Analysis and numerical simulations of the Saharan air layer and its effect on easterly wave disturbances, *Journal of the Atmospheric Sciences*, *45*(21), 3102–3136.

Karyampudi, V. M., and H. F. Pierce (2002), Synoptic-scale influence of the Saharan air layer on tropical cyclogenesis over the eastern Atlantic, *Monthly weather review*, *130*(12), 3100–3128.

Kaufman, Y. J., I. Koren, L. A. Remer, D. Rosenfeld, and Y. Rudich (2005), The effect of smoke, dust, and pollution aerosol on shallow cloud development over the

Atlantic Ocean, *Proceedings of the National Academy of Sciences of the United States of America*, *102*(32), 11207–11212.

Kim, K.-M., W. K.-M. Lau, Y. C. Sud, and G. K. Walker (2010), Influence of aerosol-radiative forcings on the diurnal and seasonal cycles of rainfall over West Africa and Eastern Atlantic Ocean using GCM simulations, *Climate dynamics*, *35*(1), 115–126.

Lau, W. K., and K. M. Kim (2006), Observational relationships between aerosol and Asian monsoon rainfall, and circulation, *Geophysical Research Letters*, *33*(21).

Lau, W. K., and K.-M. Kim (2007a), How nature foiled the 2006 hurricane forecasts, *Eos, Transactions American Geophysical Union*, *88*(9), 105–107.

Lau, K., and K. Kim (2007b), Cooling of the Atlantic by Saharan dust, *Geophysical Research Letters*, *34*(23).

Lau, K. et al. (2008), The Joint Aerosol-Monsoon Experiment: A new challenge for monsoon climate research, *Bulletin of the American Meteorological Society*, *89*(3), 369–383

Lau, K., K. Kim, Y. Sud, and G. Walker (2009), A GCM study of the response of the atmospheric water cycle of West Africa and the Atlantic to Saharan dust radiative forcing, in *Annales Geophysicae*, vol. 27, pp. 4023–4037.

Levi, Y., and D. Rosenfeld (1996), Ice nuclei, rainwater chemical composition, and static cloud seeding effects in Israel, *Journal of Applied Meteorology*, *35*(9), 1494–1501.

Levin, Z., E. Ganor, and V. Gladstein (1996), The effects of desert particles coated with sulfate on rain formation in the eastern Mediterranean, *Journal of Applied Meteorology*, *35*(9), 1511–1523.

Li, G., Y. Wang, and R. Zhang (2008), Implementation of a two-moment bulk microphysics scheme to the WRF model to investigate aerosol-cloud interaction, *Journal of Geophysical Research: Atmospheres (1984-2012)*, *113*(D15).

Lighthill, J., G. Holland, W. M. Gray, C. W. Landsea, G. Craig, J. Evans, Y. Kurihara, and C. Guard (1994), Global climate change and tropical cyclones, *Bulletin of the American Meteorological Society*, *75*(11), 2147–2158.

Liu, X., J. E. Penner, S. J. Ghan, and M. Wang (2007), Inclusion of ice microphysics in the NCAR Community Atmospheric Model version 3 (CAM3), *Journal of Climate*, *20*(18), 4526–4547.

Liu, X. et al. (2012), Toward a minimal representation of aerosols in climate models: Description and evaluation in the Community Atmosphere Model CAM5, *Geoscientific Model Development*, *5*, 709–739.

Lohmann, U. (2002), A glaciation indirect aerosol effect caused by soot aerosols, *Geophys. Res. Lett., 29(4), 11-1-11-4.*

Mahowald, N. M., and L. M. Kiehl (2003), Mineral aerosol and cloud interactions, *Geophysical Research Letters*, *30*(9).

Mahowald, N. M., and C. Luo (2003), A less dusty future?, *Geophysical Research Letters*, *30*(17).

Mahowald, N., J. Ballantine, J. Feddema, and N. Ramankutty (2007), Global trends in visibility: implications for dust sources, *Atmospheric Chemistry and Physics*, *7*(12), 3309–3339.

Martin, J. H., M. Gordon, and S. E. Fitzwater (1991), The case for iron, *Limnology and Oceanography*, *36*(8), 1793–1802.

Miller, R., and I. Tegen (1998), Climate response to soil dust aerosols, *Journal of climate*, *11*(12), 3247–3267.

Morrison, H., and A. Gettelman (2008), A new two-moment bulk stratiform cloud microphysics scheme in the Community Atmosphere Model, version 3 (CAM3). Part I: Description and numerical tests, *Journal of Climate*, *21*(15), 3642–3659.

Neale, R. B., J. H. Richter, and M. Jochum (2008), The impact of convection on ENSO: From a delayed oscillator to a series of events, *Journal of climate*, *21*(22), 5904-5924.

Ooyama, K. V. (1964), A dynamical model for the study of tropical cyclone development, *Geophys. Int.*, *4*, 187–198

Okin, G. S., N. Mahowald, O. A. Chadwick, and P. Artaxo (2004), Impact of desert dust on the biogeochemistry of phosphorus in terrestrial ecosystems, *Global Biogeochemical Cycles*, *18*(2).

Parajuli, S. P., Z.-L. Yang, and G. Kocurek (2014), Mapping erodibility in dust source regions based on geomorphology, meteorology, and remote sensing, *Journal of Geophysical Research: Earth Surface*, *119*(9), 1977–1994.

Park, S., and C. S. Bretherton (2009), The University of Washington shallow convection

and moist turbulence schemes and their impact on climate simulations with the Community Atmosphere Model, *Journal of Climate*, *22*(12), 3449–3469.

Park, S., C. S. Bretherton, and P. J. Rasch (2014), Integrating cloud processes in the community atmosphere model, Version 5, *Journal of Climate*, *27*(18), 6821- 6856.

Pratt, A. S., and J. L. Evans (2009), Potential impacts of the Saharan air layer on numerical model forecasts of North Atlantic tropical cyclogenesis, *Weather and Forecasting*, *24*(2), 420–435.

Prospero, J. M., and T. N. Carlson (1970), Radon-222 in the North Atlantic trade winds: its relationship to dust transport from Africa, *Science*, *167*(3920), 974–977.

Prospero, J. M. (1999), Long-range transport of mineral dust in the global atmosphere: Impact of African dust on the environment of the southeastern United States, *Proceedings of the National Academy of Sciences*, *96*(7), 3396–3403.

Prospero, J. M., and P. J. Lamb (2003), African droughts and dust transport to the Caribbean: Climate change implications, *Science*, *302*(5647), 1024–1027.

Ramanathan, V. et al. (2001), Indian Ocean Experiment: An integrated analysis of the climate forcing and effects of the great Indo-Asian haze, *Journal of Geophysical Research: Atmospheres (1984-2012)*, *106*(D22), 28371–28398.

Reale, O., K. Lau, and A. da Silva (2011), Impact of interactive aerosol on the African easterly Jet in the NASA GEOS-5 Global Forecasting System, *Weather and forecasting*, *26*(4), 504–519.

Reale, O., K. Lau, A. Silva, and T. Matsui (2014), Impact of assimilated and

interactive aerosol on tropical cyclogenesis, *Geophysical Research Letters*, *41*, 3282–3288.

Rosenfeld, D., and R. Nirel (1996), Seeding effectiveness—the interaction of desert dust and the southern margins of rain cloud systems in Israel, *Journal of Applied Meteorology*, *35*(9), 1502–1510.

Rosenfeld, D., and W. L. Woodley (2000), Deep convective clouds with sustained supercooled liquid water down to -37.5 ˚C, *Nature*, *405*(6785), 440–442.

Rosenfeld, D., Y. Rudich, and R. Lahav (2001), Desert dust suppressing precipitation: A possible desertification feedback loop, *Proceedings of the National Academy of Sciences*, *98*(11), 5975–5980.

Rosenfeld, D., A. Khain, B. Lynn, W. L. Woodley (2007), Simulation of hurricane response to suppression of warm rain by sub-micron aerosols, *Atmos. Chem. Phys.* 7, 5647–5674.

Rosenfeld, D., W. L. Woodley, A. Khain, W. R. Cotton, G. Carri, I. Ginis, and J. H. Golden (2012), Aerosol Effects on Microstructure and Intensity of Tropical Cyclones., *Bulletin of the American Meteorological Society*, *93*(7).

Shao, Y., K.-H. Wyrwoll, A. Chappell, J. Huang, Z. Lin, G. H. McTainsh, M. Mikami, T. Y. Tanaka, X. Wang, and S. Yoon (2011), Dust cycle: An emerging core theme in Earth system science, *Aeolian Research*, *2*(4), 181–204.

Shapiro, L. J., and S. B. Goldenberg (1998), Atlantic sea surface temperatures and tropical cyclone formation, *Journal of Climate*, *11*(4), 578–590.

Sippel, J. A., S. A. Braun, and C.-L. Shie, 2011: Environmental influences on the strength of Tropical Storm Debby (2006). *J. Atmos. Sci., 68*, 2557–2581.

Tang, B., and K. Emanuel (2012), A ventilation index for tropical cyclones, *Bulletin of the American Meteorological Society*, *93*(12), 1901–1912.

Twomey, S. A. (1977), The influence of pollution on the shortwave albedo of clouds, *Journal of Atmospheric Sciences*, *34*(5), 1149–1152.

Van den Heever, S. C., G. G. Carrió, W. R. Cotton, P. DeMott, A. J. Prenni, and others (2006), Impacts of nucleating aerosol on Florida storms. Part I: Mesoscale simulations., *Journal of the atmospheric sciences*, *63*(7).

Wang, Y., M. Wang, R. Zhang, S. J. Ghan, Y. Lin, J. Hu, B. Pan, M. Levy, J. H. Jiang, and M. J. Molina (2014a), Assessing the effects of anthropogenic aerosols on Pacific storm track using a multiscale global climate model, *Proceedings of the National Academy of Sciences*, *111*(19), 6894–6899.

Wang, Y., K.-H. Lee, Y. Lin, M. Levy, and R. Zhang (2014b), Distinct effects of anthropogenic aerosols on tropical cyclones, *Nature Climate Change*.

Willoughby, H., D. Jorgensen, R. Black, and S. Rosenthal (1985), Project STORMFURY: A Scientific Chronicle 1962-1983, *Bulletin of the American Meteorological Society*, *66*(5), 505–514.

Wilcox, E. M., K. Lau, and K.-M. Kim (2010), A northward shift of the North Atlantic Ocean Intertropical Convergence Zone in response to summertime Saharan dust outbreaks, *Geophysical Research Letters*, *37*(4).

Wong, S., and A. E. Dessler (2005), Suppression of deep convection over the tropical North Atlantic by the Saharan Air Layer, *Geophys. Res. Lett.*, *32*, L09808.

Wong, S., A. E. Dessler, N. M. Mahowald, P. R. Colarco, and A. da Silva (2008), Long-term variability in Saharan dust transport and its link to North Atlantic seasurface temperature, Geophys. Res. Lett., 35, L07812

Yin, Y., Z. Levin, T. G. Reisin, and S. Tzivion (2000), The effects of giant cloud condensation nuclei on the development of precipitation in convective clouds—A numerical study, *Atmospheric Research*, *53*(1), 91–116.

Yoshioka, M., N. M. Mahowald, A. J. Conley, W. D. Collins, D. W. Fillmore, C. S. Zender, and D. B. Coleman (2007), Impact of desert dust radiative forcing on Sahel precipitation: Relative importance of dust compared to sea surface temperature variations, vegetation changes, and greenhouse gas warming,*Journal of Climate*, *20*(8), 1445–1467.

Zender, C. S., H. Bian, and D. Newman (2003a), Mineral Dust Entrainment and Deposition (DEAD) model: Description and 1990s dust climatology, *Journal of Geophysical Research: Atmospheres (1984-2012)*, *108*(D14).

Zender, C. S., D. Newman, and O. Torres (2003b), Spatial heterogeneity in Aeolian erodibility: Uniform, topographic, geomorphic, and hydrologic hypotheses, *J. Geophys. Res.*, *108*(D17), 4543, doi:10.1029/2002JD003039.

Zhang, G. J., and N. A. McFarlane (1995), Sensitivity of climate simulations to the parameterization of cumulus convection in the Canadian Climate Centre general circulation model, *Atmosphere-Ocean*, *33*(3), 407–446.

Zhang, H., G. M. McFarquhar, S. M. Saleeby, and W. R. Cotton (2007), Impacts of Saharan dust as CCN on the evolution of an idealized tropical cyclone, *Geophysical Research Letters*, *34*(14).

Zhang, H., G. M. McFarquhar, W. R. Cotton, and Y. Deng (2009), Direct and indirect impacts of Saharan dust acting as cloud condensation nuclei on tropical cyclone eyewall development, *Geophysical Research Letters*, *36*(6).

Zhang, R., G. Li, J. Fan, D. L. Wu, and M. J. Molina (2007), Intensification of Pacific storm track linked to Asian pollution, *Proceedings of the National Academy of Sciences*, *104*(13), 5295–5299.